ELECTRONIC AND MAGNETIC PROPERTIES OF ROUGH SURFACES OF TRANSITION METALS (Fe, Co and Ni) AND THEIR ALLOYED INTERFACES WITH METAL (Ag, Cu and Au) SUBSTRATES

A Thesis Submitted

In Partial Fulfilment of the Requirement

for the Degree of

DOCTOR OF PHILOSOPHY

in

PHYSICS

by

PRIYADARSHINI PARIDA

Department of Physics & Astronomy

National Institute of Technology

Rourkela 769008, India

June 2015

Declaration

I hereby declare that the work presented in the thesis entitled **"Electronic and Magnetic Properties of Rough Surfaces of Transition Metals (Fe, Co and Ni) and Their Alloyed Interfaces with Metal (Ag, Cu and Au) Substrates"** submitted for Ph.D. degree in the Department of Physics & Astronomy, National Institute of Technology, Rourkela has been carried out by me under the supervision of Dr. Biplab Ganguli. The work is original and has not been submitted in part or full by me for any degree or diploma to this or any other University/Institute.

Priyadarshini Parida
Department of Physics & Astronomy
National Institute of Technology
Rourkela - 769008
Odisha, India.

Certificate

This is to certify that the thesis entitled **"Electronic and Magnetic Properties of Rough Surfaces of Transition Metals (Fe, Co and Ni) and Their Alloyed Interfaces with Metal (Ag, Cu and Au) Substrates"** being submitted by Ms. Priyadarshini Parida, to the National Institute of Technology Rourkela, India, for the award of the degree of Doctor of Philosophy in Physics is a record of bonafide research carried out by her under my supervision and guidance. She has fulfilled all the prescribed requirements and I am satisfied that the thesis has reached the standard fulfilling the requirements of the regulations relating to the nature of the degree. The content of the thesis is based on her own work and have not been submitted to any other university or institute for the award of any degree.

Dr. Biplab Ganguli
Associate Professor
Department of Physics and Astronomy
National Institute of Technology
Rourkela 769008, India
Email: biplabg@nitrkl.ac.in

Acknowledgements

I gratefully acknowledge my supervisor Prof. Biplab Ganguli for his excellent guidance, constant help, advice, patience and providing me with an excellent atmosphere to carry out my research work. It a pleasant and memorable experience to work with him.

I would also like to express my gratitude to Prof. Abhijit Mookerjee, S.N.Bose National Center for Basic Science, Kolkata, India for providing the ASF code for necessary amendments for the present problem. I am also thankful for his valuable input to this work. I am very much grateful to him for his suggestions and discussion I had with him to carry out this work.

I would like to thank Director, National Institute of Technology Rourkela for providing me with all necessary facilities to carry out this work. I would also like to acknowledge my DSC members Prof. D.K.Bisoyi, Prof. S.Panigrahi, Prof. P.N.Vishwakarma and Prof. Alok Satpathy for their patience reading my manuscript and adding some useful comments.

I am thankful to Satya for helping me in programming language and other tools. I also thank Vinesh for his support. I would like to thank Ambika and Rajiv from SNBNCBS, Kolkata, India, and my friends Laxman, Soumee and Pramita for their help during my research carriers.

I am very happy to have friends like Prabhat and Geeta who always motivated me to carry out this work. They always stood by my side in all my difficulties and made me feel comfortable and provided emotional courage. I am also thankful to all my friends who continuously encouraged me in every steps.

My special thanks goes to my parents Mr. Dipak Kumar Parida and Mrs. Pushpalata Parida, who always support me in all my decisions. My loving thank goes to my beloved husband Mr. Sisir Kanti Nayak for his continuous encouragement,

inspiring support and great patience at all times.

I would like to thank Prof.O.K.Anderson, Max Plank Institute, Stuttgart, Germany, for his kind permission to use TB-LMTO code developed by his group.

Finally, I would like to acknowledge INSPIRE program division, Department of Science and Technology, India for providing the financial support to carry out my thesis work under sanction number DST/INSPIRE FELLOWSHIP/2010/[175].

Priyadarshini Parida

Curriculum Vitae

Name : PRIYADARSHINI PARIDA

Date of Birth : 22nd November 1985

Mobile No : (+91)9658666661

Permanent Address: Qrs.No. A-279, Sector-4, Rourkela 769002, Odisha, India

Email: prdsni@gmail.com, paridapri@nitrkl.ac.in

Education:

- *Research Scholar* (2009 - Present), Department of Physics & Astronomy, National Institute of Technology, Rourkela 769008, India.
- *M.Sc. Physics* (2006 - 2008), 9.2 (CGPA), National Institute of Technology, Rourkela 769008, India.
- *B.Sc. (Physics)* (2003-2006), 78.63%, Sambalpur University, Odisha, India.
- *10+2* (2001-2003), 79.44%, C.H.S.E., Odisha, India.
- *10th* (2000-2001), 73.87%, B.S.E., Odisha, India.

Achievements:

- INSPIRE fellowship to carry out Ph.D. work under Department of Science and Technology, India starting from 1st January 2011 till date.
- Qualified Graduate Aptitude Test of Engineering (GATE) 2010 in Physics with all India rank 630.
- Institute Silver Medal on VI-Convocation of National Institute of Technology, Rourkela, for the 1st rank in M.Sc. (Physics).
- 2nd rank in the Sambalpur University in B.Sc. (Physics).
- "Best Graduate in Science" for the academic year 2003-2006 in S.G.W. College, Rourkela.
- Scholarship from Govt. of Odisha from 2003 to 2006 for scoring good marks in +2 Science.

Area of Research: Theoretical Condensed Matter Physics.

List of Publications:

1. Priyadarshini Parida, Biplab Ganguli and Abhijit Mookerjee, *"Magnetism on Rough Surfaces of Fe, Co and Ni : An Augmented Space Approach"*, Superlattices and Microstructures, **86**, 173 - 185, (2015).

2. Priyadarshini Parida, Biplab Ganguli and Abhijit Mookerjee, *"Electronic and Magnetic Properties at Rough and Sharp Transition Metal - Metal Interfaces: An Augmented Space Approach"*, Journal of Magnetism and Magnetic Materials, **381**, 422-432, (2015).

3. Priyadarshini Parida and Biplab Ganguli,*"Electronic and Magnetic Properties of Interfaces of Ni with Ag/Cu/Au Substrates using Augmented Space Formalism"*, Thin Solid Films, **594**, 24-29, (2015).

4. Priyadarshini Parida and Biplab Ganguli, *"Effect of Roughness on Surface Magnetism of Fe(001)"*, International Journal of Scientific & Engineering Research (ISSN 2229-5518), **5**, 81-84, (2014).

5. Priyadarshini Parida and Biplab Ganguli, *Structural, Electronic and Optical Properties of $ZnMnIn_2Te_4$ Chalcopyrite: A DFT+U study*, Transactions of the Indian Institute of Metals, **66**, 397-400, (2013).

6. Priyadarshini Parida and Biplab Ganguli, *"Electronic and Magnetic Properties at Rough Alloyed Interfaces of Fe/Co on Au Substrates: An Augmented Space Study"*, accepted in Chinese Physics B, IOP Publisher.

Workshop & Seminar Attended:

- Attended ICTS school and discussion meeting on Strongly Correlated Systems: From Models to Material at IISc, Bangalore, India from 06 - 17 Jan 2014.

- Presented a poster in ICRAPID 2014 at Sathyabama University, Chennai, India from 23 - 24 Jan 2014. Best Poster award in it.

- Presented a poster on International Symposium for Research Scholars on Metallurgy, Material Science and Engineering (ISRS 2012) at Indian Institute of Technology Madras, Chennai, India from 13 - 15 December 2012.
- Attended Lectures on Photoemission(LoP) and Workshop on Photoemission Studies of Advanced Materials (PSAM - 2011) at Institute of Physics, Bhubaneswar, India from 08 - 13 December, 2011.
- Attended Second Science Conclave: A congregation of Nobel Laureates at Indian Institute of Information Technology, Allahabad, India from 08 - 14 December 2009.

Declaration: I hereby declare that the particulars given above are true to the best of my knowledge and belief.

Priyadarshini Parida

Abstract

The real space technique, "The Augmented Space Formalism (ASF) coupled with Recursion method and Density Functional Theory (DFT) based Tight-Binding Linear Muffin-Tin Orbitals (TB-LMTO) method" is applied to carry out the layer-wise electronic and magnetic properties of transition metals (Fe, Co and Ni) rough surfaces and their alloyed interfaces with metal (Ag, Cu and Au) substrates. The potential parameters are generated by TB-LMTO method. These parameters are used to set-up augmented space hamiltonian. Finally the density of states (DOS) are calculated by recursion technique. The relativistic self-consistent calculation is based on local spin density approximation (LSDA).

A rough surface and alloyed interface resembles a binary disordered alloy. In the former case the roughness is due to random occupation of vacancies and transition metal atoms, whereas in the later case it is due to interdiffusion of transition metal atoms and metal substrate atoms. Since ASF is suitable theory to study disordered binary alloys, therefore it can also be applied to study rough surfaces and interfaces. We also show that ASF can be extended to study almost smooth surfaces and interfaces.

We consider twelve atomic layers of the transition metals along (001) direction for a surface. We also consider two layers of empty spheres above the surface to take care of charge leakage into the vacuum. Relaxation of the top most layer is carried out using minimum energy principle. Two types of roughening are considered. The first is the roughening the top most layer, and the other is roughening the first four layers with different degrees of randomness. The second type models a more realistic experimentally grown surface. As roughness changes at different layers, new peaks in DOS appear due to disorderedness. The magnetic moment of the top layer is maximum for Fe(001) and Co(001) and of 3rd layer for Ni(001) among all the roughed layers. Layered based magnetic moments differ between both types of

rough surfaces. Work functions are found to be almost same for both types of rough surfaces.

We consider nine layers of (001) bcc Fe, fcc Co and Ni to study smooth surfaces. Surface magnetic moment is found to be higher than that of the bulk and in different layers below. Magnetic moments show Friedel oscillations in agreement with other studies. Work functions of these systems are found to agree with experimental values. The orbital resolved DOS show the significant contribution of d-orbital towards the surface as well as bulk magnetic moments.

We consider one monolayer and two monolayers of transition metals on metal substrates to compare our result with other theoretical studies in the case of interface. To model a more realistic interface, an interface consisting of two layers of transition metals and two layers of metal substrates is considered. We also consider three layers of transition metals to compare our results with experimental studies.

The magnetic moment of the overlayer is more compared to its bulk for one monolayer of Fe, Co and Ni on Ag and Au with sharp interface. But it is more only for Fe overlayer and not for Co and Ni on Cu substrate. The magnetic moment of three layers of Fe/Ag having rough interface agrees with experimental results. In case of more realistic four layered rough interfaces, the layerwise magnetic moments and DOS show the effect of roughness at the interface. The magnetic moment of the transition metals as well as the average magnetic moment of interface layers decreases gradually to zero for all the systems. The effect of hybridization on the magnetic properties is also discussed here.

Keywords: Electronic and Magnetic Properties, Augmented Space Formalism, Density Functional Theory, TB-LMTO, Surfaces, Interfaces.

Contents

List of Figures

List of Tables

Chapter 1

Introduction

The valence electrons in a solid play important role to bind an atom to its neighboring atoms. Therefore, the properties of a particular material depend on its valence electrons and their interactions with neighboring atoms. The fundamental problem in solid state physics is to determine the properties of solids from the properties of their constituent atoms [1] and the correlation of electronic interaction to the crystal structure. To solve this fundamental problem, it is required to know the detailed electronic structure.

In case of insulators, magnetic ordering of atoms or group of atoms arise from local moments. But in transition metals like Fe, Co and Ni, magnetic ordering arises mainly due to the interactions among itinerant Fermi electrons. Unpaired electrons present in transition metal atoms give rise to magnetic moment. It depends on the degree of overlap of the wave functions of electrons in different shells on neighboring atoms. The overlap of the d-electron orbitals with neighboring atoms is weak in metals. The d-band is much more narrower than s-band in transition metal-based alloys. Stoner model [2, 3] is an appropriate theoretical base for the description of magnetism in transition metals. This model shows electronic energy states of the itinerant magnetic electrons split into spin-up and spin-down bands due

to the exchange interaction. The magnetic moment is proportional to the population difference in the spin-up and spin-down d-band states. Spin electronic states and therefore magnetic properties depend on the detailed electronic structure, the atomic arrangement and the composition.

The study of the effect of extended defects like surfaces and interfaces on itinerant electron magnetism takes us a step further. This effect on metallic magnets can be illustrated with simple Hubbard model, in which the electron-electron interaction is assumed to be totally local. However, our aim here is to show significant effect of extended defects on the interacting electron sea. In this model the average electron energy is given by [4]:

$$E_{k\sigma} = \varepsilon_k + \frac{U}{2}\left[N - Msign(\sigma)\right] \tag{1.1}$$

Here ε_k is the energy of non-interacting electron and U is Hubbard interaction energy. M represents magnetization and N is number of electrons. σ is spin state. Therefore, the exchange energy splitting ΔE between the up and down spins is given by [4]:

$$\Delta E = UM(\Delta E) \tag{1.2}$$

Magnetization M is a function of ΔE, because the origin of both magnetization and splitting is electron-electron interaction. The above equation constitutes an intrinsic equation for both the exchange splitting and magnetic moment and is the basis behind the Stoner criteria. For $\Delta E = 0$, the magnetic moment is also zero (figure 1.1 (a)). With the increase in ΔE, the up and down density of states (DOS) start splitting. Hence the Fermi energy shifts to accommodate electrons and therefore magnetism develops (figure 1.1(b)). But once the majority band is filled, the magnetization saturates and becomes independent of exchange splitting

(figure 1.1(c)).

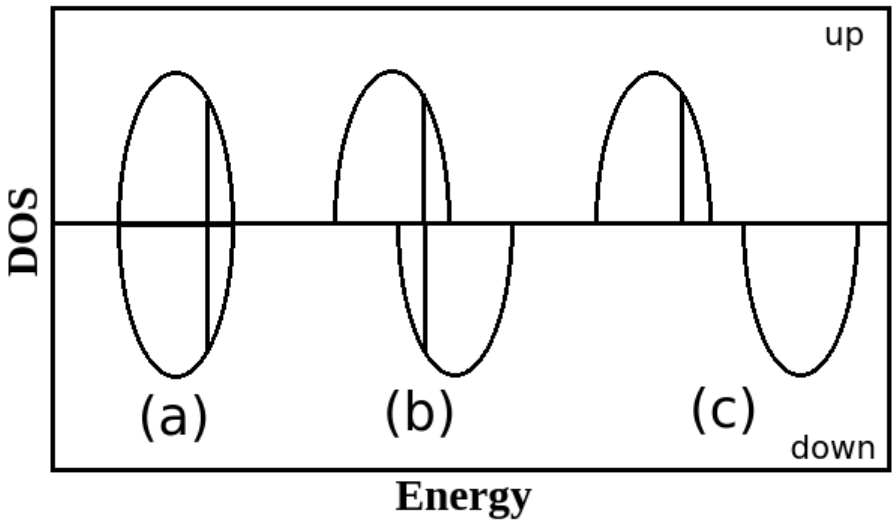

Figure 1.1: Up and down spin density of states split with increasing exchange field.

Figure 1.2 shows qualitative behavior of $M(E)$ versus E for two different values of U. As the value of U decreases, the slope of the curve increases. Hence the magnetization gets saturated with exchange splitting. It is clear that equation 1.2 has a non-zero solution if,

$$\frac{1}{U}\frac{\partial M}{\partial(\Delta E)}|_{\Delta E\to 0} > 1 \tag{1.3}$$

Atoms at surface layers are at the boundary and therefore they are loosely bonded. From these boundaries the flow of mass, charge, energy, spin and momentum occur between the environment and the material. At the boundary, translational symmetry is broken, hence the calculation of electronic states and energies are very difficult. The surface atoms have lower coordination number and reduced symmetry than that of bulk. A simple tight binding model shows that the width of the density of states is proportional to $2ZV$, where Z is the number of nearest neighbor atoms bonded to a particular atom and V is the strength of the overlap integral [4]. Therefore, band narrowing occur at the surface. If DOS is rather featureless near the Fermi energy, the DOS at the Fermi energy is inversely proportional to the width.

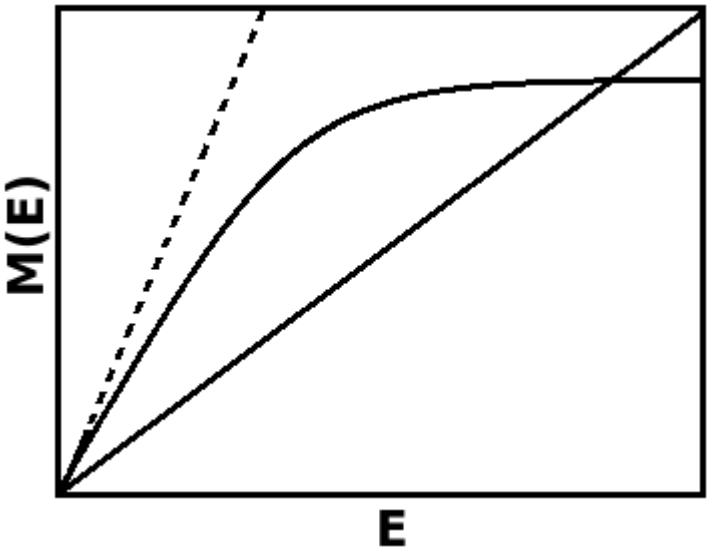

Figure 1.2: Behavior of the magnetization as a function of exchange splitting for two different values of U shown by two different solid lines. The dotted line represents the slope of the curve having smaller U value.

The Stoner criterion at the surface is more easily satisfied [4]. Figure 1.3 shows a featureless semicircular DOS. The curves (a) and (b) has band width of 1 unit and 0.8 unit respectively. It is clear that if there is a narrowing of the band, both the magnetic moment and the exchange splitting increase. Hence the magnetic moment get enhanced at surfaces [4].

Due to change in environment at the surface, like nearest neighbor atoms, nearest neighbor distance and change in symmetry, the electronic and magnetic properties of transition metals change. From the surface upto few atomic layers, the potential differs from bulk [5]. Hence surface magnetic properties are quite different from the bulk properties. In other words, there is narrowing of band width [6–9] and enhancement in surface magnetic moment [6–8, 10–20]. The band narrowing at the surface is observed due to weak bonding of the surface atoms compared to bulk. In realistic situation, surface is rough [21, 22]. The roughness is observed from the height profile analysis. When a surface is formed using molecular beam epitaxy [23] and other vapor deposition techniques, the structure of the surface is like steps, islands or pyramids. Though growth of thin films by molecular beam epitaxy

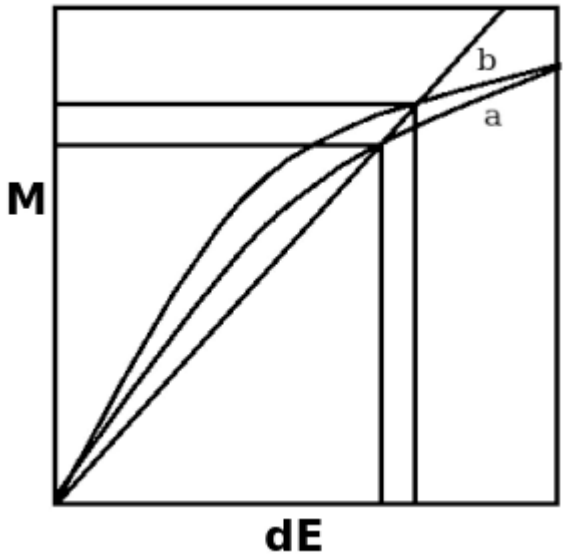

Figure 1.3: Magnetization enhancement with band-narrowing. The calculation is done for uniform density of states. The curves (a) and (b) has band width of 1 unit and 0.8 unit respectively.

is one of the most refined method, but the layer-by-layer growth leads to mound formation in this method [24]. At the same time the growth of single layer surface is unstable. Above certain critical slope, the growth becomes stable with step-mode flow. Such surface structure can be modelled by the missing of atoms at various layers. Hence the missing of atoms at a fractions of sites from the surface makes the system random. The surface roughness is due to the interaction of the surface atomic layer with the environment. So surface can be treated as a substitutional disordered alloy of the surface atom and vacancy. The roughness makes significant changes in electronic and magnetic properties at the surface. These properties are highly influenced by local environment [10, 11] like surface. To understand these surface properties, it is very important to know the surface morphology.

Due to dehybridization [9] of s-, p- and d-orbitals at the surface, the magnetic moment increases. The d-band is narrower and DOS is more at the top most layer compared to the lower layers and bulk value. The contribution of d-orbital is significant towards the magnetic moment for each layer. In case of surface and interface

properties of a transition metal overlayer on a metal substrate, the hybridization of overlayer bands with the substrate play significant role. Hybridization causes band-widening compared to band narrowing due to under-bonding [4]. The resulting surface and interface magnetism is therefore depends on the detailed band structure of both overlayer and substrate.

When transition metals are deposited on metal substrates, properties of these epitaxial films depend on substrate quality, geometrical matching, chemical interaction between adsorbate and substrate, temperature, rate of deposition, film thickness, annealing procedures and the promoting action of surfactants [25]. Band narrowing occurs at an interface due to change in nearest neighbor spacing of monolayer atoms and weak hybridization between the electronic states of overlayer and substrate [26]. This gives rise to large DOS at the Fermi level. This causes various interesting properties like localized electronic states, magnetic moment enhancement, magneto-crystalline anisotropy and complex magnetic ordering [14]. Enhancement of magnetic moment is due to loss of bonds at the overlayer [27]. We shall consider the deposition of Fe, Co and Ni overlayers along (001) surface of Ag, Cu and Au substrates.

In short, any detailed study of surface and interface magnetism should be coupled with the studies of surface growth, geometry and morphology, and first principles studies of the electronic structure at such surfaces and interfaces .

1.1 Brief Survey of Surface Properties of Transition Metals

In realistic situation, surface is rough [21]. It is confirmed from nano topographical analysis of iron by AFM [22]. Rough surface profiles are obtained from various vapor deposition technique, laser ablation method and molecular beam epitaxy [10]. The surface roughness is also observed from the height profile analysis. At the surface, due to random changes in local environment, the situation is complicated [10]. When a surface is formed using molecular beam epitaxy [23] and other vapor deposition techniques, the structure of the surface is like steps, islands or pyramids. That means roughness is not only created on the top most layer but there are some amount of roughness in the layers beneath the top most layer. Hence surface cannot be defined with a single atomic layer. The molecular beam epitaxy growth of thin films is one of the most refined method. But in this method, the layer-by-layer growth leads to mound formation [24]. And the growth of singular surface is unstable. But above certain critical slope, the growth becomes stable with step-mode flow. The imperfection in transition metals nano-wires enhances magnetic properties [28]. With increase in crystal disordered, the thickness of the weakly coupled surface increases [29]. The AFM study of highly oriented pyrolytic graphite surface with Co particles show that with the increase in electro-deposition potential of Co, the particle density increases and the size decreases [30]. Hence the study of surface roughness is very important to know the properties of realistic situations.

Very few theoretical work have been carried out for the study of rough surface. The rough surface magnetism is studied using roughness exponent of local curvatures of surface [10]. Properties of rough surface are also determined for some particular environment by randomly replacing atoms by empty spheres using real space recursion technique along with tight binding linear muffin tin orbital method [11] for Fe(100) and Ni(100). But the roughness is not defined in this case for all possible

configuration.

When iron film is deposited on noble metals, magnetic dead layers are obtained, for the first two layers of iron. But with addition of an extra layer, that is from third layers onwards, the magnetization increases and approaches to bulk value [31]. Further increase in atomic layers do not affect the magnetism of the first two layers hence the first two layers of Fe remains nonmagnetic. Similar results are also obtained for Ni on nonmagnetic substrate carried out using electrolytic deposition [32]. The number of magnetic dead layers of Ni varies with temperature, that is, four magnetic dead layers are observed at room temperature and two dead layer at $T = 0$. Such evidences of “magnetically dead layers" at the surface of ferromagnetic Fe and Ni has stimulated the development of theoretical methods for describing these surface effects.

Experimental studies of surface and bulk electronic and magnetic properties of transition metals, such as bcc Fe(001), fcc Co(001) and fcc Ni(001) are carried out earlier using spin polarized low energy electron diffraction experiment [33], spin-polarized angle-resolved photoemission [34], Weiss and Forrer's axial extraction method [35], electron capture spectroscopy [36], polarized beam spectrometer [37] and electron spin polarization (ESP) measurement [38]. From the electron spin polarization (ESP) measurement in photoemission of Ni single crystal, it is observed that the magnetic dead layers are not present in Ni surface [38]. The surface magnetism of Ni(001) is also carried out using spin polarized low energy electron diffraction experiment [33]. The temperature dependence of surface magnetization near the Curie temperature shows the magnetization of the topmost layers decreases with a critical exponent. Using spin-polarized angle-resolved photoemission [34], the magnetic surface states of Fe(001) are studied. From the study of electron-spin polarization using electron capture spectroscopy [36], the existence of local ferromagnetic order at Ni surface is confirmed. “No magnetic dead layer" at the surface is obtained for Fe surface [39] using high-resolution angle-resolved photoemission

spectra. Using Weiss and Forrer's axial extraction method, the saturation magnetization and the bulk magnetic moment of iron and nickel have been reported [35]. Using polarized beam spectrometer, 3d spin bulk magnetic moment of Ni is found to be 0.656 μ_B [37].

Various theoretical methods are also used to study the surface properties of these transition metal thin films. They are Green's function technique based on linear muffin-tin orbital (LMTO) method within tight-binding and atomic sphere approximations [18], fully relativistic LMTO method [7,17], full-potential linearized augmented plane wave (FPLAPW) method [9, 12–16, 40–42], full-potential linear muffin-tin orbital (FPLMTO) method [43], linearized augmented plane wave (LAPW) method [44], surface embedded Green's function with LAPW method [5], different basis sets in linear combination of atomic orbitals in density functional theory (LCAO-DFT) [20, 27, 45], tight binding linear muffin tin orbital (TBLMTO) with real space recursion method [10, 11, 46], TB-LMTO supercell calculation [10, 11, 19], X-ray magnetic circular dichroism (MCD) spectra and orbital magnetic moment based on FPLAPW method [6], LMTO method along with surface Green's function method [8] and local spin density functional theory [47]. FPLAPW calculation shows surface magnetic moment for bcc Fe(001), fcc Co(001) and fcc Ni(001) get enhanced by about 30%, 12% and 20% respectively over their corresponding bulk values [9, 13, 14, 40–42]. Since the enhancement in Co is less, it is more stable to the change of environment. Iron depends very strongly on the environment. Enhancement of 31% and 26% is obtained in surface magnetic moment for Fe and Ni respectively using FPLMTO method [43]. FPLAPW calculation of magnetic moment on five and nine layers of Co shows magnetic moment of subsurface layer is closed to the bulk value. This indicates a short-range effect of surface on magnetism [15]. A LMTO method [7, 17] calculations taking seven layers of bcc Fe and fcc Ni shows orbital magnetic moment for surface atoms gets enhanced over 100% and spin-moment gets enhanced by 32% and 7% for bcc Fe and fcc Ni respectively.

The study using LMTO method along with surface Green's function method [8] uses one layer of empty sphere above surface. Calculation of surface magnetic moment of Ni by real space recursion method [46] shows enhancement of surface magnetic moment decreases from 28% to 4% with the increase in slab thickness from three layers to nine layers. This is because the formation of local magnetic moment strongly depends on local environment of an atom. The surface and bulk electronic properties for transition metal are carried out using a model explaining surface atom core-level shift [48]. The difference in center of gravity for surface and bulk DOS is found to be positive for less than half-filled d-bands and negative for more than half-filled d-bands. Due to narrowing of d-band at the surface, the core-level shifts and binding energy reduce. The enhancement in surface magnetic moment is due to s-d dehybridization at the surface and the presence of electrostatic shifts in order to maintain the layer-by-layer charge neutrality [44]. Due to large difference in spin-up and spin-down electronic states at Fermi level, Ni is a strong ferromagnet [49]. The narrowing of d-band width and the shift of peak position are also observed in surface layer DOS. Near the middle of transition metal series where Fermi energy lies in the valley of d-electron of bulk DOS, the enhancement of surface DOS occurs at Fermi level [20]. All these studies show an enhancement of surface magnetic moment. But in nine layers of Ni(001) carried out using LCAO method [45], though the possibilities of magnetic dead layer is rejected, surface magnetic moment reduces by 20%. And maximum magnetic moment occur for two layers below surface. The surface roughness are not considered in all these theoretical layerwise electronic and magnetic properties study.

Interlayer relaxation is obtained at 4% using FPLAPW method [14] for bcc Fe(001). In previously studied TB-LMTO-ASR calculation for Fe(001) surface [19], surface dilatation is considered to study surface electronic and magnetic properties. But relaxation of surface atoms is not considered for bcc Fe and fcc Ni using LMTO method [7, 17] including spin-orbit coupling. In this case the bulk crystal structure

parameters are used for surface atoms. The earlier Augmented Space Formalism coupled with recursion method [19, 50] based calculations for rough surface did not consider the lattice relaxation of the top layer.

Calculations of magnetic moment using FPLAPW method [9,12] for seven layers of Fe(001) and five layers of Ni(001) thin films show small Friedel oscillations. Similar result is obtained using Green's function technique based LMTO method [18] for five layers of bcc Fe(001), fcc Co(001) and fcc Ni(001). A strong Friedel oscillation is obtained for spin density states with the enhancement of surface magnetic moment Using LCAO method [20] for seven layers of Fe(001). Using real space recursion method [11], Friedel oscillation is observed for charge and magnetic moment in bcc Fe(100), fcc Co(100) and fcc Ni(100). But local spin density functional calculation within FPLAPW method [16, 41] for seven layers of Ni(001), magnetic moment is found to decrease gradually from surface layer to the center layer, which shows no Friedel oscillation for Ni [41]. Therefore, we carry out layerwise magnetic moment for nine layers of the above mentioned systems to check the possibilities of Friedel oscillations.

Work function is a surface property and is related to the surface DOS. It is an experimentally measurable quantity and therefore theoretical calculation of it is necessary for comparison with experimental result to test the accuracy of theoretical method. Experimentally found work function for Fe(100), Co and Ni(100) are 4.67 eV, 5.0 eV and 5.22 eV respectively [51]. The work function of Ni(001) is found to be 5.71 eV using surface embedded Green's function with LAPW method [5]. Whereas FPLAPW method gives a value of 4.29 eV [12] and 4.35 eV [41] for Fe(001), 5.37 eV [16, 41] for Ni(001) and 5.05 eV & 5.17 eV respectively for five and nine layers of Co [15]. The spin-polarized Green's function technique based LMTO method within tight-binding and atomic sphere approximations calculations of work function are found to be 4.50 eV, 5.52 eV and 5.75 eV [18] respectively for bcc Fe(001), fcc Co(001) and fcc Ni(001). The effect of spin-polarization on work function is also reported.

1.2 Brief Survey of Surface and Interface Properties of Transition Metals on Metal Substrates

When Fe is grown on Cu, the magnetization of the first two layers is zero and it increases from third layers onwards and finally approaches to saturated value [32]. Hence first two Fe layers are magnetically dead. For Ni on Cu or Au, four magnetically dead layers are observed [31]. But Fe/Cu multilayer prepared by sputtering [52] shows that the top layer is ferromagnetic but the bottom layer is nonmagnetic. There are experimental and theoretical works carried out to study the layerwise properties of such transition metals, deposited on metal substrates. We shall study the deposition of Fe, Co and Ni transition metals on Ag, Cu and Au metal substrates.

The growth of Fe on Ag and Au is in bcc phase. A monolayer is two-dimensional. Therefore it is neither bcc nor fcc [53]. But in order to avoid lattice mismatch, the growth of Fe on Ag and Au takes place with a 45° rotation of Fe translational vector [13,14,40,53–56]. The lattice mismatch of Fe and Ag is wrongly interpreted in a report [57] which is corrected later [53]. This tilting of atomic layers is also proved experimentally using Rutherford backscattering spectrometry [58]. Due to dissimilarity in Fe and Au electronic structure, the hybridization gets weaken between the overlayer and substrate near Fermi level [40]. Hence the magnetic moment gets enhanced. The ferromagnetic Fe is deposited on Cu in its fcc phase [54]. This is also confirmed using spin-resolved inverse photoemission spectroscopy [59]. Using inverse photoemission spectra, the growth morphology of eight layers of fcc Fe grown on Cu(100) is carried out with Fe having lattice parameters as that of Cu. But in case of Ni on Ag, both are in fcc phase and there is 13.9% lattice mismatch. Hence the lattice relaxation of the top most Ni layer is carried out. We consider lattice relaxation of top most layer in the cases of Ni/Ag as well as Co/Ag, Co/Au and Ni/Au.

Theoretical studies of surface magnetic moment of one ML of Fe, Co and Ni

on Ag, Cu and Au substrates are carried out using FPLAPW method [9, 13, 14, 40, 41, 60–70], self consistent local orbital (SCLO) method [71–73], LCAO DFT method with SZSP and DZSP basis [27], KKR Green's function techniques [74], TB-LMTO-ASF-Recursion with and without surface dilatation [19, 50], FPLMTO method [43, 75] and TBLMTO-CPA method [76]. The layerwise surface electronic states of Ni/Ag are carried out using FPLAPW method [63, 64]. It is observed that the magnetic moment of Fe overlayer on Ag [13, 14, 40, 60–63] is less than the free standing Fe monolayers [14]. But it is approximately equal to the clean surface Fe magnetic moment [13,14,40]. The 3d electrons of transition metals hybridize with 5-sp electrons of Ag, broadening d-DOS and reducing the tendency for ferromagnetism. Ni d-electrons are more localized in Ni/Ag compared to clean Ni surface, but the surface magnetic moment of Ni/Ag is less than the clean surface [64]. Hence it is reported that the interaction of 3d electrons with substrate is significant than the localization effect. Few theoretical studies using FPLAPW method [13, 40, 60, 61, 66–68] have also been carried out to study properties of two ML of Fe and Ni on Ag and Cu substrates. Due to increase in d-d coupling, in this case, DOS of Fe monolayer broadens compared to one ML of Fe on Ag. The overlayer magnetic moment of Fe on Cu is less compared to that of Ag substrates. Comparing the monolayer moment of transition metals with Ag and Cu substrate, the Cu moments are reduced more due to 12% smaller lattice constant of Cu, which increases sp-d hybridization [14,63]. The enhancement of overlayer magnetic moment is supported by various experiments such as magnetic circular dichroism in X-ray absorption spectroscopy (XMCD) [77, 78], XMCD spectra in SQUID magnetometer [79, 80], angle-resolved photoelectron spectroscopy [67]. The overlayer magnetic moment of transition metal get enhanced on metal substrate except for Ni on Cu. Hence magnetism of Ni is very sensitive to environment. But for two ML of Ni on Cu [68], surface Ni magnetic moment is increased by 10% and the interface magnetic moment decreases by 24% [9, 41, 68, 72]. This is also supported by experiments [78].

The enhancement of the interface Fe magnetic moment at Fe/Ag interface is observed both experimentally and theoretically using first principle density functional calculation [81], molecular beam epitaxy [82], FPLAPW method [83, 84], SQUID magnetometry [85]. The layerwise magnetic moment for 3-16 ML of Fe on Ag is carried out using KKR method [86]. It is observed in all the cases that surface and interface Fe magnetic moments get enhanced compared to other layers. But the surface magnetic moment of Fe is more than the interface value. Using interface assisted ion beam mixing for ordered layer structure, the magnetic moment of Co in Co/Ag system is found to be more, whereas it is less in the case of Ni in Ni/Ag [87] compared to the bulk. The FMR studies [88] show that when thickness of Ni is between 4 and 7 nm, magnetization decreases whereas for thickness less than 4 nm it increases. Using magneto-optical sum rule [89], the enhancement of surface and interface magnetic moment for Fe/Ag is also observed for three ML of Fe deposited on Ag. Using conversion electron Mossbauer measurement [90], the enhancement of magnetic hyperfine field is observed compared to bulk value for 2.4 ML and 5.5 ML of Fe on Ag(100). Experimentally it is also observed that as the thickness of Fe layer increases, the magnetic moment per Fe atom decreases [91]. Using LMTO method along with Green's function technique [8], the interface Fe magnetic moment is found to be more compared to other Fe layers in Fe/Cu. But in the case of Co/Cu, the interface Co magnetic moment slightly less compared to its nearest Co layer. Whereas, in Ni/Cu system there is significant decrement in Ni interface magnetic moment compared to that of other Ni atomic layers. This decrement in Co magnetic moment at Co/Cu interface is also observed using spin polarized screen KKR method [92] and SQUID magnetometry [93]. At the Ni/Cu interface, the Ni magnetization reduces by 30% due to hybridization between Ni d-band and Cu conduction band. Due to short screening length, the effect of both surface and interface is only upto one or two Ni atomic layers [94]. For two ML of Cu on Ni, the interface magnetic moment of Ni decreases [94, 95]. The enhancement of Fe magnetic moment is found at Fe/Au interface by density functional theory (DFT) [56] calcula-

tion. The magnetic properties of Fe, Co, Ni sandwich between Ag or Au half planes are also carried out using layer Korringa-Kohn-Rostoker (LKKR) method [96]. The Fe interface moment converges to 2.74 μ_B with the increase in Au layers [97]. The study of electronic states for various layers of Fe on Au(100) is carried out using spin-resolved inverse photoemission study [98], FPLAPW method [70], DFT [56] and layer Korringa-Kohn-Rostoker (LKKR) band-structure technique [96].

Surface roughness are observed in various experiments [99]. When a surface is grown in case of Ni, the growth is layer-by-layer upto 3.2 ML, but beyond 4.2 ML a new layer starts before the previous layer is complete. Hence the growth of the previous layer is rough [99]. Layer-by-layer growth of Fe on Ag is observed from LEED and Auger spectroscopy [57], ultraviolet photoemission spectroscopy [26] upto three Fe layers. LEED, MEED and SMOKE analysis [100–102] show that when Fe is deposited on Cu, it gets agglomerated upto 5 ML. This leads to rough surface. Therefore, for any theoretical studies of surface and interface properties it is necessary to treat surface and interface as rough, which is missing in most of the earlier theoretical approaches. Augmented space formalism (ASF) coupled with recursion method first attempted to consider a rough interface, but interdiffusion of atoms was considered upto only one ML [19, 50]. The growth of Fe on Cu is in ferromagnetic state [101, 102]. ASF calculation finds that when Fe is deposited on Ag and Cu, induced magnetic moment on Ag is more than Cu which contradicts other theoretical studies [40, 62, 65, 66, 70, 71].

Few studies show that the interdiffusion of atoms is not allowed for immiscible systems such as Fe-Ag, Co-Ag and Ni-Ag. Therefore alloy formation is not possible at the interface [88, 103, 104]. Co-Ag is not miscible even in liquid stage [105]. Hence the possibility of intermixing is suppressed and the superlattice with sharp interface can be obtained [106, 107]. The abrupt Fe/Ag interface is also confirmed from backscattering spectroscopy [108]. From Auger electron spectroscopy [104] it is observed that for the deposition of Fe overlayers on Ag, the concentration

of Ag decreases with increase in deposited layer thickness. When the target to substrate distance is small, there is a chance of intermixing of Fe and Ag [104], which decreases with increase in target to substrate distance. From the growth morphology study of ultrathin iron films on Ag(100), carried out using thermal energy helium diffraction [25], it is observed that the sharpness of Fe on Ag interface is affected by interdiffusion and there is segregation of atoms at the interface. The presence of small islands are found from specular beam spot profile for 0.5 ML of Fe on Ag. But for 1 ML of Fe, surface roughness is not found. For Ag/Fe multilayers, the surface roughness of top Ag layer is observed from atomic force microscopy [58]. The roughness of first Fe layer is observed from RHEED pattern [58]. Initially, when growth begins, the roughness is very high. With the increase in number of Fe or Ag grown layers, the amount of roughness decreases and after few atomic layers it becomes constant [58]. When Fe is deposited on Ag layer, due to difference in surface energy, intermixing of Fe and Ag occur at the atomic level. But when Ag is deposited on Fe layer, Fe atoms do not come to the surface hence the intermixing do not occur. So Fe-on-Ag have higher interface roughness compared to Ag-on-Fe [109]. Like Fe/Ag, Ag atoms may segregate to surface due to difference in Ni and Ag surface energies to minimize the surface energy [64]. In order to minimize the surface energy in immiscible bulk systems, the surface atoms undergo elastic relaxation [110], that is, the surface alloys are formed by elastic relaxation.

The interface properties of Fe/Ag system are carried out experimentally using X-ray standing wave technique along with Mossbauer spectroscopy [109]. The intermixing of atoms of iron film of 0-10 ML thick and Ag(100) substrate at the interface is observed in an experiment of ion scattering spectroscopy [111] at low temperature where thermal diffusion is not allowed. With increase in film thickness, the amount of Ag content in surface decreases. For less concentrated Fe (about 10%), Fe atoms are dispersed in the fcc Ag matrix or in disordered regions and could not be distinguished [112]. The interface roughness is also observed in Fe/Ag multilayers with 2.4

Å and 8.8 Å thick Fe layers on Ag substrate with more than 25 Å thickness, prepared by sputtering [52]. In this work it is observed that the top and bottom interfaces are ferromagnetic and the bottom interface is less alloyed. The intermixing of 50%, 25% and 12.5% Fe atoms with Ag substrate atoms at the interface, middle and top layer respectively is also reported [89]. Two types of disorderedness at the interface are considered using TB-LMTO-ASA method [55]. One is pseudo-amorphous, that is without interdiffusion and the other is chemical disorder that is interchange of Fe and Ag atoms. The magnetic moment of Fe atoms are 2.4 μ_B/atom without considering interdiffusion of atoms at the interface. When there is 50% interdiffusion of Fe and Ag atoms at the contact layer, the magnetic moment of Fe atom get enhanced to 2.55 μ_B/atom for Fe(110)/Ag(111). Fe or Co magnetic nano particles can be dispersed in non-magnetic metallic matrix like Cu, Ag or Au [113]. Like Fe/Ag, Co/Ag rough interface is obtained when the film growth occurs at high sputtering pressure [114]. Co and Ag are highly immiscible [115], therefore intermixing of these atoms gives granular behavior. The Co/Ag granular films are prepared by MBE which shows that above 35% concentration, due to presence of Co impurities in Ag matrix, the magnetoresistance decreases [116]. It is observed that few atoms are displaced into the other side of the interface in Ni-Ag system in a molecular dynamics simulations study [117]. This roughness is only in one ML scale. The interdiffusion of atoms at Ni-Ag interface is observed from TEM analysis [118]. The abrupt interface is also obtained for Ni-Ag system [119] in scanning transmission electron microscopy. From magnetic diffuse neutron scattering data [120], it is observed that with the increase in Cu concentration from 2 to 40%, the average magnetic moment of Ni-Cu system decreases from 0.59 μ_B to 0.17 μ_B respectively. The reduction in Ni magnetic moment is due to chemical screening effect and cooperative magnetic effect between Ni atoms. From STM analysis of 0.12 ML Co on Cu, fuzzy islands are observed in Cu substrate and Co atoms are found to intermix with Cu atoms at the surface [121]. The amount of intermixing is more for 0.6 ML of Co on Cu. For 1.35 ML of Co on Cu, the second layer starts filling before the first layer is filled, called as bilayer

growth mode upto 2 ML.

The solubility of magnetic atoms are less in host metals [122]. The solubility of Co-Cu alloy is less than 5% at each end of composition range [123]. Using ion scattering equipment NODUS [124], it is observed that in Cu-rich Cu-Ni system, the Cu segregation is less. But in alloy having 84 atomic.% Cu, Ni atoms segregate to the surface. The intermixing of Ni and Cu atoms in Ni-Cu multilayer is discussed using HIKE method [125]. Due to difference in surface energies of Ni and Cu, Cu atoms segregate into Ni films deposited on Cu substrate [126]. The growth of surface is also rough. Minimum surface energy of Ni is found in second layer using Green's function technique [127]. This means Ni atoms interdiffuse to second Cu layer. Using anomalous Hall effect [122] for Co atoms on Ag surface layer, Co atoms are observed to behave as free and uncoupled magnetic ions. But when the Co concentration increases more than 10% of an atomic layer, Co atoms are no longer free. From surface x-ray diffraction and molecular dynamics study [128], interdiffusion of 30% atoms are observed at the Ni-Cu interface. And the interface is confined to two atomic layers adjacent to interface. The interdiffusion of Cu atoms upto 25% is considered in an experiment using SQUID magnetometry [93]. The dynamic evolution of Cu atoms into Ni layer is observed for 4 ML of Ni on Cu substrate using molecular dynamics simulation [129].

It is observed from RHEED analysis that the interface between Co and Au is flat [105]. LEED and STM analysis [130] show that the growth is two dimensional that is layerwise for less than or equal to one ML of Fe on Au with one Au capped layer. It is no more two dimensional for more than one layer. It is also observed that only 13% Co is soluble in Au [131]. In a molecular dynamics simulations along with embedded-atom-method (EAM) [132], it is found that the growth of Ni on Au(001) is Volmer-Weber type, that is growth is 3 dimensional from the beginning. The intermixing of atoms is also observed which lead to strained films. Au atoms are found to segregate disorderly at the surface region [133] and the growth is island

type with different heights for Fe deposited on Au(100). There is some amount of Au present at the surface region for thick Fe layer. Fe/Au rough interface is also observed in scanning tunneling microscopy studies [134]. From the study using spin-polarized embedded-cluster method [135], it is observed that with Fe impurities in Au, the magnetic energy increases, that is, the magnetic moment of the single Fe impurity in Au is more than the pure bulk Fe magnetic moment. It is observed using SQUID magnetometry that with increase in Fe content the induced magnetic moment on Au increases [136].

1.3 Motivation

Based on the literature survey, the motivations to carry out this work are as follows.

1. Study of electronic and magnetic properties of transition metals (Fe, Co and Ni) rough surfaces with surface thickness upto few monolayers.
2. Layerwise variation of roughness is considered.
3. Study of electronic and magnetic properties of rough and alloyed interface of transition metals (Fe, Co and Ni) and metal substrates (Ag, Cu and Au) with interdiffusion of atoms upto few monolayers on both sides.
4. Consideration of lattice relaxation of the top most layer.
5. Extension of Augmented space formalism to almost smooth surface and sharp interface properties.

1.4 Plan of Work

The detailed plan to carry work this thesis work is as follows.

1. To implement TB-LMTO code to generate potential parameters to be used in "Augmented Space Hamiltonian".

2. To develop code for nearest neighbor map for recursion calculation.

3. The nearest neighbor map code is coupled with ASF code and apply this full code to study a known binary alloy for test.

4. We roughen the surface with empty spheres and consider surface as an alloy of surface atoms and empty spheres and generate potential parameter for empty sphere and surface atom.

5. We apply ASF with recursion using the potential parameters as generated above to calculate density of states, work functions and magnetic moments of Fe, Co and Ni layers.

6. To avoid the lattice mismatch between Fe and Ag or Au, we shall deposit Fe in its bcc phase with 45° rotation. But in case of Co and Ni overlayer on Ag and Au, we shall consider the effect of lattice relaxation in surface.

7. To study interface properties we apply TB-LMTO to generate transition metal and substrate metal potential parameters.

8. Due to interdiffusion of transition metal atoms into metal substrate and vice versa, the rough interface is a binary alloy. We set up ASF hamiltonian for the binary alloy transition metal (Fe, Co and Ni) and substrate metal (Ag, Cu and Au) atoms using the potential parameters generated. We then calculate density of states and magnetic moments.

1.5 Research Outlines

The outlines of the present work are as follows.

1. Electronic and magnetic properties of (001) surface are calculated upto twelve layers of bcc Fe, fcc Co and fcc Ni transition metals. Two different cases of roughness are considered

   (a) Top four layers are treated with varying roughness and rest smooth.

   (b) Top one layer with different degree of roughness and rest smooth.

2. Electronic and magnetic properties of (001) surface are studied for almost smooth surface by considering nine atomic layers of bcc Fe, fcc Co and fcc Ni.

3. Electronic and magnetic properties are studied for sharp interface of one ML transition metal (Fe, Co and Ni) with semi-infinite metal substrates (Ag, Cu and Au). In this case no interdiffusion is considered.

4. Electronic and magnetic properties are studied for alloyed interface of one ML transition metal (Fe, Co and Ni) with one ML of metal substrates (Ag, Cu and Au) while taking semi-infinite substrates. 5% and 10% interdiffusion of atoms are considered.

5. Electronic and magnetic properties are studied for sharp interface of two ML transition metal (Fe, Co and Ni) with semi-infinite metal substrates (Ag, Cu and Au). In this case no interdiffusion is considered.

6. Electronic and magnetic properties are studied for alloyed interface of two layers transition metal (Fe, Co and Ni) with two layers of metal substrates (Ag, Cu and Au) with varying degree of interdiffusion of atoms into different layers.

7. Electronic and magnetic properties are studied for sharp interface of three layers transition metal (Fe, Co and Ni) with semi-infinite metal substrates (Ag, Cu and Au) without any interdiffusion of atoms.

8. Electronic and magnetic properties are studied for rough interface of one ML transition metal (Fe, Co and Ni) with one ML metal substrates (Ag, Cu and Au) while taking three layers of transition metal deposition on semi-infinite metal substrates. 5% interdiffusion of atoms is considered.

Chapter 2

First Principle Methods

2.1 Density Functional Theory

The wave function Ψ carries all information about a quantum mechanical system. So it is very important to find the wave function from Schroedinger's equation. In the stationary states of a time independent potential, the Schroedinger's equation is:

$$\left[-\nabla^2 + V(\mathbf{r})\right]\Psi_n(\mathbf{r}) \;=\; E_n\Psi_n(\mathbf{r}) \tag{2.1}$$

Here $\frac{-\hbar^2}{2m} = 1$ is taken in atomic Rydberg unit. In the above equation r represents the distance between electron and nucleus, Ψ_n and E_n are the wave functions and energy levels respectively. For a simple case having a single particle like Hydrogen atom, Schroedinger's equation can be solved exactly. But for elements having higher atomic number (Z) and their compounds, that is for many-body problems, the solution of such equations is very difficult. This difficulty is due to the electrostatic repulsion among many electrons in presence of attractive nuclei. For N number of particles, Schroedinger's equation will be of the form:

$$\left[\sum_i^N \left(-\nabla^2 + V(\mathbf{r}_i)\right) + \sum_{i<j} U(\mathbf{r}_i, \mathbf{r}_j)\right]\Psi_n(\mathbf{r}_1, \mathbf{r}_2, ..., \mathbf{r}_N) \;=\; E_n\Psi_n(\mathbf{r}_1, \mathbf{r}_2, ..., \mathbf{r}_N) \tag{2.2}$$

The first term in the left hand side represents the kinetic energy operator. The second term $V(\mathbf{r}_i)$ is the potential energy of many electrons due to attractive nuclei. The third term U deals with electron-electron interaction. If the potentials $V(\mathbf{r}_i)$ and $U(\mathbf{r}_i, \mathbf{r}_j)$ are known, Schroedinger's equation can be solved to obtain the wave function $\Psi(\mathbf{r})$. In general U is not exactly known and there is no simple direct solution of such a many body equations. We require approximations and indirect method to solve such a Schroedinger's equation. In an indirect method, a many-body Schroedinger's equation is reduced to an equivalent single particle Schroedinger's equation like Hydrogen atom.

First approximation is Born-Oppenheimer adiabatic approximation [137], in which electrons and nuclei are considered as two separate systems and their behavior is studied independently. Next come Hartree approximation. In this approximation each electron experiences an effective potential due to other electrons which is classical Coulomb potential [137]. The further approximation is Hartree-Fock theory which includes quantum mechanical exchange potentials among the electrons. Hartree-Fock method does not take into account electron correlation, that is spin contribution to Coulomb interaction energy.

The density functional theory (DFT) takes into account all the above mentioned approximations including electron-electron correlation. In this theory the basic idea is to write all physical quantities as a functional of electron density. The formulation of theory began in 1927 by Thomas and Fermi. According Thomas-Fermi theory [138], the variation in potential experience by the electron is very slow and the kinetic energy of the of the systems of electrons is an explicit functional of the density, as that of non-interacting electrons in a homogeneous gas with density equal to the local density at any given point. Then the total energy of the system can be expressed with the single particle density. But Thomas and Fermi did not consider the effect of exchange and correlation. The problem in exchange part was corrected by Dirac in 1930. However Thomas-Fermi-Dirac theory was also inaccurate. Because according

to this theory, the kinetic energy which is a major contribution to the total energy is poorly approximated and the electronic correlation is completely neglected.

In 1964, Hohenberg and Kohn [139] formulated the most successful DFT which include both electron correlation and exchange also. Hohenberg and Kohn formally proved that all the ground state physical quantities can be written as a functional of ground state density $n_0(\mathbf{r})$. Starting from the density of the particle, all information about ground state as well as excited state can be determined. Therefore all the observables can be calculated from the ground state density. Thomas-Fermi theory is then considered as an approximation to DFT. The two **Hohenberg and Kohn theorems** are [138, 139]:

- **Theorem 1: Density as Basic Variable:** For any system of interacting particles in an external potential $V_{ext}(\mathbf{r})$, the potential $V_{ext}(\mathbf{r})$ is determined uniquely, except for a constant, by the ground state particle density $n_0(\mathbf{r})$. Therefore, all ground state properties of a system are completely determined by the ground state density.

- **Theorem 2: The Variational Principle:** A universal functional for the energy $E[n]$ in terms of the density $n(\mathbf{r})$ can be defined, valid for any external potential $V_{ext}(\mathbf{r})$. For any particular $V_{ext}(\mathbf{r})$, the exact ground state energy of the system is global minimum value of this functional, and the density $n(\mathbf{r})$ that minimizes the functional is the exact ground state density $n_0(\mathbf{r})$.

  This theorem gives the total energy as:

$$\begin{aligned} E_{HK}[n] &= T[n] + E_{int}[n] + \int d^3\mathbf{r} V_{ext}(\mathbf{r}) n(\mathbf{r}) + E_{II} \\ &= F_{HK}[n] + \int d^3\mathbf{r} V_{ext}(\mathbf{r}) n(\mathbf{r}) + E_{II} \end{aligned}$$

  where, E_{II} is electrostatic ion-ion interaction.

In 1965, **Kohn and Sham** [140] proposed a method to carry out electronic structure calculations. In this, the original many-body hamiltonian is replaced by

an auxiliary system. The ground state density of original interacting system is taken as the density of the non-interacting auxiliary system. Hence the many-body Schroedinger's equation can be expressed as independent particle equation which can be easily solved to get ground state density and energy. The Kohn-Sham equation is:

$$\sum_{i=1}^{N}\left[-\nabla^2 + V_{eff}(\mathbf{r})\right]\Psi_i(\mathbf{r}) = \sum_{i=1}^{N} E_i\Psi_i(\mathbf{r}) \tag{2.3}$$

Here $\frac{-\hbar^2}{2m} = 1$ is taken in atomic Rydberg unit. The effective potential term $V_{eff}(\mathbf{r})$ consists of external potential, Hartree potential and exchange-correlation potential and is given by:

$$V_{eff}(\mathbf{r}) = V_{ext}(\mathbf{r}) + V_{Hartree}(\mathbf{r}) + V_{xc}(\mathbf{r}) \tag{2.4}$$

$$= V_{ext}(\mathbf{r}) + \int \frac{2n(\mathbf{r}')}{|\mathbf{r}-\mathbf{r}'|}d^3\mathbf{r}' + \frac{\delta E_{xc}[n]}{\delta n(\mathbf{r})} \tag{2.5}$$

where, the density is:

$$n(\mathbf{r}) = \sum_{i=1}^{N}|\Psi_i(\mathbf{r})|^2 \tag{2.6}$$

The last term in the right hand side of equation 2.5 is not known exactly and need to be modeled. These equations can be solved self consistently to get ground state energy for a system of N interacting particles. The step-by-step procedure to solve Kohn-Sham equation is given in figure 2.1 [138]. The accuracy of the solution depends on various exchange-correlation used. In an exchange-correlation term for weakly inhomogeneous system, the deviation of single particle density from its homogeneous value is small. This is called as **Local density approximation** (LDA). The exchange-correlation energy in this approximation is:

$$E_{xc}[n] = \int n(\mathbf{r})\epsilon_{xc}[n(\mathbf{r})]d^3\mathbf{r} \tag{2.7}$$

Considering the spin of the particle, this approximation is called as local spin density approximation (LSDA) and is given by:

$$E_{xc}[n_\uparrow, n_\downarrow] = \int n(\mathbf{r})\epsilon_{xc}[n_\uparrow(\mathbf{r}), n_\downarrow(\mathbf{r})]d^3\mathbf{r} \tag{2.8}$$

LDA is very successful to calculate cohesive properties as well as for band structure calculations. But it is not a good approximation for strongly correlated systems.

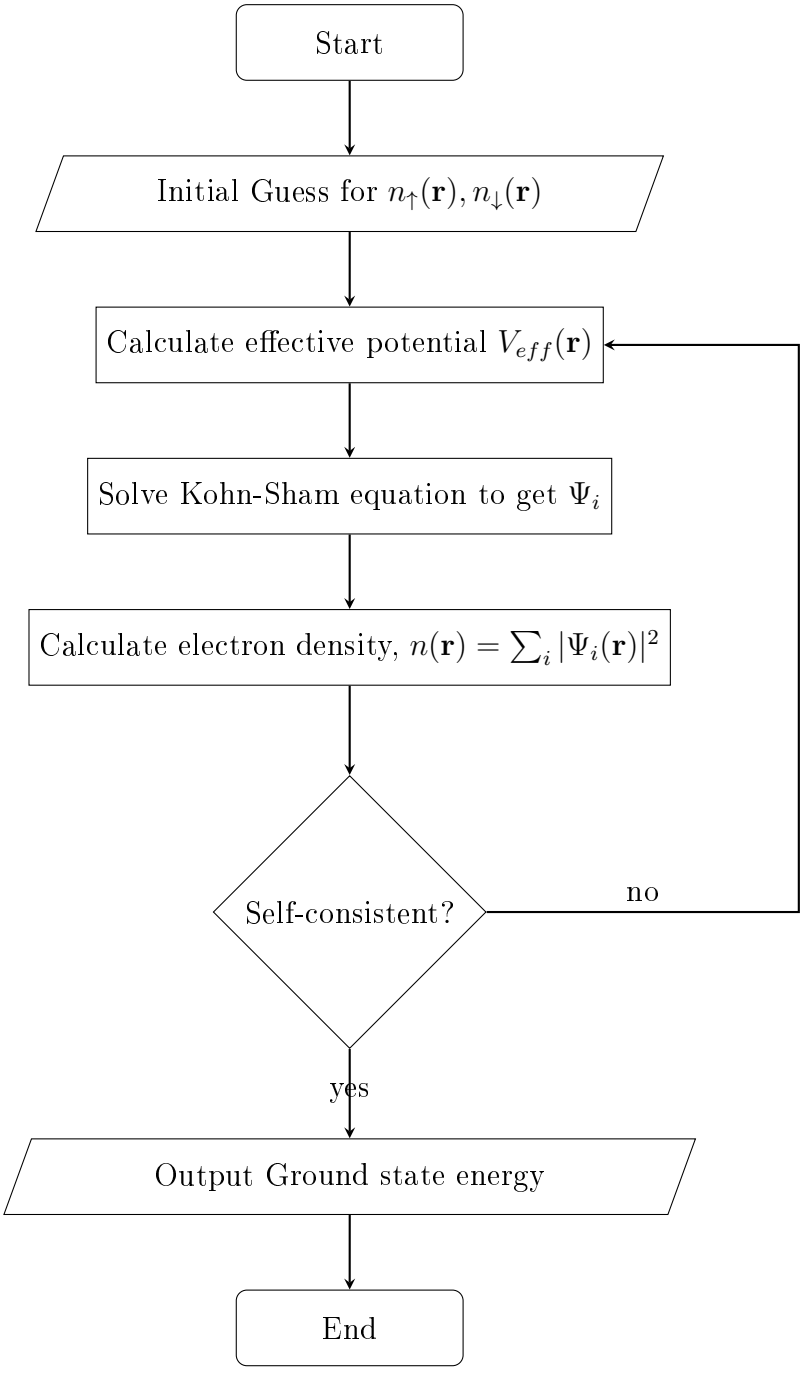

Figure 2.1: Flow Chart showing Solution of Kohn-Sham Equation.

2.2 First Principle Methods for Periodic Potential

First principle or 'Ab-initio' methods do not include experimental data to calculate the electronic structure using Schroedinger's equation within a set of approximations. There are many first principle methods used for band structure calculation. We discuss briefly various methods and in detail TB-LMTO method which is used for our calculations in the next section.

Wigner and Seitz have proposed cellular method [141–143] to calculate the energy level in valence band of sodium metal. In this method, the Schroedinger's equation is solved by replacing the periodic potential within the Wigner-Seitz cell with spherically symmetric potential. They have also considered the polyhedron type primitive cell as a sphere such that the potential at the boundary is also spherical. It gives spherically symmetric cellular wave functions and energies. The problem in this method is that it gives discontinuous derivative at the boundary, whereas in actual case the potential in interstitial region is flat. This problem was removed using muffin-tin potential, in which potential is spherically symmetric in core atomic region with radius r_0 and constant elsewhere (figure 2.2). The muffin-tin potential is:

$$\begin{aligned} U(\mathbf{r}) &= V(|\mathbf{r}-\mathbf{R}|), \quad \text{when } |\mathbf{r}-\mathbf{R}| < r_0 \quad \text{(core region)} \\ &= V(r_0) = V_0, \quad \text{when } |\mathbf{r}-\mathbf{R}| > r_0 \quad \text{(interstitial region)} \end{aligned} \tag{2.9}$$

To calculate band structure in muffin-tin potential, augmented plane wave (APW) or Korringa, Kohn and Rostoker (KKR) methods are used. APW method was given by Slater [144]. It is a full potential method. In this method, the interstitial region is defined by plane wave:

$$\phi_{\mathbf{k},\epsilon} = e^{i\mathbf{k}.\mathbf{r}} \tag{2.10}$$

It is continuous and rapidly oscillatory in core region. At the boundary of atomic and interstitial region, the derivative is discontinuous. In KKR method [145, 146],

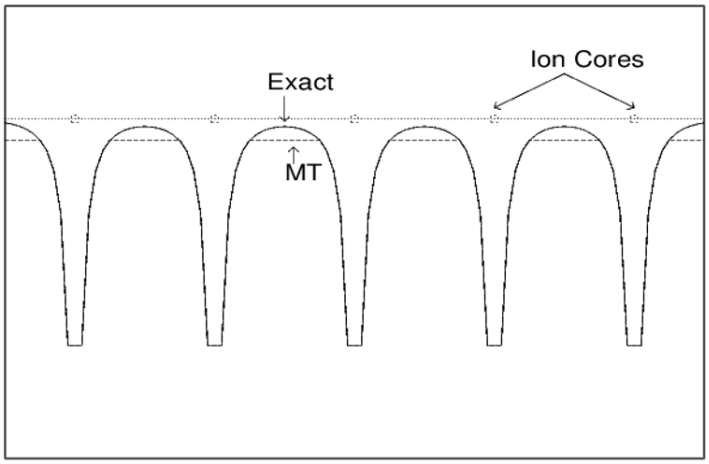

Figure 2.2: Muffin-tin Potential.

the potential is considered as spherically symmetric in atomic region and constant in space between them. In this type, though the potential is spherical in core region, but unlike Wigner-Seitz cellular method, the actual polyhedron shape is considered [146].

Orthogonalized planewave (OPW) method given by Herring [147] deals with plane wave in the interstitial region. This method is not based on muffin-tin potential. The plane waves are orthogonal to core regions so that the oscillatory behavior in these regions can be maintained. The orthogonalized plane wave is [141]:

$$\phi_{\mathbf{k}} = e^{i\mathbf{k}.\mathbf{r}} + \sum_{c} b_c \Psi^c_{\mathbf{k}}(\mathbf{r}) \tag{2.11}$$

Here $\sum_c$ is sum over all core level with Bloch vector $\mathbf{k}$. It reduces actual electron periodic potential to an effectively nearly free electron calculation.

In pseudopotential method, the effect of core region is neglected. When molecules are formed, valence electrons plays significant role and the effect of core electrons are negligible. Hence the Coulomb potential and core region are replaced with an effective pseudopotential and the valence electron wave function with pseudo-wavefunction. The pseudo-wavefunction vary smoothly in core region.

2.3 Tight-binding Linear Muffin Tin Orbital Method

In tight binding approximation, the electronic wave function is given by linear combination of localized atomic orbitals centered at each atomic site. The tight-binding one-electron hamiltonian is:

$$H = -\nabla^2 + \sum_R V_R(\mathbf{r} - \mathbf{R}) \tag{2.12}$$

where the effective potential is replaced by $V_R(\mathbf{r} - \mathbf{R})$ centered at sites R. For a spherically symmetric potential $V_{\mathbf{R}}$, the Schroedinger's equation is [137]:

$$\left[-\nabla^2 + V_R(r)\right] \phi_{Rl} Y_L(\hat{\mathbf{r}}) = \epsilon_{Rl} \phi_{Rl} Y_L(\hat{\mathbf{r}}) \tag{2.13}$$

$$\left[-\nabla^2 + V_R(r) - E\right] \psi(\mathbf{r}) = 0 \tag{2.14}$$

Here L represents angular momentum indices (l, m), $\phi_{Rl}(r)$ are radial amplitude and $Y_L(\hat{\mathbf{r}})$ are spherical harmonics. ϵ_{Rl} is the free atomic energies for an atom having potential $V_R(r)$. Using muffin-tin potential given by equations 2.9, the solution of the above Schroedinger's equation is divided into two parts. First one is the radial part of the solution which is for the inside part of the muffin-tin sphere. The other part is the solution in the interstitial region between the muffin-tin spheres. This part depends on the structure constant. These structure constants contain information about the position of muffin-tin spheres.

According to atomic sphere approximation (ASA), the Wigner-Seitz spheres centered at nuclei have spherical potentials at the center and it neglects electronic kinetic energy at the interstitial region. That is the atomic spheres do not overlap with each other. And this problem is similar to muffin-tin spheres with an interstitial region in between. Since the electronic kinetic energy is neglected, the wave function satisfy Laplace equation in the interstitial region. The spherical potential in the core

region is defined as $V_R(\mathbf{r}-\mathbf{R}) = V_R(r_R)$ where $r_R \leq s_R$. s_R is the radius of the R-th sphere. ASA is reasonable when an infinite collection of atomic spheres are considered.

In the absence of any atomic sphere, the Laplace equation is valid in whole region. Since Laplace equation is independent of the rotation of coordinate systems, its solution can be given by $\Psi(\mathbf{r}) = a_l(r)Y_L(\hat{\mathbf{r}})$ where $\hat{r} = \mathbf{r}/r$ is unit vector parallel to $\mathbf{r}$ and $L = (l, m)$ is the angular momentum index, l and m are orbital and magnetic quantum numbers. $Y_L(\hat{\mathbf{r}})$ is spherical harmonic and $a_l(r)$ is radial amplitude. The differential equation for radial amplitude is [137]:

$$\left[-\frac{\partial^2}{\partial r^2} - \frac{2}{r}\frac{\partial}{\partial r} + \frac{l(l+1)}{r^2}\right] a_l(r) \;=\; 0 \tag{2.15}$$

The above equation have both regular $J_L(\mathbf{r})$ and irregular $K_L(\mathbf{r})$ solutions of the original Laplace equation. These solutions are:

$$J_L(\mathbf{r}) = J_l(r), \qquad J_l(r) = \frac{1}{2(2l+1)}\left(\frac{r}{w}\right)^l \tag{2.16}$$

$$K_L(\mathbf{r}) = K_l(r), \qquad K_l(r) = \left(\frac{w}{r}\right)^{l+1} \tag{2.17}$$

The quantity w makes these functions dimensionless. $Y_L(\hat{\mathbf{r}})$ satisfy orthonormality condition. These two solutions are related to each other in terms of canonical structure constant.

$$K_L(\mathbf{r}_\mathbf{R}) \;=\; -\sum_{L'} S_{RL,R'L'} J_{L'}(\mathbf{r}_{\mathbf{R}'}) \tag{2.18}$$

$$\text{where, } S_{R'L',R''L''} \;=\; \sum_L (-1)^{l''+1} \frac{8\pi(2l-1)!!C_{LL'L''}}{(2l'-1)!!(2l''-1)!!} K_L(\mathbf{R}''-\mathbf{R}') \tag{2.19}$$

Here $l = l' + l''$. $S_{R'L',R''L''}$ are the canonical structure constant and $C_{LL'L''}$ is Gaunt coefficient. Canonical structure constants are symmetric in nature and

they obey inverse power law. In order to get a smooth matching of a function with linear combination of other functions, for a system having several atomic spheres, the Wronskian is considered. The Wronskian for $J_l(r)$ and $K_l(r)$ is:

$$\{J_l(r), K_l(r)\} \;=\; -\frac{w}{2} \tag{2.20}$$

Hence the matching condition at the sphere boundary $r = s_R$ for radial amplitude, $\phi_{Rl}(r, E)$, with the linear combination of $J_l(r)$ and $K_l(r)$ is:

$$\phi_{Rl}(r, E) \rightarrow \frac{2}{w}\left[\{\phi_{Rl}(r, E), J_l(r)\}|_{r=s_R} K_l(r) - \{\phi_{Rl}(r, E), K_l(r)\}|_{r=s_R} J_l(r)\right] \tag{2.21}$$

And a potential function $P_{Rl}(E)$ in terms of two Wronskian and the normalization function $N_{Rl}(E)$ are:

$$\begin{aligned} P_{Rl}(E) =& \frac{\{K_l(r), \phi_{Rl}(r, E)\}}{\{J_l(r), \phi_{Rl}(r, E)\}}|_{r=s_R} = 2(2l+1)\left(\frac{w}{s_R}\right)^{2l+1} \frac{D_{Rl}(E) + l + 1}{D_{Rl}(E) - l} \\ N_{Rl}(E) =& \frac{w}{2}\frac{1}{\{\phi_{Rl}(r, E), J_l(r)\}}|_{r=s_R} = (2l+1)\left(\frac{w}{s_R}\right)^{l+1} \frac{1}{\phi_{Rl}(s_R, E)} \frac{1}{l - D_{Rl}(E)} \end{aligned} \tag{2.22}$$

Here $D_{Rl}(E)$ represents logarithmic derivative. The matching condition now reduces to,in terms of the above two functions:

$$N_{Rl}(E)\phi_{Rl}(r, E) \;\rightarrow\; K_l(r) - P_{Rl}(E)J_l(r) \tag{2.23}$$

Returning to original muffin-tin potential with several atomic spheres, we consider a linear superposition

$$\psi(\mathbf{r}) = \sum_{RL} a_{RL}\Psi_{RL}(\mathbf{r}, E) \tag{2.24}$$

$\Psi_{RL}(\mathbf{r}, E)$ are called muffin-tin orbitals and given by:

$$\begin{aligned}\Psi_{RL}(\mathbf{r},E) = &\quad N_{Rl}(E)\phi_{Rl}(\mathbf{r_R},E) + P_{Rl}(E)J_L(\mathbf{r_R}) \qquad \text{for} \quad r_R \leq s_R, \\ = &\quad K_L(\mathbf{r_R}) \qquad\qquad\qquad\qquad\qquad\qquad\quad \text{for} \quad r_R \geq s_R\end{aligned} \tag{2.25}$$

The muffin-tin orbitals are the smooth function in the whole space, and it satisfies Laplace equation outside muffin-tin sphere and the boundary conditions are well defined at infinitesimal distant point. When the function $K_L(\mathbf{r_R})$ is defined in the whole space, the muffin-tin orbitals inside and outside the muffin-tin sphere are called as the head and tail of the orbital. But Schroedinger's equation is not satisfied inside the sphere. To find the condition that $\psi(\mathbf{r})$ (equation 2.24) satisfy the Schroedinger's equation inside the atomic sphere, we rewrite equation 2.25 in terms of its tail orbitals ($K_L(\mathbf{r_R})$) for the points inside another atomic sphere into the function $J_{L'}(\mathbf{r_{R'}})$:

$$\begin{aligned}\Psi_{RL}(\mathbf{r},E) &= N_{Rl}(E)\phi_{Rl}(\mathbf{r_R},E) + P_{Rl}(E)J_L(\mathbf{r_R}), \qquad r_R \leq s_R, \\ &= -\sum_{L'} S_{RL,R'L'}J_{L'}(\mathbf{r_R}), \qquad\qquad r_{R'} \leq s_{R'}(\mathbf{R'} \neq \mathbf{R}) \\ &= K_L(\mathbf{r_R}), \qquad\qquad\qquad\qquad \mathbf{r} \in I\end{aligned} \tag{2.26}$$

Substituting equation 2.26 into equation 2.24, $\psi(r)$ satisfy the Schroedinger's equation provided the coefficient of $J_{L'}(\mathbf{r_{R'}})$ vanish. This leads to so-called **tail cancellation of muffin-tin orbitals**:

$$\sum_{RL} a_{RL}[P_{Rl}(E)\delta_{RL,R'L'} - S_{RL,R'L'}] = 0 \tag{2.27}$$

Non-trivial solution of a_{RL} exist if the secular determinant vanishes:

$$det[P_{Rl}(E)\delta_{RL,R'L'} - S_{RL,R'L'}] = 0 \tag{2.28}$$

This equation is called KKR-ASA secular equation and it divides the eigenvalue problem into two parts, that is, the potential function and the structural constant.

The potential function tells about individual atomic properties and the structural constant which are energy independent tells about the position of atomic spheres. But these potential parameters are non-linear in energy dependence. Therefore the secular equation cannot be reduced to standard matrix eigenvalue equation. It is necessary to linearize these potential parameters using variational principle. The linearisation of the KKR-ASA secular equation means the energy linearisation of the radial amplitude in the neighborhood of some energy $E = E_{\nu,Rl}$ taken along the centre of occupied valence density of states. Therefore using energy linearisation, the secular equation is:

$$det[E\delta_{RR',LL'} - H^{orth}_{RR',LL'}] = 0 \tag{2.29}$$

such that the orthogonal LMTO hamiltonian is:

$$\begin{aligned} H^{orth} &= E_\nu - (\{K,\Phi\} - \{J,\Phi\}S)\,(\{K,\dot{\Phi}\} - \{J,\dot{\Phi}\}S)^{-1} \\ &= C + \sqrt{\Delta}S(1-\gamma S)^{-1}\sqrt{\Delta} \end{aligned} \tag{2.30}$$

Here, S is the structure matrix. C, Δ and γ are the diagonal matrices corresponding to potential parameters C_{Rl}, Δ_{Rl} and γ_{Rl}. The potential parameter C_{Rl} correspond to the centre, Δ_{Rl} to width and γ_{Rl} to the distortion of a pure that is unhybridized $Rl-$th band. The concept of these potential parameters depend on the concept of canonical bands. In terms of Wronskian the potential parameters are defined by:

$$\begin{aligned} C_{Rl} &= E_{\nu,Rl} - \frac{\{K,\Phi\}_{Rl}}{\{K,\dot{\Phi}\}_{Rl}} \\ \Delta_{Rl} &= \frac{w}{2}\frac{1}{\{K,\dot{\Phi}\}^2_{Rl}} \\ \gamma_{Rl} &= \frac{\{J,\dot{\Phi}\}_{Rl}}{\{K,\dot{\Phi}\}_{Rl}} \end{aligned} \tag{2.31}$$

Chapter 3

Augmented Space Formalism

Prior to Augmented space formalism (ASF), the theories which were mostly applied to study binary disordered alloys were virtual crystal approximation (VCA) and coherent potential approximation (CPA). These are mean field theories. In VCA, the potential at each lattice site is replaced by an average potential. This approximation does not consider any scattering caused by random potential fluctuations about the average. The approximation is applicable only if the random variation of the diagonal terms is very small. CPA was introduced by Soven [148]. He modeled a substitutional alloy based on the concept of an effective or coherent potential. The coherent potential placed at every site of the lattice and stimulate the electronic properties of the actual alloy. The coherent potentials are complex energy dependent quantity which describes the average effect of the medium. CPA is a single-site mean field approximation so it cannot deal with multi-site properties like off-diagonal disorder, short range ordering, effects of random clustering in impurity bands and the effects of extended defects [149]. Extended effects involve correlated random fluctuations from more than one site. But the generalization of the CPA for multi site problems is difficult. Therefore a general configuration averaging method is developed. This is called augmented space formalism.

3.1 Configuration Averaging

Why there is a need of configuration averaging? Let us consider an example of an experimenter carrying out energy resolved photo-emission studies on a disordered metallic alloy to find the density of states of the valence electrons. He keeps the energy window of the excited outgoing electrons narrow and varies the frequency of the incident photon. If he carries out the experiment on ten different samples of the same alloy, he should obtain slightly different result. The alloy is random and different samples will give different results but the variation is well within the experimental error bar. Here he actually observes the physical property with the average over different realizable configurations of atomic arrangement in a single sample, that is, he observes the configuration averaged result. These measured properties are global to the system. In quantum mechanics and statistical physics, it is very common to deal with the averages of all possible states. In statistical physics, if different possible states of a canonical ensemble are occupied with Boltzmann probabilities, then at finite temperature the observable physical properties are the average over the ensemble. Similarly, in quantum mechanics, the observable physical system is the average over different possible states with probabilities given by the squared amplitude of the wave function projection onto these states. And configuration averaging is meaningless for local properties. Consider a macroscopically large system made up of subsystems such that each subsystem resembles the configuration of the system. Using the idea of spatial ergodicity, in the limit of the size and number of subsystems of a macroscopically large system, the subsystems of a single sample exactly replicate all its possible configurations. A global property which averages over the subsystems becomes the same as the average over all configurations. Configuration averaging is very relevant for study of disordered systems. In a binary alloy, atomic position are occupied by two different atoms, A and B, randomly with certain probability. Therefore, there can be large number of occupational configuration. ASF indeed takes care of each configuration to find out the average property

unlike in VCA and CPA.

3.2 Augmented Space Formalism

To visualize the configuration space [149] of a set of random variables, let us consider the Ising model which consists of spins $\{\sigma_R\}$ arranged on a discrete lattice labelled by R. Each spin σ_R can have two possible states or configurations which is denoted by $|\uparrow_R\rangle$ and $|\downarrow_R\rangle$. The collection of all linear combinations of these two states, that is, $\{|\uparrow_R\rangle + |\uparrow_R\rangle\}$, $\{|\uparrow_R\rangle + |\downarrow_R\rangle\}$, $\{|\downarrow_R\rangle + |\uparrow_R\rangle\}$ and $\{|\downarrow_R\rangle + |\downarrow_R\rangle\}$ is called the configuration space of σ_R. In general, the configuration space is given by $\{a|\uparrow_R\rangle + b|\downarrow_R\rangle\}$. Here it has 2^2 configurations. But for a set of N spins, the number of possible configurations are 2^N. For this N spins each of 2^N configurations can be written as a sequence of m up-states and $N-m$ down-states. The number $N-m$ is called the cardinality of the configuration and the sequence is called the cardinality sequence of the configuration space. For example, for a particular configuration of 5 spins $|\uparrow_1\downarrow_2\downarrow_3\uparrow_4\downarrow_5\rangle$, the cardinality sequence is $\{2, 3, 5\}$. Cardinality sequence is the unique way for labelling the configuration of a system. The rank of configuration space Φ is 2^N in this case and is given by the direct product of the configuration spaces of the individual spins, that is:

$$\Phi = \prod_R \otimes \phi_R \tag{3.1}$$

For the spins that can have more than 2 states, that is, $n > 2$, the set of N spins can have n^N configurations. Now instead of σ_R consider the random variable ε_R of the Anderson model such that ε_R are independently distributed. The configuration space of this Anderson model is isomorphic to the collection of Ising spins. The probability density $p(\varepsilon_R)$ for the distribution of random variable ε_R is a positive definite function. The density of states corresponding to the hamiltonian H is also a positive definite function and is related to H as:

$$n(\varepsilon) = -\frac{1}{\pi}\Im\langle\psi|((\varepsilon_R + i0)I - H)^{-1}|\psi\rangle \tag{3.2}$$

$$= -\frac{1}{\pi}\Im G(\varepsilon_R + i0) \tag{3.3}$$

Since $p(\varepsilon_R)$ is a positive definite function like density of states, therefore one can construct an operator M_R in configuration space similar to H in Hilbert space such that $p(\varepsilon_R)$ can be written as [149–151]:

$$p(\varepsilon_R) = -\frac{1}{\pi}\,\Im\langle\phi|((\varepsilon_R + i0)I - M_R)^{-1}|\phi\rangle \tag{3.4}$$

$$= \Im g(\varepsilon_R + i0) \tag{3.5}$$

The operator M_R in the configuration space is associated with the random variable ε_R. If ε_R is a binary distribution having values 0 and 1 with probabilities x and $y = 1 - x$, then M is:

$$M = \begin{pmatrix} x & \sqrt{xy} \\ \sqrt{xy} & y \end{pmatrix} \tag{3.6}$$

The average of a well-behaved function $f(\varepsilon_R)$ of ε_R is defined as:

$$\langle\langle f(\varepsilon_R)\rangle\rangle = \int f(\varepsilon_R)p(\varepsilon_R))d\varepsilon_R \tag{3.7}$$

In terms of $g(z)$, this reduces to:

$$\Rightarrow \langle\langle f(\varepsilon_R)\rangle\rangle = \oint f(z)g(z)dz \tag{3.8}$$

The integral is taken over closed contour enclosing the singularities of $g(z)$ but not any of $f(z)$. Here $f(z)$ is well-behaved, that is, it has no singularities in the neighborhood of a singularity of $g(z)$. If the function $g(z)$ is expanded in the basis

of its eigenstates $\{|\mu\rangle\}$ of M_i with a spectral density function $\rho(\mu)$ of M_i the above equation reduces to:

$$\langle\langle f(\varepsilon_R)\rangle\rangle = \int d\rho(\mu)\langle\phi|\mu\rangle \left[\oint f(z)(z-\mu)^{-1}\right] \langle\mu|\phi\rangle \tag{3.9}$$

$$= \langle\phi| \left[\int d\rho(\mu)|\mu\rangle f(\mu)\langle\mu|\right] |\phi\rangle \tag{3.10}$$

$$= \langle\phi|f(M_R)|\phi\rangle \tag{3.11}$$

The second line requires the function to be well behaved at infinity. $f(M_R)$ is the same functional of M_R as $f(\varepsilon_R)$ of ε_R, that is, if $f(\varepsilon_R)$ is ε_R^2 then $f(M_R)$ is M_R^2. This generalization of the above equation to the averages of functions of the set of random variables is:

$$\langle\langle f(\{\varepsilon_R\})\rangle\rangle = \langle\phi|\tilde{f}(\{\tilde{M}_R\})|\phi\rangle \tag{3.12}$$

All operators in the full configuration space is denoted by the tilde variables. The operator $\tilde{M}_R$ is:

$$\tilde{M}_R = I \otimes I \otimes \cdots \otimes M_R \otimes I \otimes \cdots \tag{3.13}$$

This is augmented space theorem [149–151]. Hence the configuration average of the Green's function is:

$$\langle\langle G_{RR}(z)\rangle\rangle = \langle R\otimes\phi|(z\tilde{I} - \tilde{H}(\{\tilde{M}_R\}))^{-1}|R\otimes\phi\rangle \tag{3.14}$$

Here
$$\tilde{H} = \sum_R \mathcal{P}_R \otimes \tilde{M}_R + \sum_R \sum_{R'} V_{RR'}\mathcal{T}_{RR'} \otimes \tilde{I} \tag{3.15}$$

In this hamiltonian the original random variables are replaced by the corresponding configuration space operators found from their probability distributions. This augmented hamiltonian is an operator in the augmented space $\Psi = \mathcal{H} \otimes \Phi$ where $\mathcal{H}$ is the space spanned by the tight binding basis and ϕ is the full configuration space. The augmented hamiltonian has no randomness in it. And the result is exact.

3.3 Recursion Method

A new orbital basis set $\{u_1, u_2 ..., u_n, ...\}$ is generated from the original orbital basis of the hamiltonian using the following recurrence relation [1, 152]:

$$Hu_n = a_n u_n + b_{n+1} u_{n+1} + b_n u_{n-1} \tag{3.16}$$

The initial orbital u_0 is chosen to be any orbital of the original basis. Here $u_{-1} = 0$. The advantage of this new basis set is that the hamiltonian in this basis takes a tridiagonal form. The resolvent G is then found to be as a continued fraction which can easily be evaluated. The elements of this tridiagonal hamiltonian are the recursive parameters a's and b's. $\{a_n\}$ are the real numbers and $\{b_n\}$ are the positive numbers. The first recursion orbital is u_0 and it is normalized to unity. Other states are projected on this first orbital. When the hamiltonian is operated on the first orbital, the result is the linear combination of u_0 and u_1 given by:

$$Hu_0 = a_0 u_0 + b_1 u_1 \tag{3.17}$$

The orthogonalization of Hu_0 to u_0 gives the first recursive parameter a_0:

$$a_0 = u_0^\dagger S H u_0 \tag{3.18}$$

Here S is the overlap matrix element in the old basis. $u_0^\dagger$ is the column vector of elements which are complex conjugates of the elements of u_0. Normalizing u_1 we get:

$$b_1 = \left[(Hu_0 - a_0 u_0)^\dagger S (Hu_0 - a_0 u_0)\right]^{1/2} \tag{3.19}$$

This gives the first b value. Using first a and b values, we can get the next recursive orbital, that is,

$$u_1 = \frac{(Hu_0 - a_0u_0)}{b_1} \tag{3.20}$$

b_1 is the matrix element of the hamiltonian between u_0 and u_1. In this way, starting from a single orbital, all successive orbitals can be calculated. In general:

$$\begin{aligned} a_n =& u_n^\dagger SHu_n \\ b_{n+1} =& \left[(Hu_n - a_nu_n - b_nu_{n-1})^\dagger S(Hu_n - a_nu_n - b_nu_{n-1})\right]^{1/2} \end{aligned} \tag{3.21}$$

and

$$u_{n+1} = \frac{(Hu_n - a_nu_n - b_nu_{n-1})}{b_{n+1}} \tag{3.22}$$

The tridiagonal matrix is symmetric and hence the recurrence relation is also symmetric. From the a's and b's, the projected resolvent ($R_0(E)$) is [153]:

$$R_0(E) = \cfrac{1}{(E-a_0) - \cfrac{b_1^2}{(E-a_1) - \cfrac{b_2^2}{(E-a_2) - ...}}} \tag{3.23}$$

And the partial density of states is:

$$n(u_0; E) = \lim_{\epsilon \to 0^+} -\frac{1}{\pi}\Im R_0(E + i\epsilon) \tag{3.24}$$

Since the new recursive orbital depends on the previous orbital, so the error in the recursion calculation multiplies, that is, grow exponentially. But this does not affect the accuracy of the recurrence relation [1]. Recursion method is an effective tool to study the localization properties.

3.4 Augmented Space in TB-LMTO Basis

To study the first principle properties of random system, the augmented space hamiltonian is written within TB-LMTO basis. The localized tight binding hamiltonian derived from LMTO-ASA theory is written for substitutionally disordered random binary alloys as [149]:

$$\begin{aligned} H^{\alpha}_{RL,R'L'} &= \hat{C}_{RL}\delta_{RR'}\delta_{LL'} + \hat{\triangle}^{1/2}_{RL} S^{\alpha}_{RL,R'L'} \hat{\triangle}^{1/2}_{R'L'} \\ \hat{C}_{RL} &= C^{A}_{RL} n_R + C^{B}_{RL}(1-n_R) \\ \hat{\triangle}^{1/2}_{RL} &= (\triangle^{A}_{RL})^{1/2} n_R + (\triangle^{B}_{RL})^{1/2}(1-n_R) \end{aligned}$$

Here R is the lattice sites and $L = (lm)$ are the orbitals indices. For transition metal $l < 2$. C^{A}_{RL}, C^{B}_{RL}, $\triangle^{A}_{RL}$ and $\triangle^{B}_{RL}$ are the potential parameters of the constituents A and B of the alloy. n_R are the local site occupation variables which randomly takes value 1 and 0 according to whether the site is occupied by an A atom or not. Now replacing the local site occupation variable $\{n_R\}$ by $\{\tilde{M}_R\}$, we get the augmented hamiltonian:

$$\begin{aligned} \tilde{H} = & \sum_{RL} \left(C^{B}_{RL}\tilde{I} + \delta C_{RL}\tilde{M}_R \right) \otimes a^{\dagger}_R a_R + \cdots \\ & + \sum_{RL}\sum_{R'L'} \left(\triangle^{B}_{RL}\tilde{I} + \delta\triangle_{RL}\tilde{M}_R \right) S^{\alpha}_{RL,R'L'} \left(\triangle^{B}_{R'L'}\tilde{I} + \delta\triangle_{R'L'}\tilde{M}_{R'} \right) \otimes a^{\dagger}_R a_R \end{aligned} \tag{3.25}$$

where

$$\delta C_{RL} = \left(C^{A}_{RL} - C^{B}_{RL} \right) \tag{3.26}$$

$$\delta\triangle_{RL} = \left((\triangle^{A}_{RL})^{1/2} - (\triangle^{B}_{RL})^{1/2} \right) \tag{3.27}$$

$\tilde{I}$ is the identity operator in the augmented space. $\tilde{M}^R$ in the second quantized notation [154] is:

$$\tilde{M}^R = x b^\dagger_{R0} b_{R0} + (1-x) b^\dagger_{R1} b_{R1} + \sqrt{x(1-x)} \left(b^\dagger_{R0} b_{R1} + b^\dagger_{R1} b_{R0} \right) \quad (3.28)$$

$(b^\dagger_{R0}, b_{R0})$ and $(b^\dagger_{R1}, b_{R1})$ are the creation and annihilation operators in the augmented space, where each site is characterized by two states (0,1), which may be identified with the up and down states of an Ising system. The augmented hamiltonian is an operator in the augmented space $\Phi = \mathcal{H} \otimes \prod \phi^R$, where $\mathcal{H}$ is the Hilbert space spanned by the countable basis set $\{|r\rangle\}$. The operators used in the augmented hamiltonian are:

(a) $a^\dagger_R a_{R'}$ with $R = R'$ and $R \neq R'$ are the operators acting on a vector in the augmented space change only the real space label but keeps the configuration part unchanged.

(b) $a^\dagger_R a_{R'} b^\dagger_{k\lambda} b_{k\mu}$ with $R = R'$ and $R \neq R'$ are the operators acting on an augmented space vector may change real space label (if $R \neq R'$)and may also change configuration at site R or R' (if $\lambda \neq \mu$). k is R or R'. λ and μ takes values only 0 and 1. This resembles a single-spin-flip Ising operator in configuration space.

(c) $a^\dagger_R a_{R'} b^\dagger_{R\lambda} b_{R\mu} b^\dagger_{R'\nu} b_{R'\xi}$, with λ, μ, ν, ξ taking values 0 and 1, are the operators that may change the real-space label (if $R \neq R'$), as well as the configuration either at R or R' or both. This resembles a double-spin-flip Ising operator in the configuration space.

In configuration space, the operations (a) to (c) change the cardinality and cardinality sequence. In the Hilbert space, the basis $|m\rangle$ is given by a column vector with zero everywhere except at the m^{th} position such that the inner product are:

$$\begin{aligned} \langle m|n\rangle &= C^T_m C_n \\ a^\dagger_m a_n C_p &= \delta_{np} C_m \end{aligned} \quad (3.29)$$

The basis in $\prod^{\otimes} \phi_R$ has the form $|f^1_{\lambda_1} \otimes f^1_{\lambda_1} \otimes ...\rangle$ such that each λ_i may be either 0 or 1. In ASF, the number 1 define the cardinality of the basis and the cardinality sequence is given by $\{S_C\}$. Thus the binary sequence is given by $B[C, \{S_C\}]$. This is a member of the basis in the configuration space. The dot product between the basis members is:

$$B[C, \{S_C\}] \odot B[C', \{S_{C'}\}] \quad = \quad \delta_{CC'} \delta_{\{S_C S_{C'}\}} \tag{3.30}$$

Applying recursion on the augmented hamiltonian (equation 3.25) the resolvent which is in continued fraction form is configuration averaged Green's function and is given by:

$$\langle\langle G_{RL,RL}(z) \rangle\rangle \quad = \quad \cfrac{1}{z - a_0 - \cfrac{b_1^2}{z - a_1 - \cfrac{b_2^2}{\ddots \cfrac{b_N^2}{z - a_N - b_{N+1}^2 T(z)}}}} \tag{3.31}$$

Here $T(z)$ is the terminator used to estimate the asymptotic part of the continued fraction. In our case, the system is infinite. The terminator must be determined from a set of initial coefficients such that the continued fraction approach is convergent. This asymptotic part determines the essential singularities of the Green's function such as band edges (e_{min} and e_{max}) and band weights (w). Band edges are first crudely determined from few initial continued fraction coefficients. It is further refined by how they are converging when few more coefficients are included. The terminator is so determined from band edges and band weights that the Green's function satisfy the herglotz properties [149].

Luchini and Nex [149, 155] proposed a method of joining the terminator coefficients to the first few exactly calculated coefficient. According to their method:

$$\hat{a}_n = \begin{cases} a_n, & n < n_1 \\ 1/2\{(1-\sin\{\delta(n+\phi)\}a_n) + (1+\sin\{\delta(n+\phi)\}\hat{a}_n)\}, & n_1 < n < n_2 \\ \hat{a}_n, & n_2 < n \end{cases}$$

$$\hat{b}_n = \begin{cases} b_n, & n < n_1 \\ 1/2\{(1-\sin\{\delta(n+\phi)\}b_n) + (1+\sin\{\delta(n+\phi)\}\hat{b}_n)\}, & n_1 < n < n_2 \\ \hat{b}_n, & n_2 < n \end{cases}$$

Here $\delta = \pi/(n_2 - n_1)$ and $\phi = -(n_1+n_2)/2$. Two sets of recursion equations are used to calculate the terminator. In one type, two sets of orthogonal polynomials are obtained, given by:

$$\begin{aligned} P_{n+1}(z) =& (z-a_n)P_n(z) - b_n^2 P_{n-1}(z) \\ Q_{n+1}(z) =& (z-a_n)Q_n(z) - b_n^2 Q_{n-1}(z) \end{aligned} \tag{3.32}$$

such that, $P_1(z) = 0 = Q_0$ and $P_0 = 1 = Q_{-1}$. The second recursive relation used to find the set of coefficient $\{\gamma_n, \delta_n\}$ starting from the state $|0\rangle = F(z)$, where $F(z)$ is herglotz function given by:

$$F(z) \;=\; 8w\left[z - \frac{e_{max}+e_{min}}{2} - \sqrt{(z-e_{min})(z-e_{max})}\right]/(e_{max}-e_{min})^2 \tag{3.33}$$

This recursive relation is:

$$|n+1\rangle \;=\; (z-\gamma_n)|n\rangle - \delta_n^2|n-1\rangle \tag{3.34}$$

with the inner product defined by $\langle f|g\rangle = \sum_i w_i f(\alpha_i)g(\alpha_i)$ with

$$\begin{aligned} w_i =& \frac{\pi w}{n+1}\sin^2 v_i \\ \alpha_i =& a_i + (1-\cos v_i)(e_{max}-e_{min})/2 \\ v_i =& \frac{i\pi}{n+1} \end{aligned} \tag{3.35}$$

Using these continued fraction coefficients, the two orthogonal polynomials are:

$$\begin{aligned} R_{n+1}(z) =& (z-\gamma_n)R_n(z) - \delta_n^2 R_{n-1}(z) \\ S_{n+1}(z) =& (z-\gamma_n)S_n(z) - \delta_n^2 S_{n-1}(z) \end{aligned} \tag{3.36}$$

Using these polynomials, the terminator ($T(z)$) and hence the Green's function ($G(z)$) is:

$$T(z) = \frac{S_{n_2-2}(z) - F(z)R_{n_2-1}(z)}{\delta_{n_2-1}^2[S_{n_2-3}(z) - F(z)R_{n_2-2}(z)]} \tag{3.37}$$

$$G(z) = \frac{Q_{n_2-2}(z) - b_{n_2-1}^2 T(z) Q_{n_2-3}(z)}{P_{n_2-1}(z) - b_{n_2}^2 T(z) P_{n_2-2}(z)} \tag{3.38}$$

When a single atom is added to a large but finite system, it shifts all the eigenvalues of the system. This arbitrary small perturbation leads to non-convergence of Green's function. This can infinitely change the Green's function near its corresponding poles. Hence the convergence of ASR is very important. Most physical quantities are averages over the spectrum of the type.

$$F(E) = \int_{-\infty}^{E} f(E')n(E')dE'$$

The convergence of the recursion depends upon the convergence of these physical quantities. For example, the Fermi energy is defined by:

$$\int_{-\infty}^{E_F} n(E')dE' = n_e$$

here n_e is the total number of electrons, and the band energy is:

$$U = \int_{-\infty}^{E_F} E'n(E')dE'$$

Then study is for the convergence of the indefinite integrals of the kind

$$M_k(E) = \int_{-\infty}^{E} (E')^k n(E')dE'$$

$(E')^k$ is monotonic and well behaved within the integration range.

In the recursion method, the errors can arise due to a finite number of recursion steps and the termination of the continued fraction using one of the available terminator; a large but finite cluster in real space; and a finite subspace of the configuration space.

3.5 Transition to Smooth Surfaces

ASF can also be applied to cases where surface roughness is negligible, that is, almost smooth surfaces. One would have thought, given the way we modeled the roughness of surfaces, that if we simply let the concentration of the empty spheres go to zero and we would recover the smooth surfaces. However, that is not the case. As the concentration of the empty sphere decreases, these 'impurities' become more and more isolated and form highly spikey impurity states. The coherent potential approximation for example fails in this composition range and do not adequately reproduce the impurity structures in the density of states. Originally it was also thought that the ASF too misses out these structures. However, careful analysis of the "terminator" or the asymptotic behaviour of the continued fraction, indicated that this reproduces impurity peaks quite accurately. We have to incorporate not only the singularities at the band edges, but also those lying on the compact spectrum of H. Viswanath and Müller [156,157] has proposed a terminator:

$$T(z) = \frac{2\pi(E_m)^{(p+2q+1)/2}}{B\left(\frac{p+1}{2}, 1+q\right)} |z - E_0|^p \{(z - E_1)(E_2 - z)\}^q \tag{3.39}$$

The spectral bounds are at E_1, E_2 with square-root singularities, $E_m^2 = E_1 E_2$ and there is a cusp singularity at E_0 if $p = 1, q = 1$ or infra-red divergence if $p = -1/2, q = 0$. E_0 sits on the compact spectrum of H. Magnus [158] has cited a closed form of the convergent continued fraction coefficients of the terminator :

$$\begin{aligned} \beta_{2n}^2 &= E_m^2 \frac{4n(n+q)}{(4n+2q+p-1)(4n+2q+p+1)} \\ \beta_{2n+1}^2 &= E_m^2 \frac{(2n+2p+1)(2n+2q+p+1)}{(4n+2q+p+1)(4n+2q+p+3)} \end{aligned} \tag{3.40}$$

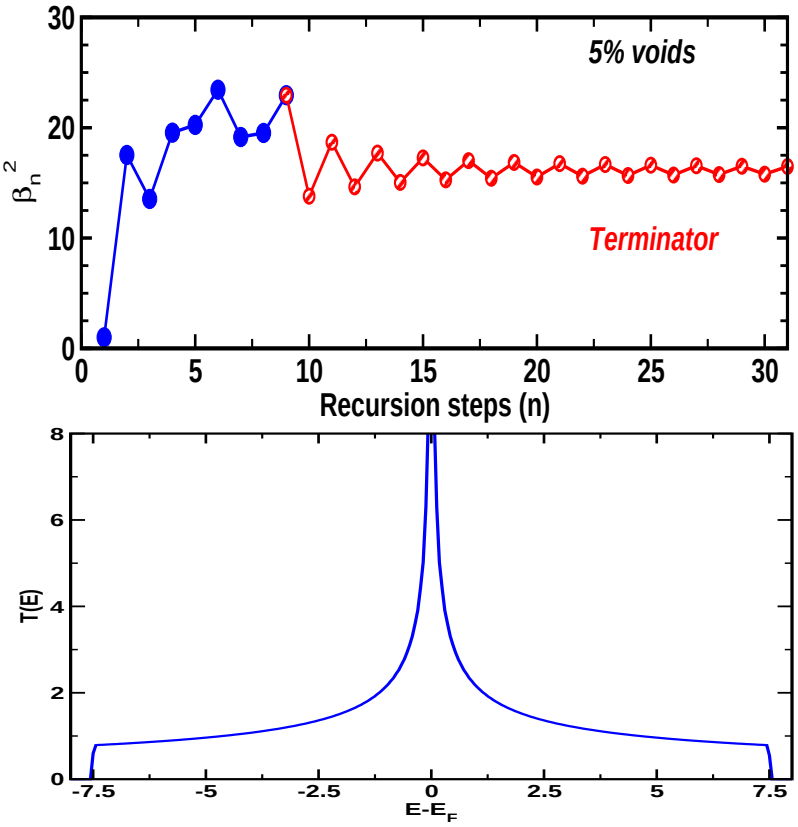

Figure 3.1: (Top) Recursion coefficients β_n^2 from the recursive calculations (blue) and terminator (red) smoothly enmeshed. (Bottom) Density of states with a peak at the origin.

The parameters of the terminator are estimated from the asymptotic part of the continued fraction coefficients calculated from our recursion. The Viswanath-Müller terminator [156, 157] is appropriate for infra-red divergences and seamlessly enmeshed with the calculated coefficients as shown in Figure 3.1.

Chapter 4

Transition Metals Surfaces

In this chapter we discuss electronic and magnetic properties of (001) surfaces of bcc Fe(001), fcc Co(001) and fcc Ni(001). We consider few atomic layers for a surface. We choose twelve layers in total and considered two more layers with empty spheres which contain charge but no atoms above surface layer. These empty spheres take care of the charge leakage into the vacuum. The potential parameters are generated from TB-LMTO within local spin density approximation (LSDA) using Barth and Hedin exchange correlation potential [159]. Wave equations are solved by the scalar-relativistic calculations. Atoms at top most layer are more weekly bound than atoms at inner atomic layers. The lattice relaxation for top most layer in these three systems is carried out by minimum energy principle. The lattice relaxation for bcc Fe(001) is found at 5%. Similarly the lattice relaxation for fcc Co(001) and Ni(001) are respectively found to be 16% and 9%. With these relaxed lattice constants potential parameters are generated for the top most layer. The TB-LMTO potential parameters for rest of the layer are generated using bulk lattice parameter [160].

As discussed in the introduction, the surface roughness is not only created on the top most layer but there are some amount of roughness in the subsurface layers.

Hence surface cannot be defined with a single atomic layer. In order to deal with such realistic situation, we roughen top four layers with different amount of roughness. As we go down from the top layer, roughness of these four layers decreases from 20% to 5%. We also consider different amount of roughness of the top most layer only and compare the results for these two types of rough surfaces considered.

We show ASF can also be extended to smooth surfaces. The smooth surface is not achieved by simply putting the concentration of the empty spheres to zero. However, as the concentration of the empty sphere decreases, these 'impurities' become more and more isolated. The smooth surface properties are obtained using a suitable terminator as discussed in previous chapter. Our results for smooth surface agree with earlier reported theoretical studies which proves ASF can be used for smooth surface calculation. To carry out such smooth surface calculations, we choose nine layers of bcc Fe(001), fcc Co(001) and fcc Ni(001) with two layers of empty spheres above surface. In this case also the potential parameters for top most layer are generated considering the lattice relaxation as in the case of rough surface. We use eight shell augmented space calculation and nine steps of recursion.

We also generate potential parameters for the top most layer without relaxing the lattice parameter in the case of Fe(001). Lattice parameter of the top most layer is expected to be more than other layers due to loose bonding. This situation can be modeled by creating regular voids in bcc Fe so that bonding is weaker. Therefore we remove body centered atom in bcc lattice which reduces number of bonds. This way we generate the potential parameters for bcc Fe with missing body centered atom. But the results with relaxed lattice parameter gives better results than this. Therefore we consider relaxation procedure for all other systems.

4.1 Effect of Roughness on Surface Properties of Fe(001), Co(001) and Ni(001)

Figures 4.1, 4.2 and 4.3 show layerwise spin resolved DOS for top five layers as well as for bulk layers for Fe(001), Co(001) and Ni(001) respectively. In these systems, the amount of roughness decreases from 20% to 0% with a difference of 5% as we go down from the top most layer. In the case of smooth surfaces the width of the density of states (DOS) of the top most surface layer (S) is narrower as compared to the bulk [11, 17], which gradually increases in the inner layers to approach bulk DOS. This trend changes when different layers are roughened with different amount of roughness. These figures show that width of DOS increases substantially at S-1 layer and then reaches to the bulk values very slowly. Though width of DOS from S-2 layer onwards changes slowly, but there are significant changes in structure of DOS. This is due to variation in roughness. The width of DOS of the top most surface layer (S) is narrower as compared to the bulk which is expected. DOS attain the bulk value at the S-9^{th} layer down the top most layer in the case of Fe(001) whereas at the S-8^{th} layer in case of Co(001) and Ni(001).

These figures show variation in spin resolved DOS. We note that down spin electrons contribute significantly to DOS at the Fermi level at the layers S & S-1 in the case of Fe(001) (figure 4.1). This trend is changed at the S-2 level where both up and down spins have significant contributions indicating that this layer is less magnetic. It is other way round at S-3 layer where up has significant contribution and down is negligible. In the case of Co(001) (figure 4.2) contributions of spin-down to the DOS at the Fermi level is significant compared to spin-up at all the layers. This is also true in the case of Ni(001) (figure 4.3) except at S-1 layer where both have significant contributions. This means S-1 layer of Ni is almost non-magnetic at Fermi level. The appearance of new peaks in DOS, with change in roughness correspond to disorderedness.

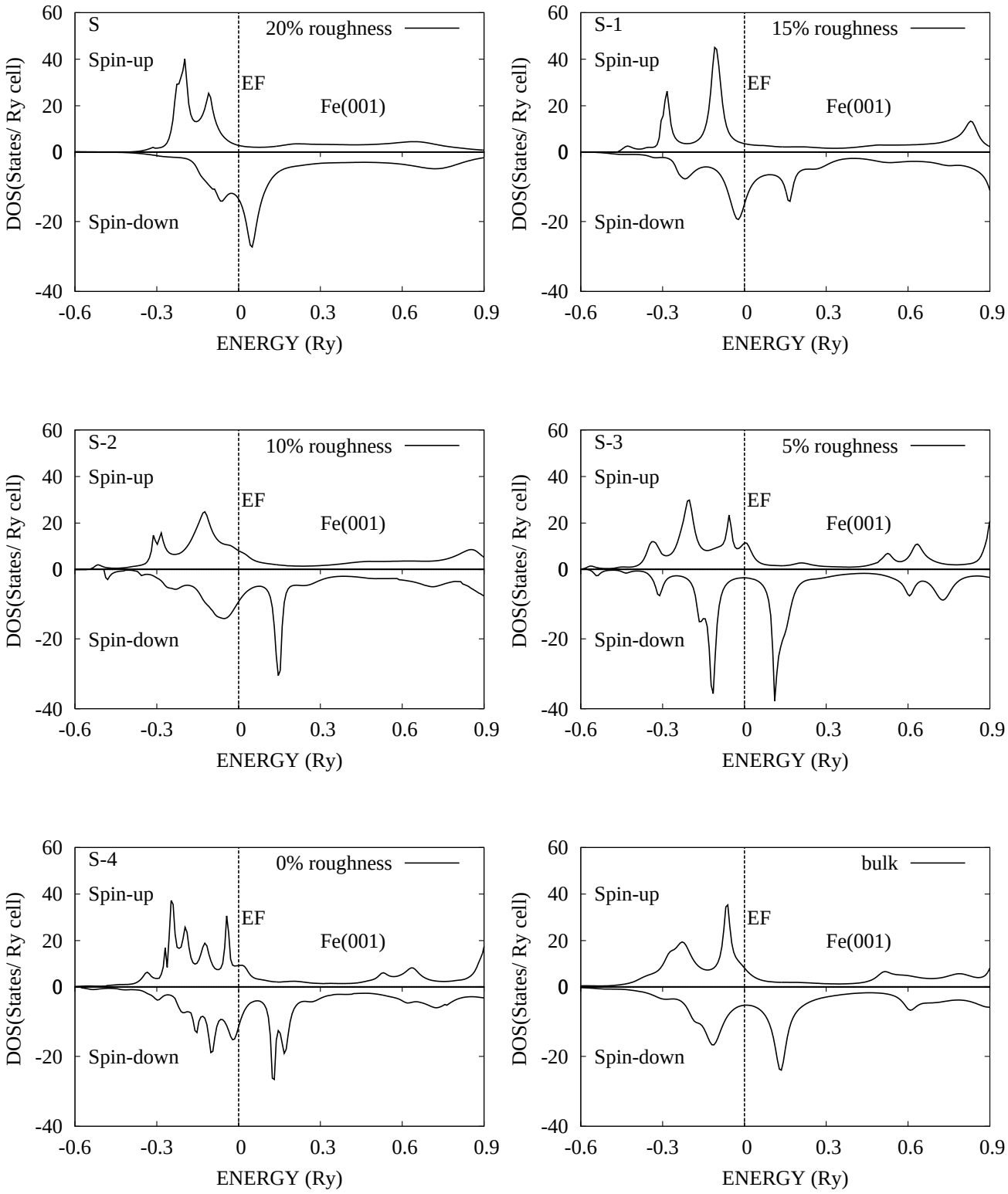

Figure 4.1: Comparison of layer based spin resolved DOS with different amount of roughness in top four layers of Fe(001). Fermi energy is reset at zero.

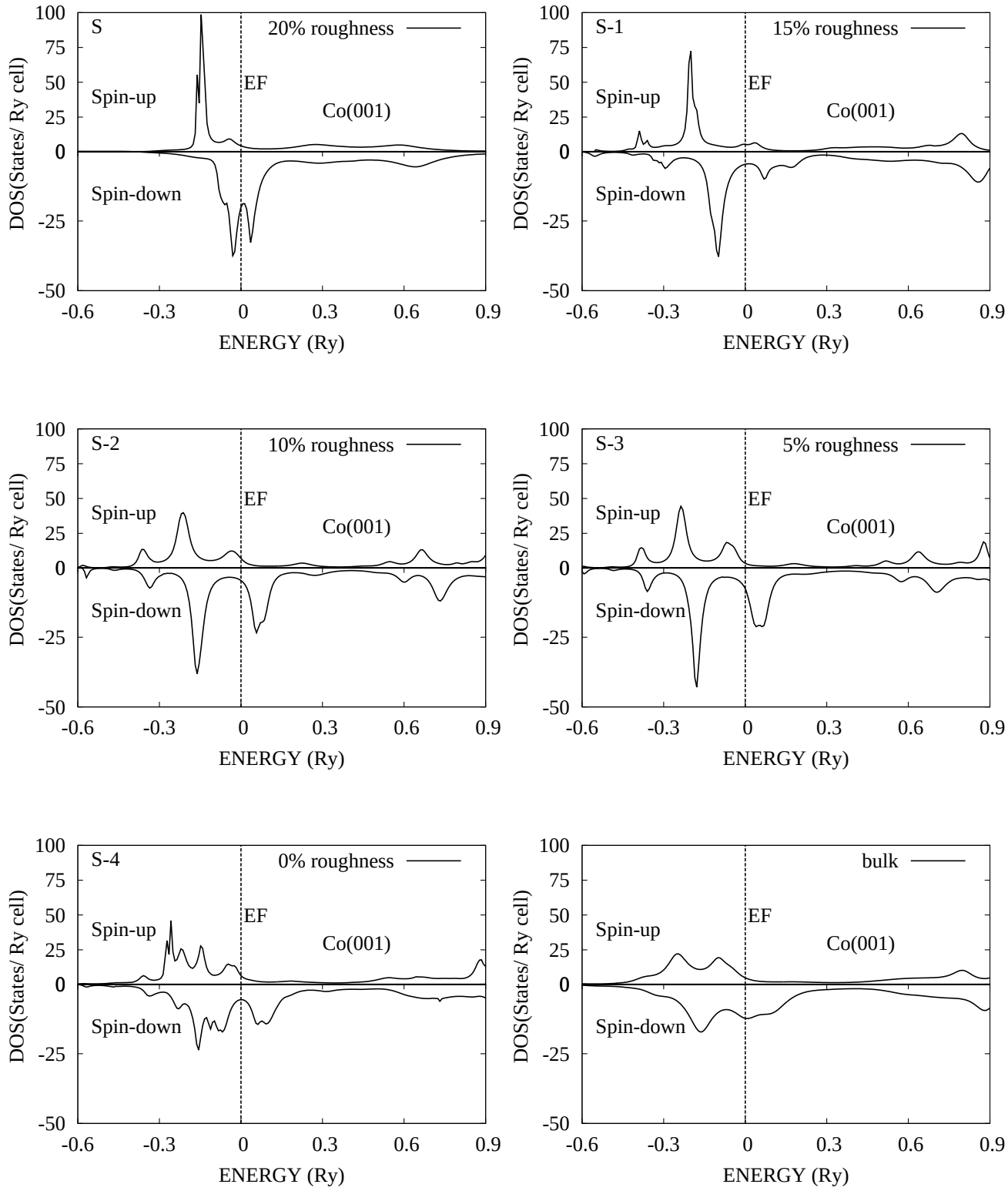

Figure 4.2: Comparison of layer based spin resolved DOS with different amount of roughness in top four layers of Co(001). Fermi energy is reset at zero.

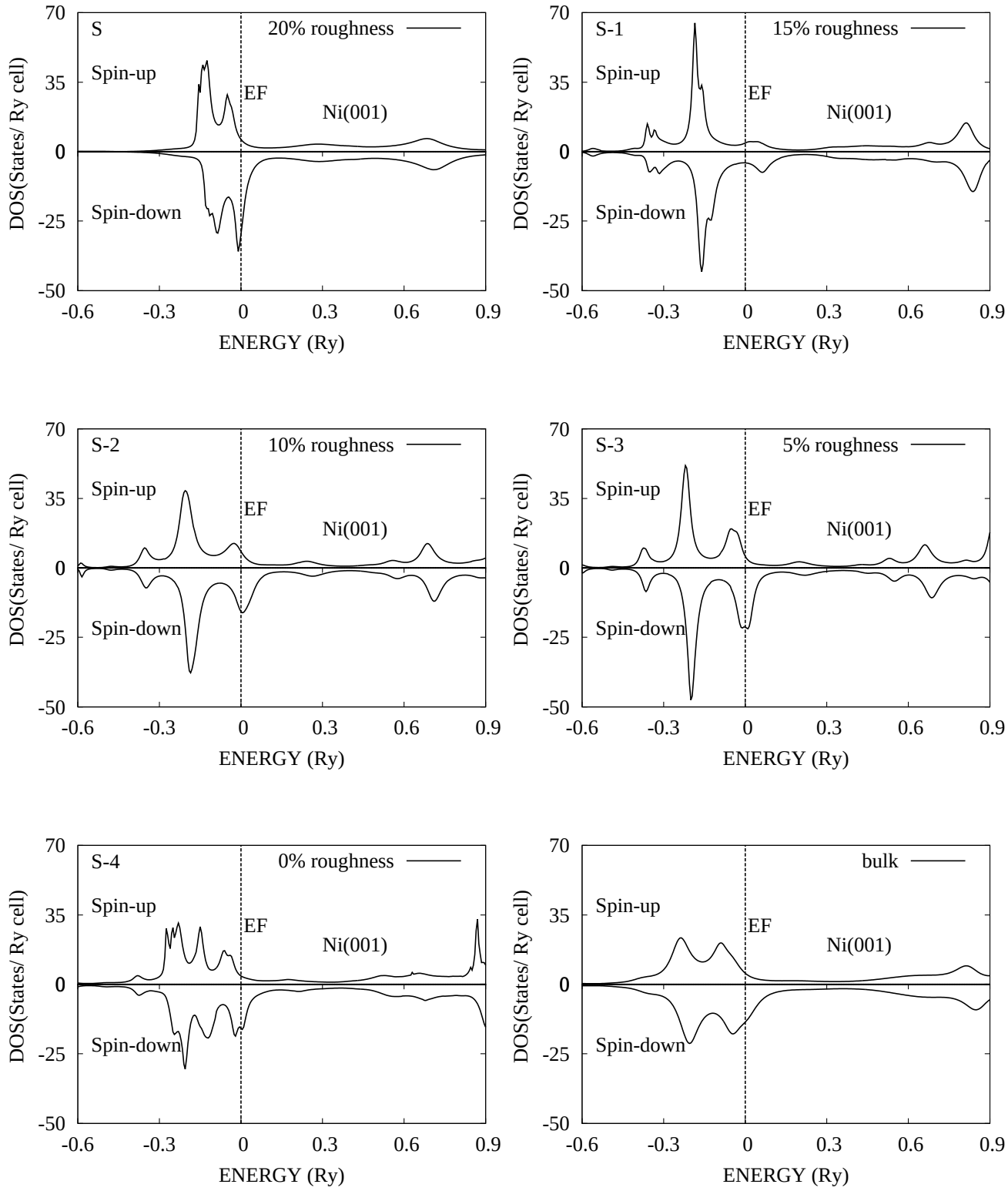

Figure 4.3: Comparison of layer based spin resolved DOS with different amount of roughness in top four layers of Ni(001). Fermi energy is reset at zero.

Table 4.1: Fermi energies and Work Functions.

Properties	Four layered rough surface			Smooth surface		
	Fe(001)	Co(001)	Ni(001)	Fe(001)	Co(001)	Ni(001)
Fermi Energy (Ry)	-0.07	-0.06	-0.08	-0.07	-0.06	-0.08
Work Function (eV)	4.15	5.42	4.79	4.15	5.33	4.79

Table 4.2: Layered based and bulk (B) orbital resolved magnetic moment in μ_B/atom for the three systems with different amount of roughness on top four layers.

Layers	Roughness (%)	Fe(001)				Co(001)				Ni(001)			
		s	p	d	Total	s	p	d	Total	s	p	d	Total
S	20	-0.06	0.03	2.82	2.79	-0.01	0.03	2.30	2.32	0.0	0.0	0.63	0.63
S-1	15	-0.05	-0.03	2.15	2.07	-0.07	-0.01	1.20	1.12	-0.02	0.0	0.43	0.41
S-2	10	-0.02	-0.03	1.89	1.84	-0.02	-0.04	1.82	1.76	-0.01	-0.01	0.64	0.62
S-3	5	-0.02	-0.05	2.13	2.06	-0.01	-0.05	1.97	1.91	-0.01	-0.02	0.74	0.71
S-4	0	-0.01	0.00	2.02	2.01	0.04	-0.06	1.72	1.70	0.01	-0.02	0.36	0.35
S-5	0	-0.04	-0.08	2.20	2.08	0.00	-0.06	1.68	1.62	0.00	-0.03	0.46	0.43
S-6	0	-0.02	-0.05	2.29	2.22	0.00	-0.05	1.71	1.66	0.00	-0.02	0.57	0.55
S-7	0	-0.02	-0.06	2.56	2.48	-0.01	-0.06	1.62	1.55	-0.00	-0.02	0.55	0.53
S-8	0	-0.02	-0.06	2.27	2.19	-0.02	-0.06	1.62	1.54	-0.01	-0.02	0.55	0.52
S-9/B	0	-0.02	-0.06	2.25	2.17								

Table 4.1 shows the Fermi energies and work function. The Fermi energy is carried out using TB-LMTO method. There is negligible effect of roughness on work function for the case of Fe and Ni but there is slight change in the case of Co.

Orbital resolved layerwise magnetic moment for all the three systems with different amount of roughness at the top four layers is tabulated in the table 4.2. The topmost layer (S) of Fe(001) & Co(001) has the maximum magnetic moment. Whereas layer S-3 of Ni(001) has maximum magnetic moment. This is indeed true because splitting of spin up and down DOS is maximum at these respective layers

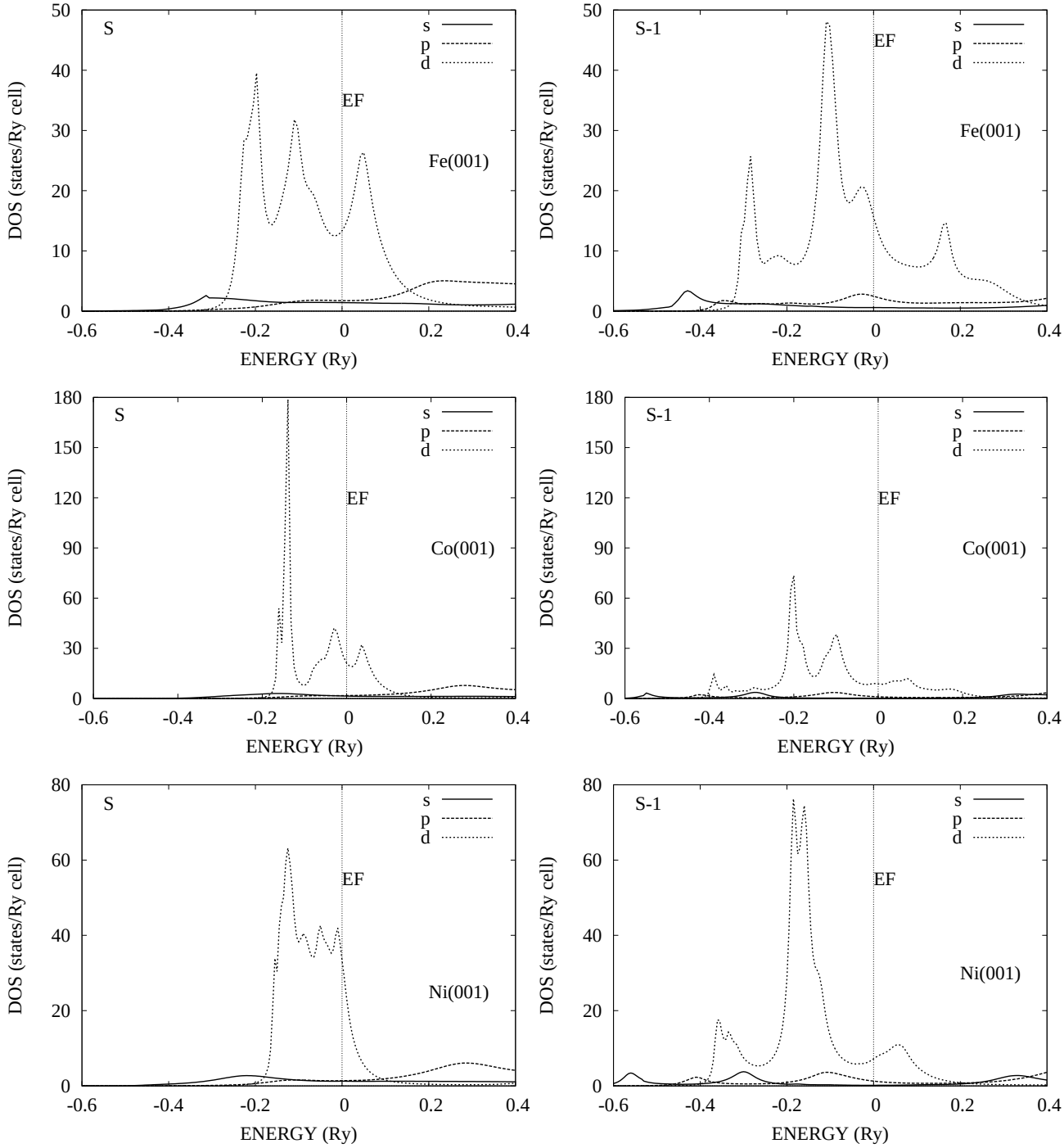

Figure 4.4: Orbital resolved total DOS for surface (S) and sub-surface (S-1) layer of Fe(001), Co(001) and Ni(001). Fermi energy is reset at zero.

as shown in the figures 4.1, 4.2 and 4.3. The bulk magnetic moment is attained at the S-9^{th} layer in the case of bcc Fe(001) whereas it is attained at the S-8^{th} layer in the case fcc Co(001) and fcc Ni(001). The average magnetic moment of the top four layers having different amount of roughness is more than its bulk value for all the three systems. This is expected as surface magnetic moment is enhanced compared to the bulk. The table 4.2 shows d-orbital alone contributes most to the the magnetic moment. Similarly, figure 4.4 shows d-orbital DOS is maximum whereas others are almost negligible. Among the three systems, the most significant change in d-band DOS of the S layer is found in Co(001). Its magnetic moment at the S^{th} layer is almost double than that of S-1 layer. Change in p-band magnetic moment is observed whereas negligible change in s-band in the case of Fe(001). Though the effect of d-band is significant but changes in s- and p-band magnetic moments are also observed in the case of Co(001). A slight change in s- and p-band magnetic moments and significant change in d-band are found in the case of Ni(001).

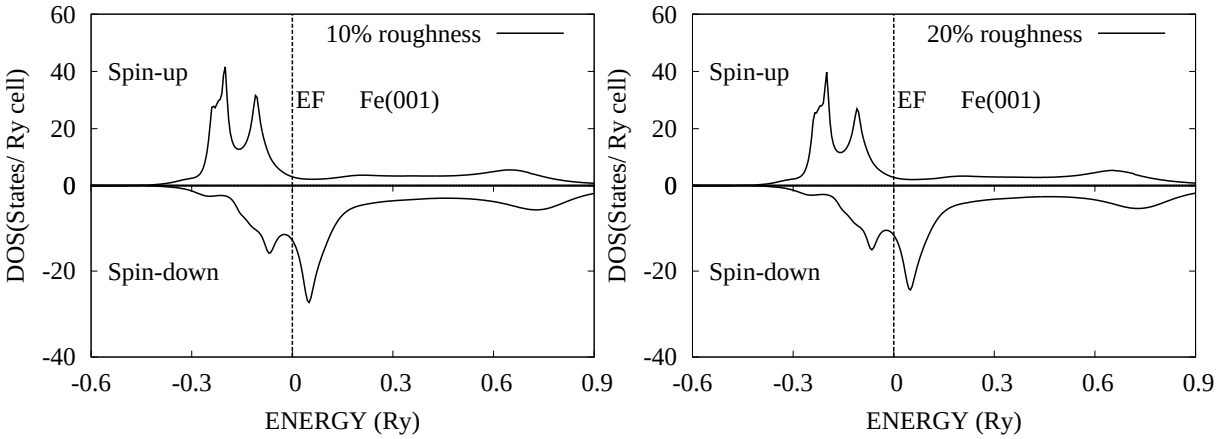

Figure 4.5: DOS of top most layer with different amount of roughness for Fe(001). Fermi energy is reset at zero.

We also roughen the top most layer with different degrees of roughness (with 10% & 20% empty spheres). Figures 4.5, 4.6 and 4.7 show DOS of the top most layer for Fe(001), Co(001) and Ni(001) respectively. It is clear that peaks near the Fermi level, change significantly when roughness is varied in all the three systems.

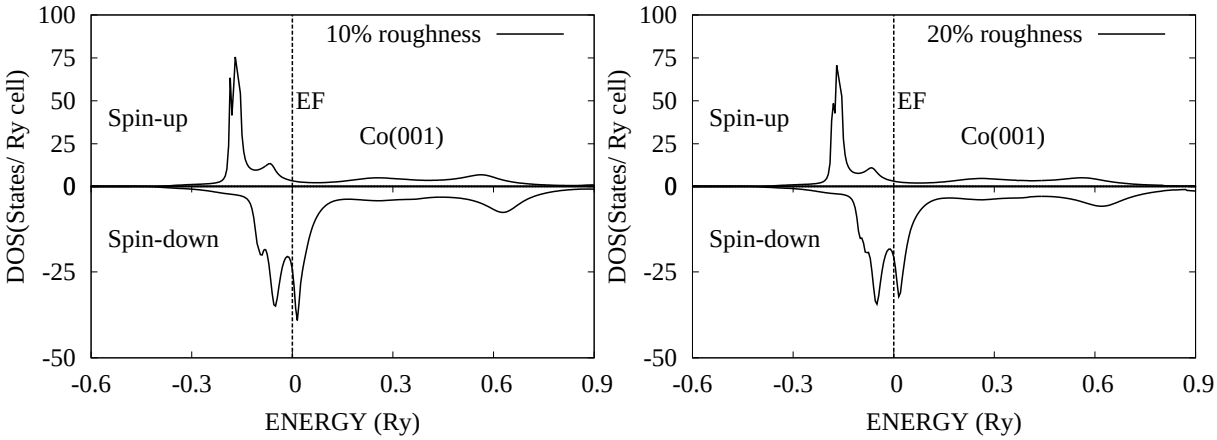

Figure 4.6: DOS of top most layer with different amount of roughness for Co(001). Fermi energy is reset at zero.

Hence electrons near the Fermi level are more affected when roughness is varied. The average magnetic moment, i.e., $M_{avg} = xM_{es} + (1-x)M_{TM}$ is calculated for different amount of roughness. Here, x is the concentration of empty spheres. M_{es} and M_{TM} are the magnetic moment of empty sphere and transition metal atoms (Fe, Co, Ni) respectively. It is found that average magnetic moment decreases for all the systems when roughness is increased. It is observed that work function of the top layer changes slightly when roughness is varied and is almost equivalent to smooth surface case as shown in table 4.1. Table 4.3 shows the layer based magnetic moment with 20% roughness at the top layer. In this case also we observe the magnetic moment of the top most layer is more than all other layers for Fe and Co whereas layer S-3 has maximum magnetic moment for Ni.

Comparison between the DOS for the two cases, i.e., a realistic case when top four layers are roughened (figures 4.1, 4.2 and 4.3) and the other when only the top layer is roughened with 20% (figures 4.5, 4.6 and 4.7) indicates there is minor difference in Fe(001) and Ni(001) DOS. But there is significant difference in the case of Co(001). Similarly comparison of Tables 4.2 and 4.3 show magnetic moments of Co get enhanced significantly for the realistic case than the other.

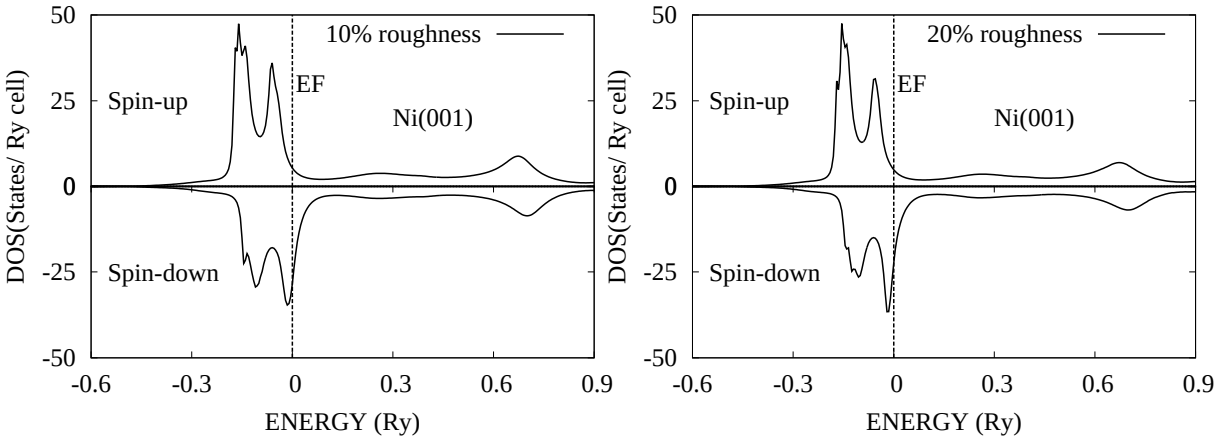

Figure 4.7: DOS of top most layer with different amount of roughness for Ni(001). Fermi energy is reset at zero.

Table 4.3: Layer based orbital resolved magnetic moment with 20% roughness on top most layer in μ_B/atom.

Layers	Fe(001)				Co(001)				Ni(001)			
	s	p	d	Total	s	p	d	Total	s	p	d	Total
S	0.01	0.03	2.81	2.85	-0.01	0.03	1.93	1.95	-0.01	0.0	0.65	0.64
S-1	0.0	0.0	1.27	1.27	0.02	-0.03	0.92	0.91	0.02	-0.01	0.29	0.30
S-2	-0.03	-0.05	1.82	1.74	-0.07	-0.05	1.75	1.63	-0.02	-0.05	0.47	0.40
S-3	-0.03	-0.04	2.33	2.26	-0.02	-0.05	1.74	1.67	0.01	-0.03	0.76	0.74
S-4	-0.03	-0.05	2.64	2.56	-0.01	-0.06	1.65	1.58	0.0	-0.02	0.55	0.53
B	-0.02	-0.06	2.25	2.17	-0.02	-0.06	1.62	1.54	-0.01	-0.02	0.55	0.52

Figures 4.8, 4.9 and table 4.4 are the results of Fe(001) without consideration of lattice relaxation. Figure 4.8 shows spin resolved DOS of the top most Fe(001) layer with various amount of roughness without relaxation of lattice parameter. This figure shows width of DOS increases when roughness is increased. The magnetic moment is 3.10 μ_B/atom for 80% roughness, whereas, it reduces to 2.85μ_B/atom for 20% roughness as shown in table 4.4.

Both table 4.4 and figure 4.9 show the average magnetic moment of the top layer increases as the roughness decreases. Table 4.4 also shows the local magnetic

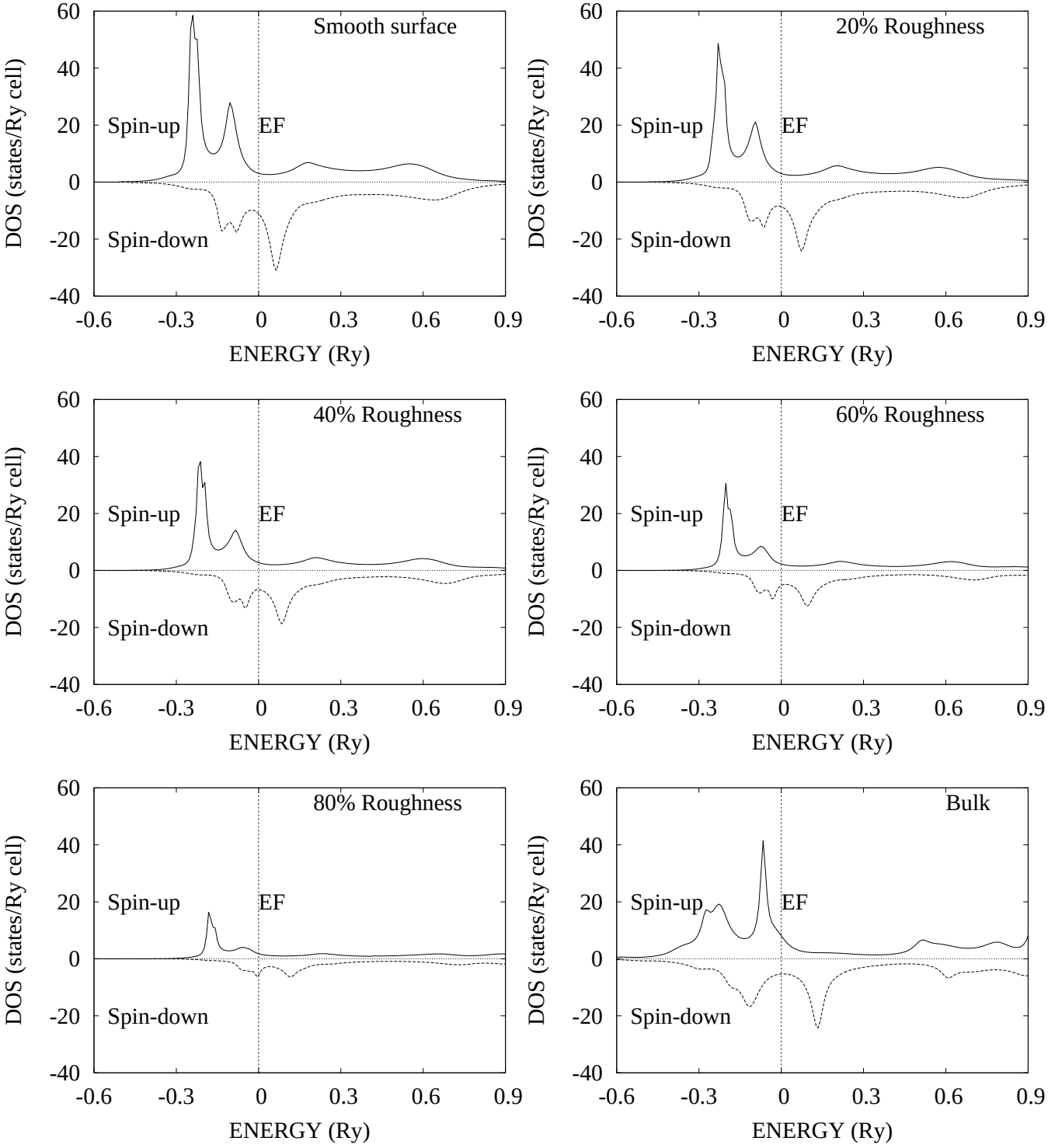

Figure 4.8: Spin up and spin down DOS for smooth surface, surface with different amount of roughness and bulk bcc Fe. Vertical line represents Fermi level.

Table 4.4: Variation of local magnetic moment of Fe in surface layer and average magnetic moment of surface layer with roughness in μ_B/atom

Percentage of roughness	Magnetic moment of Fe	Average Magnetic Moment of surface
80	3.10	0.63
60	2.91	1.17
40	2.86	1.72
20	2.85	2.28
0	2.78	2.78

moment of Fe atom at the top most layer increases with increase in roughness. This is because amount of empty spheres increases when roughness is increased. This reduces coordination number of Fe atom. This reduction in coordination number results in the decrement of interaction among Fe atoms. Therefore when the roughness is more, the surface magnetic moment increases and it approaches to atomic magnetic moment.

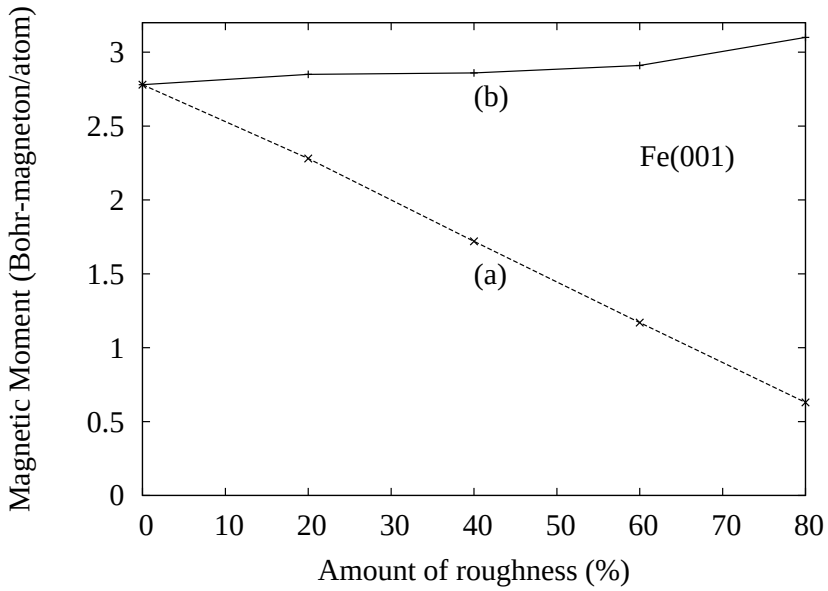

Figure 4.9: Variation of (a) average magnetic moment of the top most layer and (b) magnetic moment of Fe in top most layer with different amount of roughness.

4.2 Surface Properties of almost Smooth Fe, Co and Ni (001) Surfaces

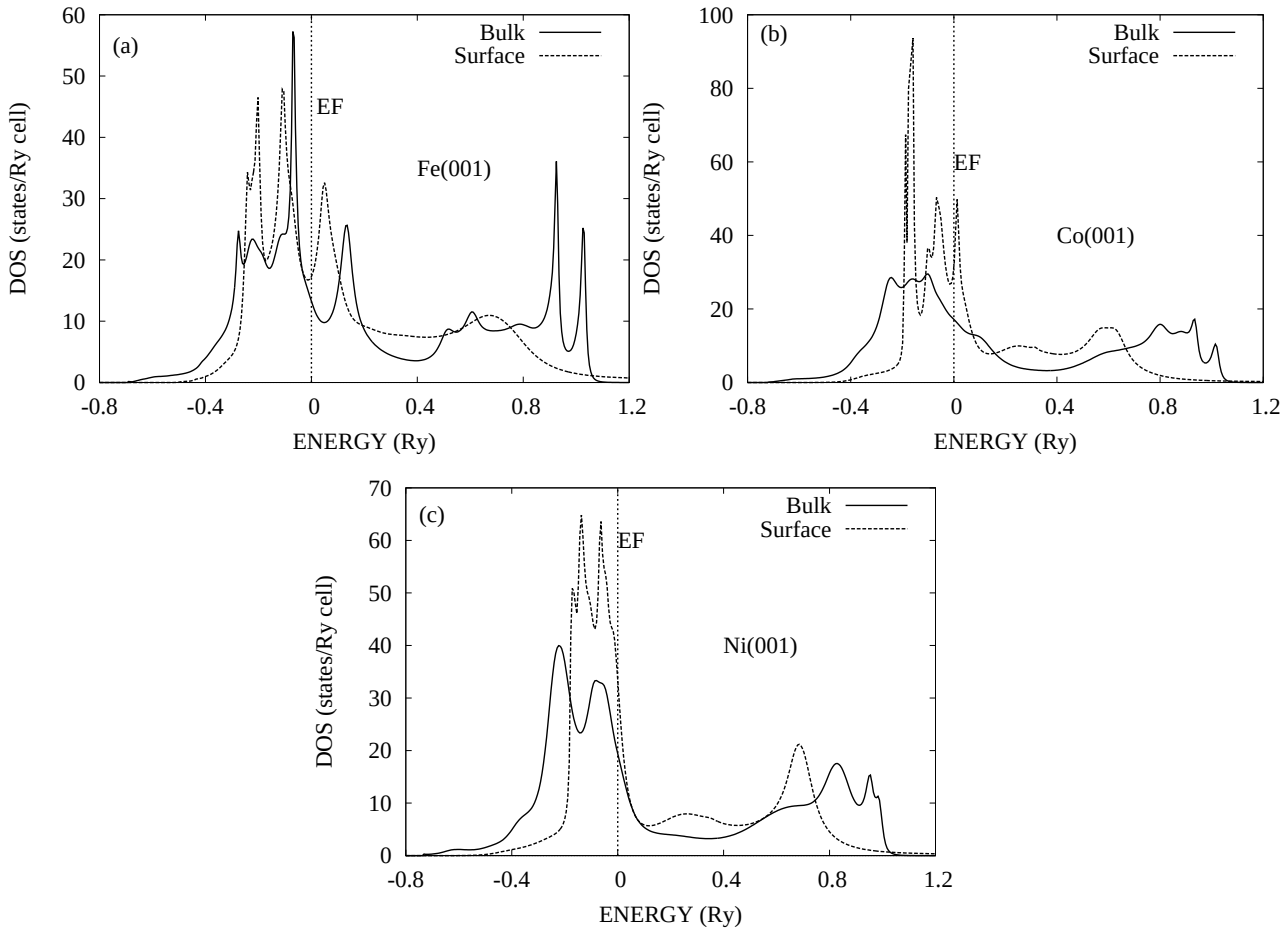

Figure 4.10: Comparison of total density of states for bulk and surface (top most layer). Fermi energy is reset at zero.

We discuss surface properties of almost smooth surfaces. Figure 4.10 shows energy bands of the surface states near Fermi level get narrower compared to bulk. This is due to weakening of interaction by symmetry breaking and reduction in co-ordination number. Similar picture arises in the spin resolved DOS as shown in the Figure 4.11. The spin resolved DOS for surface and bulk bcc Fe matches well with that of LMTO method [7,17], TB-LMTO recursion method [11], FP-LMTO method [43], FPLAPW method [6,12] and LCAO method [20] reported earlier. Apart from narrowing of band there is change in number of spin-up surface states compared to the bulk states at the Fermi level (figure 4.11). The amount of change is maximum

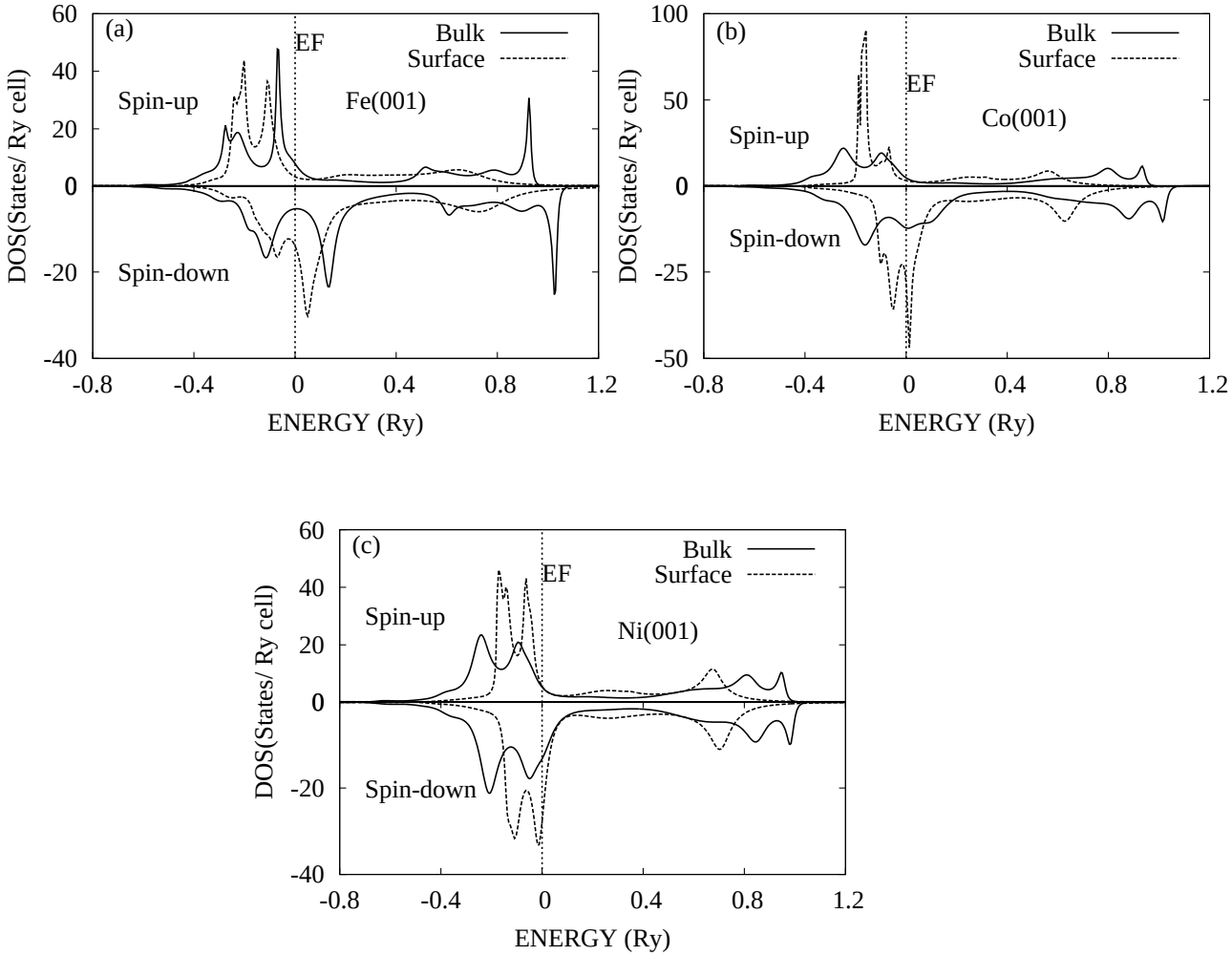

Figure 4.11: Comparison of spin resolved density of states for bulk and surface (top most layer). Fermi energy is reset at zero.

in the case of Fe(001) and negligible in the case of Ni(001). But in all the three cases, there is significant change in the spin-down states (figure 4.11). This shows spin-down states are mainly responsible for the enhancement of magnetic moment at the surface. The splitting of spin-up and spin-down states near Fermi level is maximum for Fe(001) and least for Ni(001). This is expected because magnetic moment of Fe is maximum and it is least for Ni. The magnetic moment is directly related to the amount of splitting in spin up and spin down states. From figure 4.11, it is clear that Ni is a strong ferromagnet because it has large difference between spin-up and spin-down DOS at the Fermi level. The splitting of spin-up and spin-

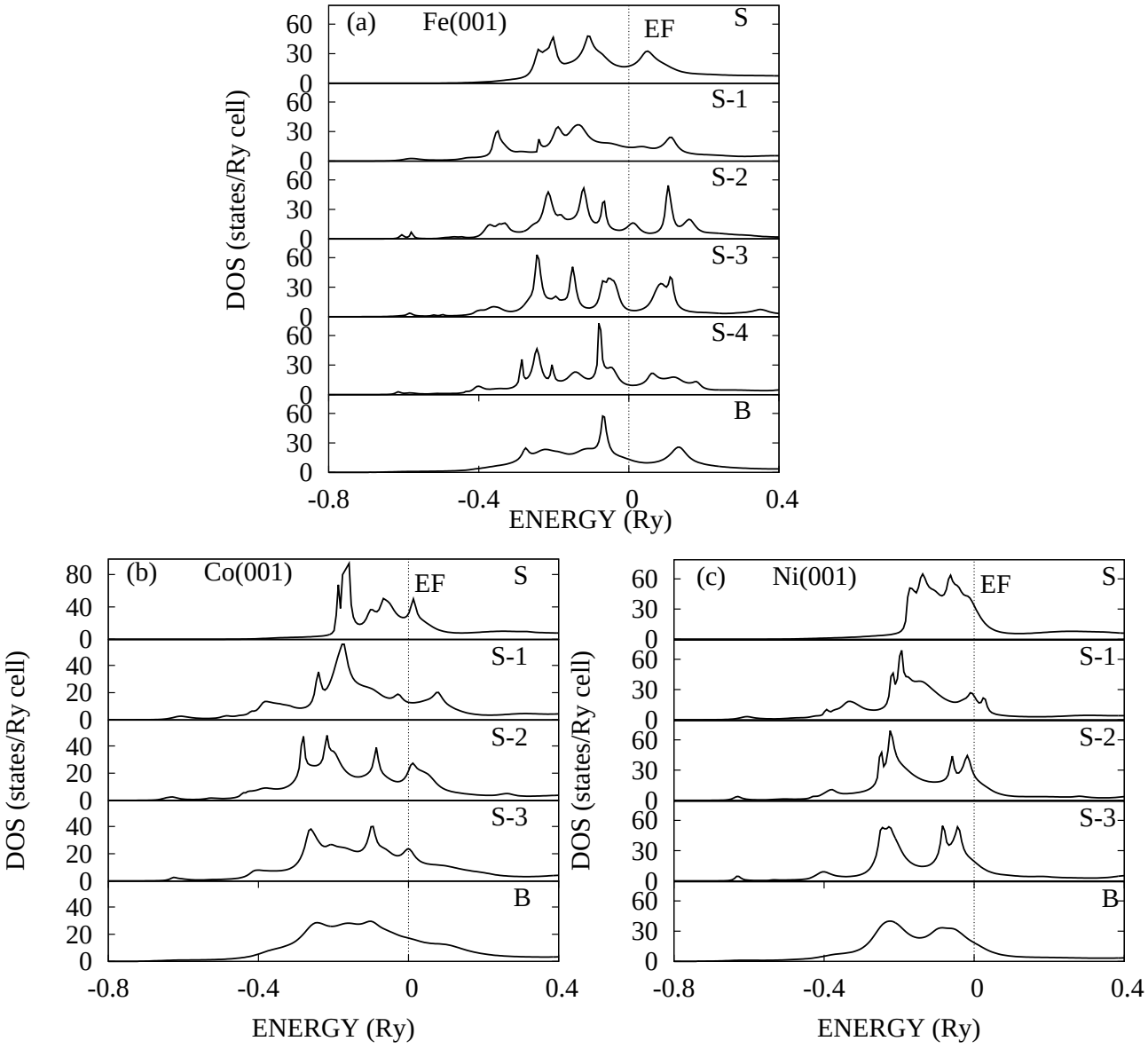

Figure 4.12: Layer based and bulk total DOS. Fermi energy is reset at zero.

down states is more for Fe(001), and hence plays significant role for enhancement of surface magnetic moment.

Table 4.1 shows the Fermi energies for these systems. The layer based total DOS, shown in the figure 4.12 indicates that as we go down from the top layer, the width of the DOS increases. It also shows that DOS approaches the bulk value from 5^{th} layer down the top most layer in the case of Fe(001) whereas it approaches to the bulk from 4^{th} layer in the other two, Co(001) and Ni(001), cases. Further going down

Table 4.5: Layer based and bulk (B) orbital resolved magnetic moment in μ_B/atom for almost smooth surfaces.

Layers	Fe(001)				Co(001)				Ni(001)			
	s	p	d	Total	s	p	d	Total	s	p	d	Total
S	0.01	0.02	2.80	2.83	-0.01	0.02	1.82	1.83	-0.01	0.0	0.69	0.68
S-1	-0.02	-0.03	2.13	2.08	-0.01	-0.03	1.49	1.45	-0.01	-0.01	0.60	0.58
S-2	-0.03	-0.06	2.06	1.97	-0.01	-0.04	1.79	1.74	0.0	-0.02	0.62	0.60
S-3	-0.02	-0.04	2.70	2.64	-0.01	-0.06	1.66	1.59	0.0	-0.02	0.56	0.54
S-4	-0.01	-0.06	2.43	2.36	-0.02	-0.06	1.62	1.54	-0.01	-0.02	0.55	0.52
S-5/B	-0.02	-0.06	2.25	2.17								

to the inner atomic layer, there is no change in DOS. Hence bulk electronic properties are obtained after four layers down in the case of Fe(001) and after three layers in the cases of Co(001) and Ni(001). The bulk DOS of the three systems calculated in this case are same as calculated for rough surfaces (figures 4.11, 4.1, 4.2 and 4.3).

In transition metals, d-electrons contribute mainly to the formation of bands. Therefore, any surface effects must be reflected into d-band. This is evident from the orbital resolved DOS (figure 4.13). The narrowing of d-band is due to the dehybridization of s-, p-, and d-electrons [9]. It is clear that for surface as well as for bulk, the DOS of s- and p-orbitals are negligible but that of d-orbitals is significant. Hence d-electrons give significant contribution towards the magnetic moment than that of s- and p-orbitals (table 4.5). Because of narrowing of peaks, states are more localized and their heights are more.

The orbital resolved layer based magnetic moment of different layers and the bulk are tabulated in table 4.5. The table shows magnetic moment approaches to the bulk value at 5^{th} layer down in case of Fe(001) and at 4^{th} layer in the other two cases as expected from DOS result. Magnetic moments for different layers exhibit Friedel oscillation. This is also shown in the figure 4.14. This figure further shows that the enhancement of surface magnetic moment is more for Fe(001) and Ni(001)

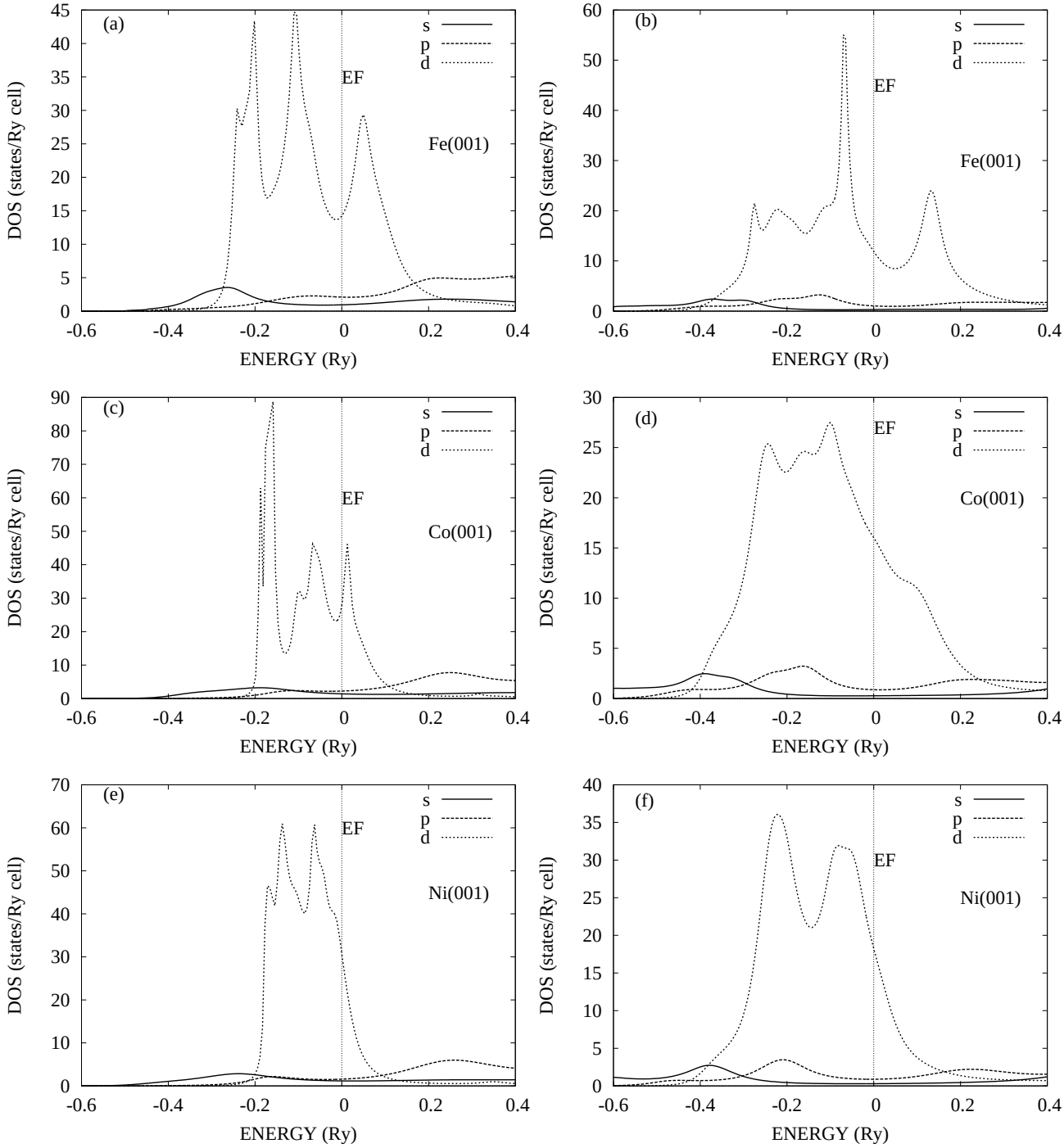

Figure 4.13: Orbital resolved DOS: surface : (a), (c) & (e), and bulk : (b), (d) & (f). Fermi energy is reset at zero.

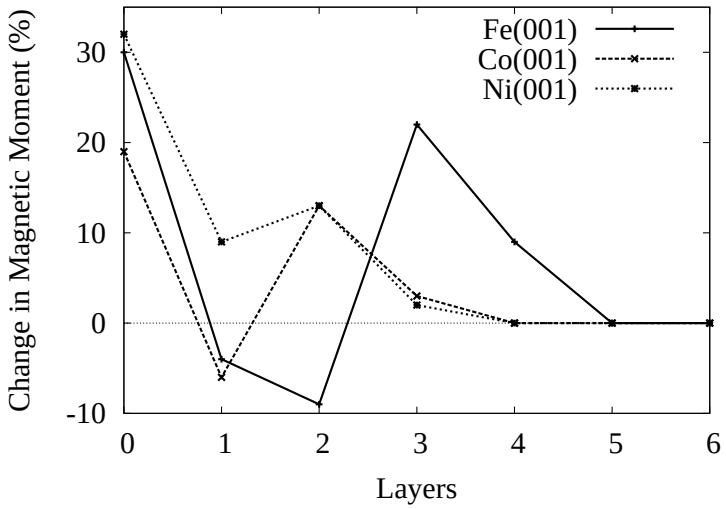

Figure 4.14: Percentage variation of magnetic moment with respect to the bulk value for different layers. Layer 0 represents the top most layer.

but it is less for Co(001). Table 4.5 also shows that d-electrons contribute most to the magnetic moment compared to s- and p-electrons as expected form DOS. In all the three cases, the contribution of s- and p-orbital are comparable to TB-LMTO Green's function method [18].

The present result of layer based magnetic moment and other available theoretical and experimental values are tabulated in tables 4.6, 4.7 and 4.8 for comparison. These tables show the enhancements of surface magnetic moment compared to the bulk by 30% for Fe(001), 19% for Co(001) and 32% for Ni(001). Our result of bulk magnetic moment for Fe is within 5% difference from experimental value [35, 161].

Experimental values of local magnetic moment for surface layer and layers below are not available for comparison. It is only the bulk magnetic moment for which experimental results are available [35, 161]. Work function is a surface property and is related to the surface DOS. It is an experimentally measurable quantity. It is therefore necessary to calculate work function to compare our results with experimental observations. Table 4.9 shows our calculated work functions agree quite well with experimental [39, 51] and other theoretical [5, 9, 12, 15–18, 49] calculations for all the systems.

Table 4.6: Comparison of magnetic moment in μ_B/atom for surface (S), sub-surfaces (S-1, S-2, S-3) and central layer or bulk (C/B) for Fe. Numbers in the square brackets represent the reference numbers.

Methods	Fe(001)			
	S	S-1	S-2	C/B
FPLAPW	2.98 [6, 12, 13, 40]	2.35 [12]	2.39 [12]	2.25 [12]
	2.80 [14]	2.38 [6]	2.43 [6]	2.15 [13]
				2.30 [6]
LMTO	2.87 [7, 17]	2.34 [7, 17]	2.33 [7, 17]	2.18 [7, 17]
FPLMTO	2.94 [43]	2.33 [43]	2.38 [43]	2.25 [43]
TB-LMTO	2.97 [18]	2.30 [18]	2.37 [18]	2.24 [18]
	2.97 [8]	2.3 [8]	2.37 [8]	2.25 [8]
	2.86 [19]	2.16 [19]	2.38 [19]	2.17 [19]
	2.98 [10]	2.17 [10]	2.40 [10],	2.26 [10]
	2.99 [10]	2.21 [10]	2.38 [10]	2.26 [10]
	2.95 [11]	2.2 [11]	2.387 [11]	2.28 [11]
	2.92 [27]	2.07 [27]	2.28 [27]	2.12 [27]
	2.99 [27]	2.13 [27]	2.35 [27]	2.16 [27]
LCAO	3.01 [20]	1.69 [20]	2.13 [20]	1.84 [20]
	3.04 [27]	2.43 [27]	2.50 [27]	2.36 [27]
	3.08 [27]	2.46 [27]	2.52 [27]	2.39 [27]
ASR	2.99 [19]	2.17 [19]	2.38 [19]	2.27 [19]
Experiment				2.21 [35]
				2.22 [161]
Present work	2.83	2.08	1.97	2.17

References [8, 18] includes Green's function techniques; [19] includes surface dilatation; [10, 19] is supercell calculation; [10, 11] Real space recursion study; [27] with SZSP and DZSP basis; [27] with LDA and GGA.

Table 4.7: Comparison of magnetic moment in μ_B/atom for surface (S), sub-surfaces (S-1, S-2, S-3) and central layer or bulk (C/B) for Co. Numbers in the square brackets represent the reference numbers.

Methods	Co(001)				
	S	S-1	S-2	S-3	S-4/B
FPLAPW	1.86 [14, 15]	1.64 [15]	1.65 [15]	1.64 [15]	1.65 [15]
TB-LMTO	1.76 [11]	1.46 [11]	1.58 [11]	1.56 [11]	1.58 [11]
	1.84 [18]	1.63 [18]	1.66 [18]	1.64 [18]	
	1.84 [8]	1.63 [8]	1.66 [8]	1.65 [8]	1.66 [8]
Experiment					1.71 [161]
Present work	1.83	1.45	1.74	1.59	1.54

References [8, 18] includes Green's function techniques; [11] is Real space recursion study.

We now discuss surface properties of Fe(001) without surface relaxation. As discussed earlier, the weak bonding of the surface atoms is modeled by removing the body centered atom in bcc Fe(001). We choose seven layers of Fe(001) and two layers of empty spheres above the top layer. The Fermi energy is found to be -0.07 Ry. This value is closed to bulk (-0.08 Ry) value. Figure 4.15 shows DOS in this case. Comparing total DOS in both calculations (figures 4.15(a) and 4.10(a)), we observe no significant difference in bulk electronic states, but slight difference in surface DOS at low energy region. Similar difference is also observed in spin resolved DOS (figures 4.15(b) and 4.11(a)). The increases in spin-up surface states at lower energy region is responsible for less surface magnetic moment in this case. Comparison of total layer based DOS in both the cases (figures 4.15(c) and 4.12(a)) show slight variation in DOS for the top three layers. But from layer S-3 onwards, the DOS are equivalent on both type of calculations. The surface magnetic moment is found to be 2.78 μ_B/atom and that of the bulk is 2.17 μ_B/atom in this case.

Table 4.8: Comparison of magnetic moment in μ_B/atom for surface (S), sub-surfaces (S-1, S-2, S-3) and central layer or bulk (C/B) for Ni. Numbers in the square brackets represent the reference numbers.

Methods	Ni(001)				
	S	S-1	S-2	S-3	S-4/B
FPLAPW	0.73 [6] 0.68 [16] 0.73 [9, 41, 44] 0.68 [9, 13, 14, 40–42]	0.68 [6] 0.60 [16] 0.68 [9, 41, 44]	0.66 [6] 0.59 [16] 0.69 [9, 41, 44]	0.63 [6] 0.56 [16] 0.56 [13, 14, 40, 41]	
LMTO	0.59 [7, 17]	0.58 [7, 17]	0.57 [7, 17]	0.55 [7, 17]	
FPLMTO	0.73 [43]	0.61 [43]	0.61 [43]	0.59 [43]	
TB-LMTO	0.69 [18] 0.69 [8] 0.65 [11]	0.64 [18] 0.64 [8] 0.53 [11]	0.66 [18] 0.66 [8] 0.61 [11]	0.64 [18] 0.64 [8] 0.60 [11]	0.65 [8] 0.595 [11]
LCAO	0.44 [45]	0.58 [45]	0.62 [45]	0.56 [45]	0.54 [45]
TB-GF	0.74 [94]	0.55 [94]	0.56 [94]		0.56 [94]
Experiment					0.616 [35] 0.656 [37]
Present work	0.68	0.58	0.60	0.54	0.52

References [8, 16, 18] includes Green's function techniques; [11] is real space recursion study; [94] based on tight binding hamiltonian with single-site approximation including Green's function.

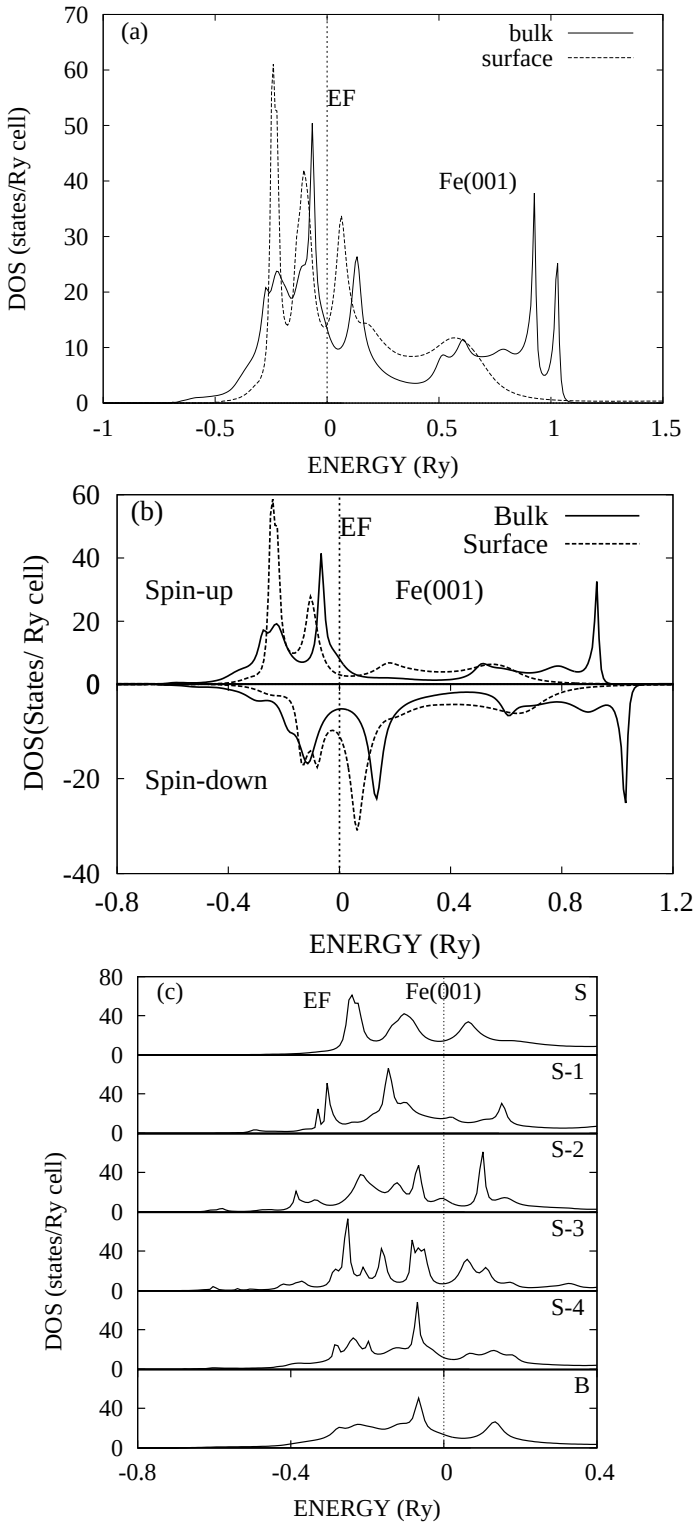

Figure 4.15: (a) Total density of states and (b) Spin density of states for surface and bulk bcc Fe(001) with 50% empty spheres on top most layer. (c) Layerwise total density of states for surface (S), subsurfaces (S-1, S-2, S-3, S-4) and bulk bcc Fe (001). Fermi energy is reset at zero.

Table 4.9: Work functions of Fe(001), Co(001) and Ni(001) in eV. Numbers in the square brackets represent the reference numbers.

Methods	Fe (001)	Co(001)	Ni(001)
FPLAPW	4.29 [12]	5.17 [15]	5.37 [16], 5.5 [9],5.31 [49]
LAPW			5.71 [5]
LMTO	4.30 [17]		5.02 [17]
TB-LMTO	4.5 [18]	5.52 [18]	5.75 [18]
Experimental	4.67 [51], 4.4 [39]	5.0 [51]	5.22 [51]
Present work	4.15	5.33	4.79

Reference [18]: with Green's function; and [5,9,49]: with surface embedded Green's function.

The surface magnetic moment is less in this case whereas the bulk value is same. The enhancement of surface magnetic moment is 28%. This enhancement is less compared to when lattice relaxation is considered. Figure 4.16 shows an oscillatory behavior of magnetic moments. The DOS and magnetic moment approach to bulk value after five layers down the top most layer.

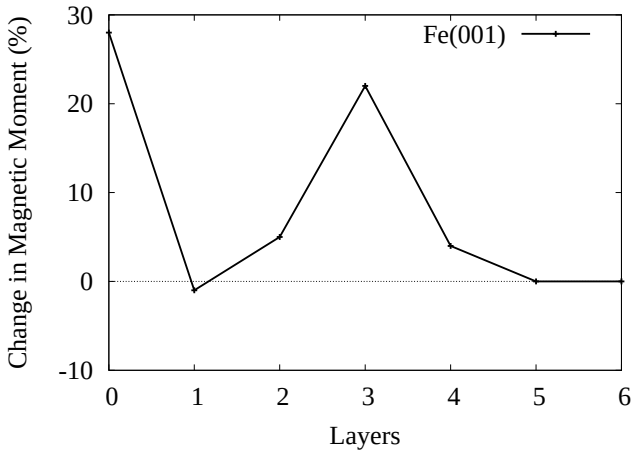

Figure 4.16: Change in magnetic moment from surface to the bulk. Layer 0 represents the top layer.

Chapter 5

Transition Metal - Metal Interfaces

In this chapter, we discuss layerwise electronic and magnetic properties of transition metals overlayers on metal substrates. There is a significant change in the electronic and magnetic properties at an interface due to weak hybridization and roughness. In its first application to interface, ASF was applied to only single monolayer (ML) of Fe on metal substrates with 5% and 10% interdiffusion of atoms [19, 50]. As discussed in the introduction, the interdiffusion is possible upto few layers on both sides. Therefore we consider two, three and four monolayers (ML) of transition metals on metal substrates other than one ML. We first study one and two monolayers thick film to compare our results with other reported works [9,41,43,63,64,68,69,73,74,76, 127] and test the accuracy of our method. We also compare the properties of one ML with (5% and 10%) and without interdiffusion of atoms at the interface. There are experimental studies of magnetic properties on 2.9 ML using SQUID magnetometry [85] and on 3 ML using X-ray magnetic circular dichroism (XMCD) [89]. Therefore we consider three ML of overlayer growth to compare our result with experimental works. The interface is considered as an alloy due to interdiffusion of atoms between transition metal overlayer and substrate. Two different thickness of interfaces, two and four alloyed layers, are considered. We shall consider interdiffusion upto two ML into each side of the interface. Since the amount of interdiffusion of two types of

atoms is different at different atomic layers at the interface, therefore it is imperative to treat varying degree of randomness at different layers. Here this formalism is also extended to carry out sharp interface properties, when interdiffusion is negligible.

We represent metal substrate as M and deposited transition metal layers as T. Therefore, when x fraction of atoms interdiffuse into both sides, substrate is an alloy of $M_{1-x}T_x$ and overlayer is $T_{1-x}M_x$ at the interface. We choose $x = 0.0$, 0.05 and 0.1. The justification of applying ASF to nearly zero disorder (x=0) is discussed in chapter-3.

We consider growth of Fe, Co and Ni transition metals on (001) surface of Ag, Cu and Au metal substrates. Fe is deposited on Ag and Au in its bcc phases. There is a large lattice mismatch (42%) between bcc Fe and fcc Ag / fcc Au. When Fe is deposited on Ag or Au, the layers of bcc Fe is rotated by 45° [13, 14, 40, 53–57, 90]. This reduces the lattice mismatch to only 0.8% and 0.5% respectively. But interfaces of other transition metal overlayers with metal substrates are found to be in fcc phase. There is about 15% lattice mismatch between Co and Ag / Au. Therefore we have carried out lattice relaxation of the top layer in these cases. This is done by minimising the total energy by varying the lattice constant of the top layer. After relaxation, the Co lattice parameter increases by 17% and 15.5% respectively for Ag and Au metal substrate such that the lattice mismatch reduces to within 2%. There is also sufficient lattice mismatch between Ni and Ag or Au (16%). Here also we consider lattice relaxation for Ni. The lattice parameter are relaxed by 10%. This reduces the lattice mismatch to within 6% with both Ag and Au. Fe is deposited on Cu in its fcc phases [50]. The lattice mismatch in this case is within 1%. The lattice mismatch of Co/Cu and Ni/Cu interfaces are also small, 2% and 3% respectively. Since the lattice mismatch is less for Cu based systems, so lattice relaxation is not considered in such cases.

We consider two layers of empty spheres which contain charge but no atoms

above surface layer to take care of the charge leakage into the vacuum for different types of study using different ML. The potential parameters are generated from TB-LMTO within local spin density approximation (LSDA) using Barth and Hedin exchange correlation potential [159]. Wave equations are solved by the scalar-relativistic calculations. We use eight shell augmented space calculation and nine steps of recursion.

5.1 Single Monolayer of Transition Metals on Metal Substrates

In this case, we consider sharp interfaces first. Interdiffusion of atoms from both sides of interface is taken negligible. The result for this case can be compared with other calculations using different first principle methods. This is because most of the other reported work are for sharp interface.

Figures 5.1, 5.2 and 5.3 show layerwise density of states (DOS) for all the systems. Spin polarized DOS shows the amount of splitting in spin up and spin-down electronic states, the nature of hybridization and its contribution towards the magnetic moments for the transitional metal layer. Figure 5.1 shows that spin-down DOS of Co is more than Fe at Fermi energy in the case of Ag based systems. This agrees with earlier study [63]. The spin-down band width is more than spin-up in the case of Fe/Ag and Co/Ag. There is slight difference between these two bandwidths in the case of Ni/Ag which agrees with earlier study [63]. The spin resolved DOS of top most layer for Ag based systems matches with earlier study using FPLAPW method [63, 64]. The splitting of spin-up and spin-down states are more for Fe overlayers with Ag and Au substrates. Therefore the peaks of transition metal atoms do not coincide with that of substrate atoms at layer S-1. This means sp-d hybridization between Fe and Ag or Au is comparatively weak. The weak hybridization narrows down the Fe bands and hence the magnetic moment of Fe on Ag or Au is more compared to others.

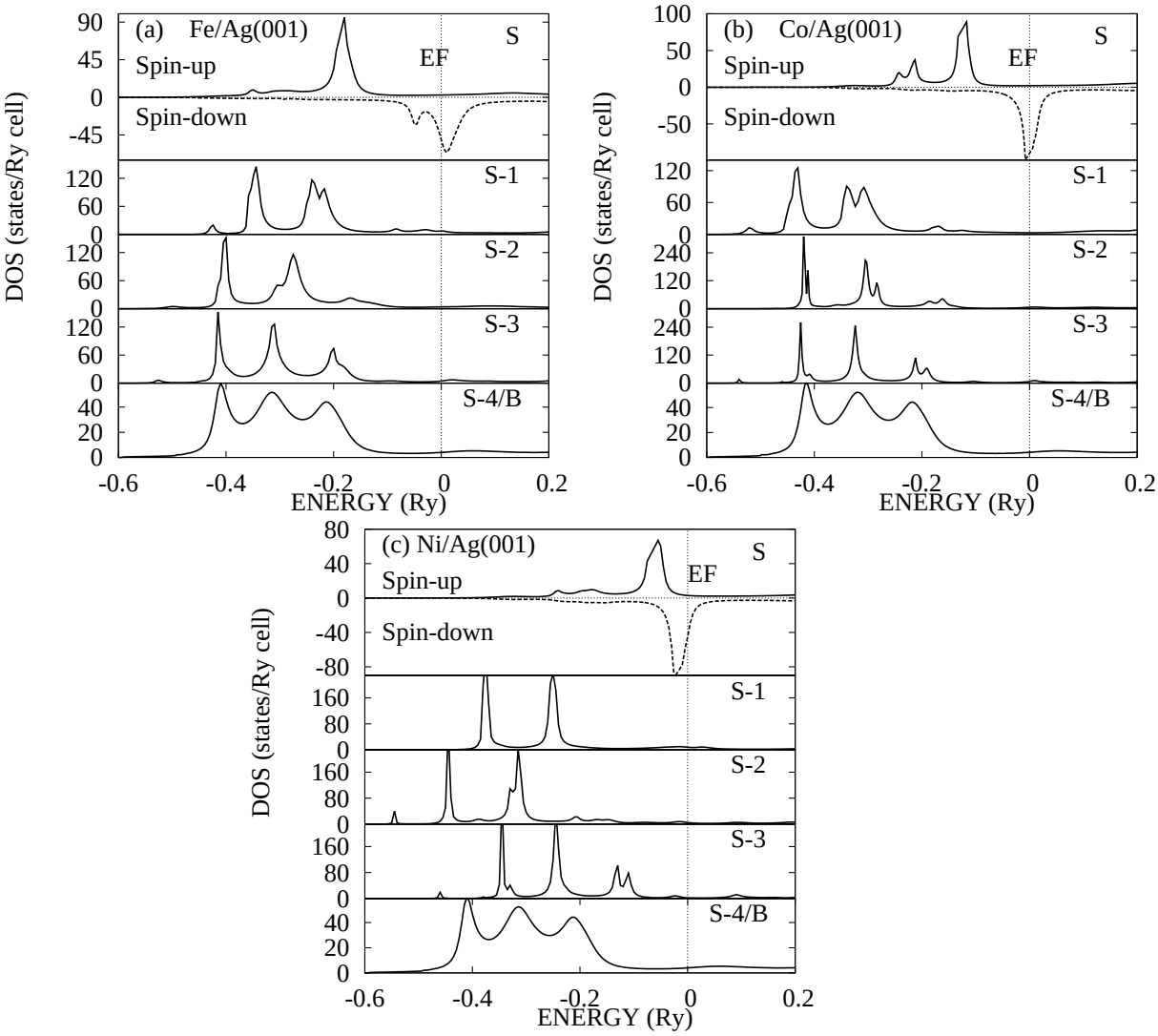

Figure 5.1: Layerwise variation of DOS for one ML of transition metal (Fe, Co and Ni) on Ag metal substrates from top most surface (S) layer to inner atomic layers. Fermi level is reset at zero

In case of Cu based systems as shown in figure 5.2, the spin DOS of Fe and Co on Cu agrees with earlier studies using FPLAPW method [66], LAPW method [68] and FPLMTO method [43]. Our calculated DOS is slight different from first principle Green's function method [127]. The spin-up DOS contribute more towards the magnetic moment of these systems. The spin-down states have significant contribution in case of Ni/Cu. Comparing spin-down DOS of the top most layer, Co has more electronic states than Fe at Fermi energy and also wider than the spin-up bands. Figure 5.2 shows the splitting of spin-up and spin-down states are more for

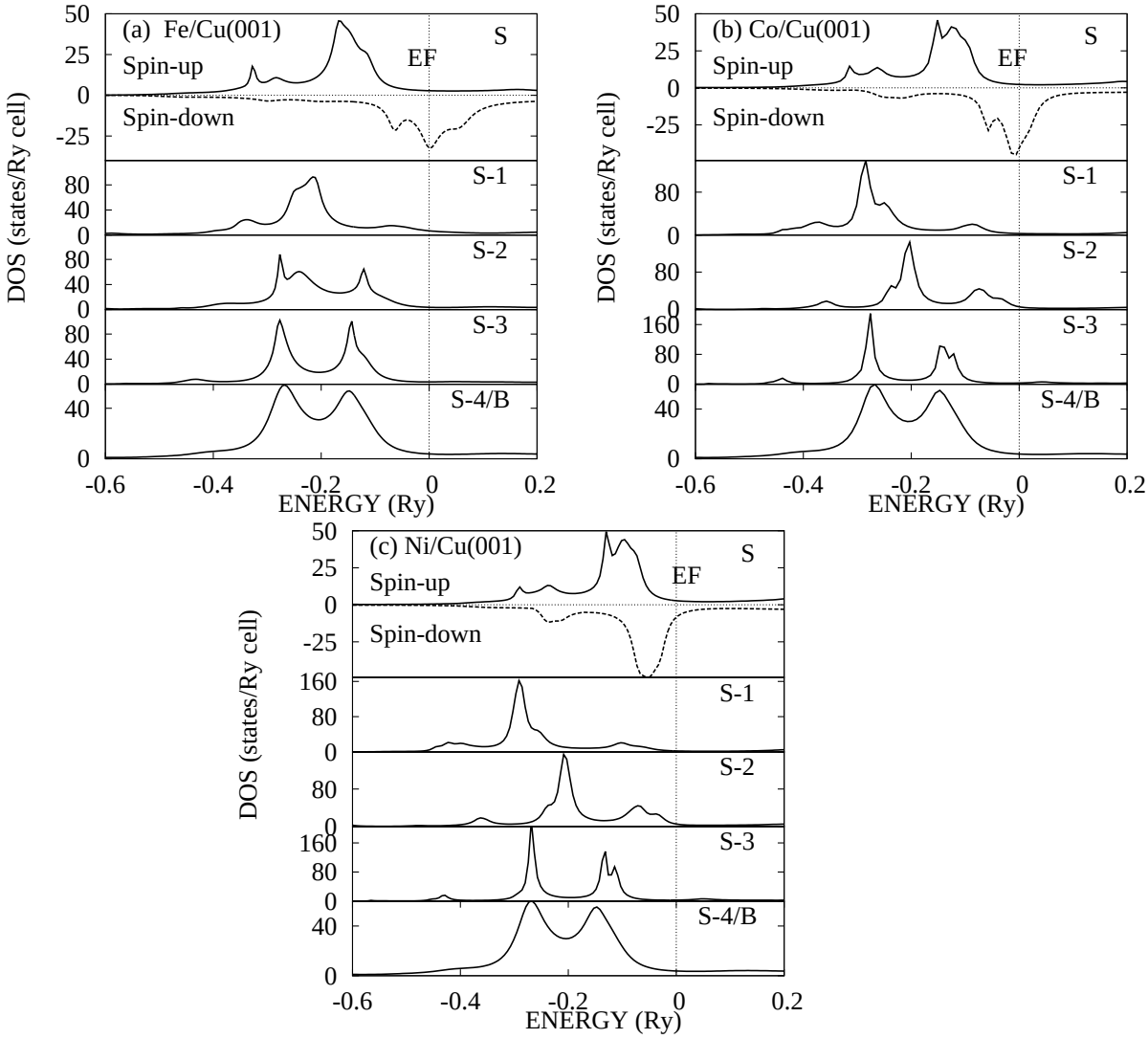

Figure 5.2: Layerwise variation of DOS for one ML of transition metal (Fe, Co and Ni) on Cu metal substrates from top most surface (S) layer to inner atomic layers. Fermi level is reset at zero.

Fe/Cu(001) than other systems. There is overlap of electronic states of Cu with the transition metal electronic states. Therefore sp-d hybridization is strong in these systems compared to Ag based systems. The strong sp-d hybridization of Cu based systems is due to lattice constant contraction by about 11% [14].

Figure 5.3 shows spin-down DOS of Co is more than Fe and Ni at Fermi energy. The spin-down band is wider than the spin-up bands. The splitting of spin-up and spin-down electronic states are more for Fe/Au(001) than other systems. The spin resolved DOS for top Fe layer in Fe/Au(001) system matches well with the result

by FPLAPW method [70].

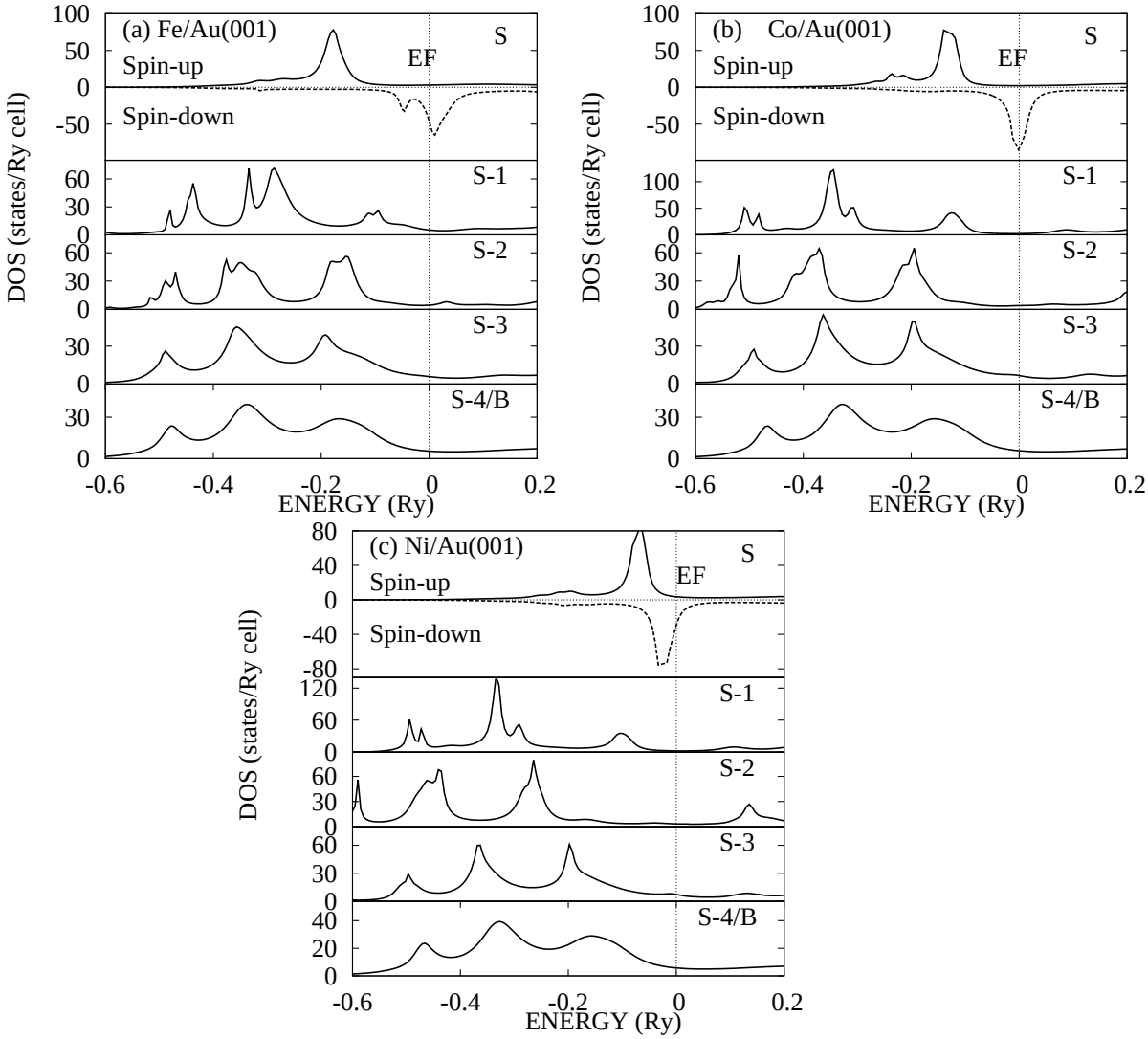

Figure 5.3: Layerwise variation of DOS for one ML of transition metal (Fe, Co and Ni) on Au metal substrates from top most surface (S) layer to inner atomic layers. Fermi level is reset at zero.

The layerwise magnetic moments for all the systems are tabulated in table 5.1. The spin-up DOS contribute more towards the magnetic moment of these systems. This table shows the magnetic moment goes to zero at S-4^{th} substrate layer. This is also shown in figures 5.4, 5.5 and 5.6. These figures show that as we move towards the inner layer, magnetic moment exhibits oscillatory behavior except for Ni/Ag, Fe/Cu and Fe/Au. Hence metal substrates obtain their bulk properties at the fourth layer down the top most transition metal overlayer.

Table 5.1: Layer-wise magnetic moment(μ_B/atom) for a single layer of transition metal deposited on metal substrate. S stands for top most layer of the interface. x = 0.0 (sharp interface).

Layers	Ag(001)			Cu(001)			Au(001)		
	Fe	Co	Ni	Fe	Co	Ni	Fe	Co	Ni
S	2.994	2.03	0.61	2.49	1.51	0.43	3.00	2.01	0.55
S-1	0.03	0.001	0.11	0.04	0.003	-0.02	0.09	-0.03	-0.003
S-2	0.005	-0.004	0.08	0.01	0.006	0.002	0.02	0.21	-0.07
S-3	0.02	-0.04	0.02	0.00	-0.04	0.00	0.001	0.001	0.001
S-4	0.00	0.00	0.00	0.00	0.00	0.00	0.00	0.00	0.00

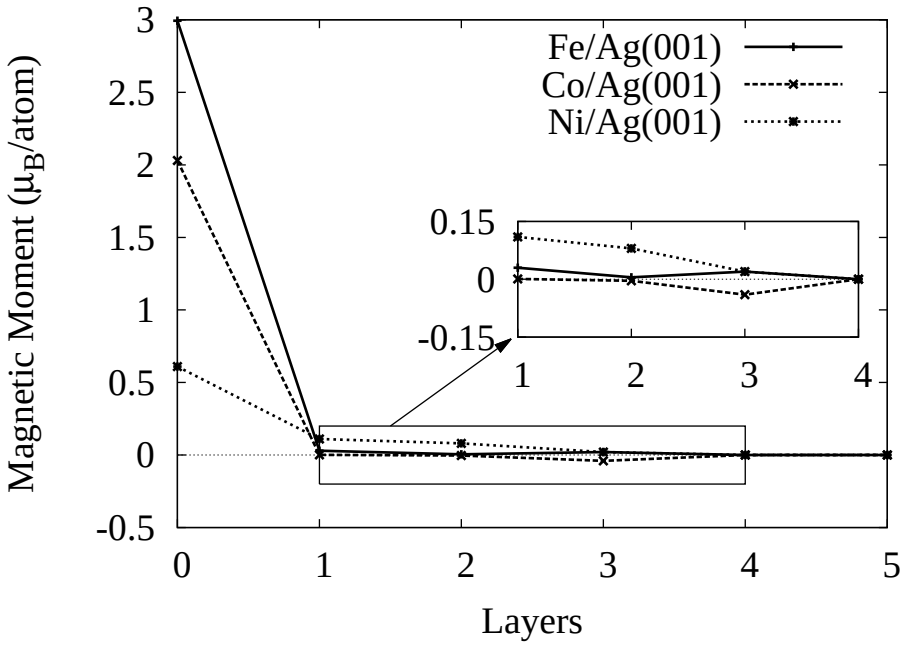

Figure 5.4: Layerwise variation of magnetic moment for 1 ML of transition metal on Ag metal substrates. Layer 0 represents surface layer.

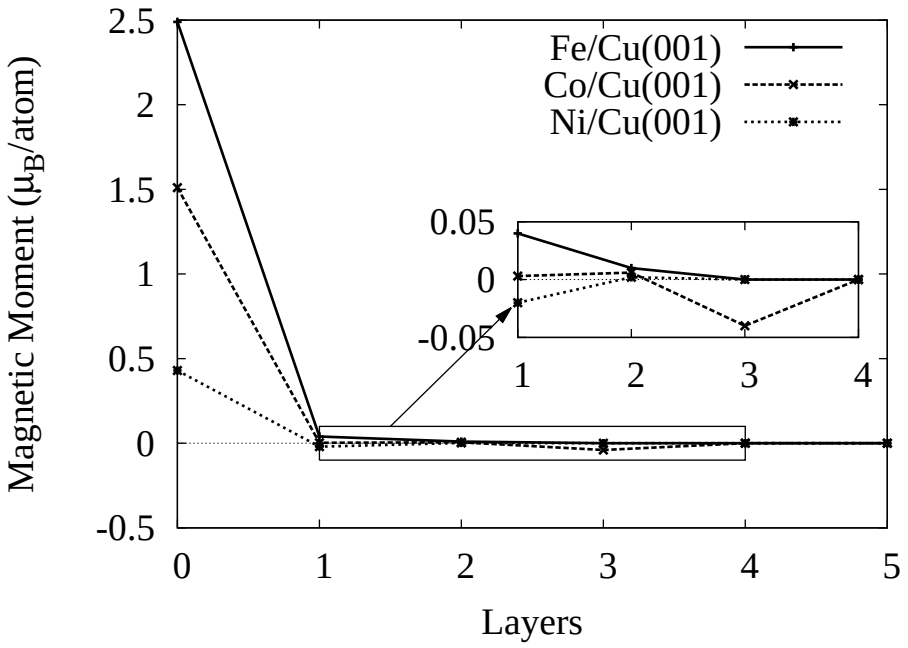

Figure 5.5: Layerwise variation of magnetic moment for 1 ML of transition metal on Cu metal substrates. Layer 0 represents surface layer.

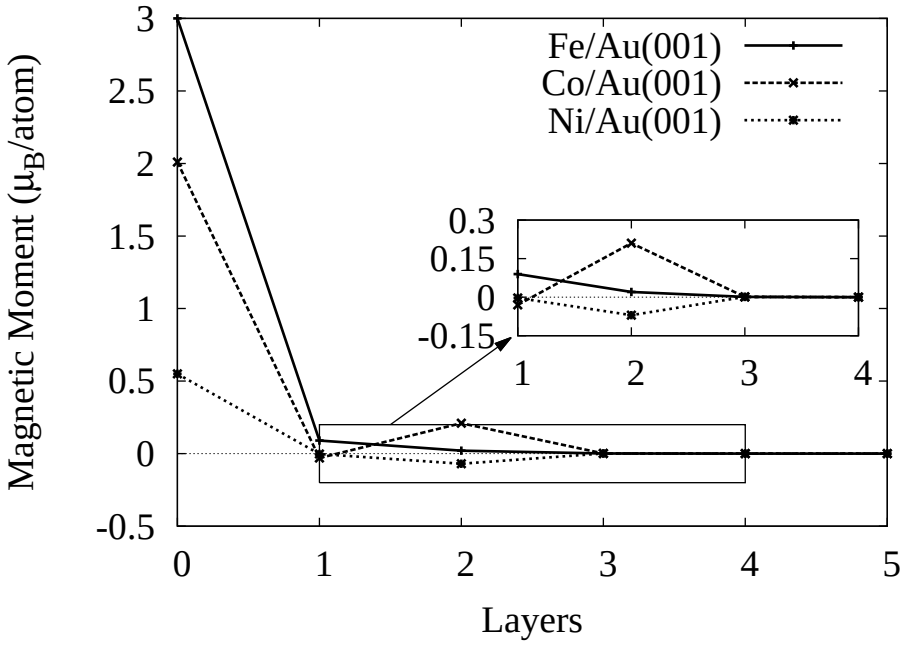

Figure 5.6: Layerwise variation of magnetic moment for 1 ML of transition metal on Au metal substrates. Layer 0 represents surface layer.

Table 5.2: Magnetic moments (in μ_B/atom) for sharp interface: A Comparison with other method for one layer transition metal deposition on Ag substrate. Numbers in square brackets show reference numbers.

Methods	Fe/Ag(001)		Co/Ag(001)		Ni/Ag(001)	
	S	S-1	S	S-1	S	S-1
FPLAPW	3.01 [63]	0.03 [62, 65]	2.03 [63]		0.65 [63]	
	2.96 [13, 40, 60–62, 65]				0.57 [64]	
SCLO	3.0 [71]	0.03 [71]				
ASR	3.02[a] [19],2.93[a] [50]					
	2.86[b] [19],2.76[b] [50]					
TBLMTO-ASA	2.86 [55]					
LCAO	3.02 [27]					
	3.10 [27]					
KKR-GF	3.00 [74]		1.9 [74]		0.70 [74]	
	3.15 [162]		2.03 [162]			
Present	2.994	0.03	2.03	0.001	0.61	0.11
work	2.80[a]		1.68[a]		0.53[a]	
	2.54[b]		1.69[b]		0.43[b]	

[a]5% and [b]10% Ag in top most transition metal layers.

Table 5.3: Magnetic moments (in μ_B/atom) for sharp interface: A Comparison with other method for one layer transition metal deposition on Cu substrate. Numbers in square brackets show reference numbers.

Methods	Fe/Cu(001)		Co/Cu(001)		Ni/Cu(001)	
	S	S-1	S	S-1	S	S-1
FPLAPW	2.69 [65]	0.06 [65]	1.79 [65]	0.05 [65]	0.39 [9, 41, 68]	
	2.85 [13, 40, 66, 67]					
LAPW					0.37 [69]	
SCLO					0.24 [73]	
ASR	2.25[a] [50]					
	2.13[b] [50]					
TBLMTO-CPA	2.80 [76]		1.80 [76]		0.41 [76]	
GF					0.30 [127]	
FPLMTO	2.81 [43]	0.05 [43]	1.85 [43]	0.03 [43]	0.45 [43]	0.01 [43]
Present	2.49	0.04	1.51	0.003	0.43	-0.02
work	2.37 [a]		1.40 [a]		0.41 [a]	
	2.26 [b]		1.32 [b]		0.39 [b]	

[a]5% and [b]10% Cu in top most transition metal layers.

Table 5.4: Magnetic moments (in μ_B/atom) for sharp interface: A Comparison with other method for one layer transition metal deposition on Au substrate. Numbers in square brackets show reference numbers.

Methods	Fe/Au(001)		Co/Au(001)		Ni/Au(001)	
	S	S-1	S	S-1	S	S-1
FPLAPW	2.98 [62]	0.08 [62, 65]				
	2.97 [65, 70])	0.03 [70]				
ASR	2.85[a] [50]					
	2.68[b] [50]					
Present	3.00	0.09	2.01	-0.03	0.55	-0.003
work	2.84 [a]		1.93 [a]		0.51 [a]	
	2.70 [b]		1.65 [b]		0.47 [b]	

[a]5% and [b]10% Au in top most transition metal layers.

Tables 5.2, 5.3 and 5.4 show that our calculated values are well comparable to the other theoretical calculations. The magnetic moment of Fe and Co overlayers on Ag and Au are more than that of smooth bcc Fe(001) and fcc Co(001) surfaces (table 4.5). This is because sp-3d hybridization between these transition metal and Ag or Au metal is weak comparison to interlayer 3d-3d hybridization for Fe(001) and Co(001). But the magnetic moment of Ni is less than sharp Ni(001) surface. That is, though the coupling between Ni and Ag or Au is weak but there is reduction in Ni magnetic moment compared to smooth Ni(001) surface magnetic moment [64]. Hence band narrowing does not play important role in this case. The hybridization between Fe/Cu is strong than the other two systems (figure 5.2), therefore the induced magnetic moment in Fe/Cu is more than other which agrees with earlier studies [43, 65]. The decrease of Ni spin moment is due to an effect of strong hybridization between the Ni 3d and Cu s and p states [43]. The magnetic moment of Co is more for Co/Ag than Co/Cu. This result matches with experiment [122]. The induced magnetic moment of Fe on Cu is more than Ag, which is contradictory to earlier study [50], but matches with study using FPLAPW method [62,65]. This may be because of weak hybridization between Fe and Ag than Fe and Cu, less amount of magnetism will be induced on Ag than Cu substrates. The layer-by-layer magnetic moment for one ML of Fe on Au agrees with FPLAPW method [70].

We now discuss the effect of roughness at the interface. The interface roughness due to interdiffusion of atoms is observed in such systems [19, 50, 58, 104, 112, 117, 121, 125, 128, 133, 134]. We consider 5% and 10% interdiffusion of atoms for single ML of transition metal on metal substrates.

Figures 5.7, 5.8 and 5.9 show the effect of roughness on the spin polarized DOS at the interface (S and S-1) layers for one ML of transition metals on Ag, Cu and Au respectively. Tables 5.5 and 5.6 show the layerwise variation of magnetic moment for Ag based systems with 5% and 10% interdiffusion of atoms at the interface, respectively. When 5% of Ag impurity is introduced in Fe atomic layer, there is

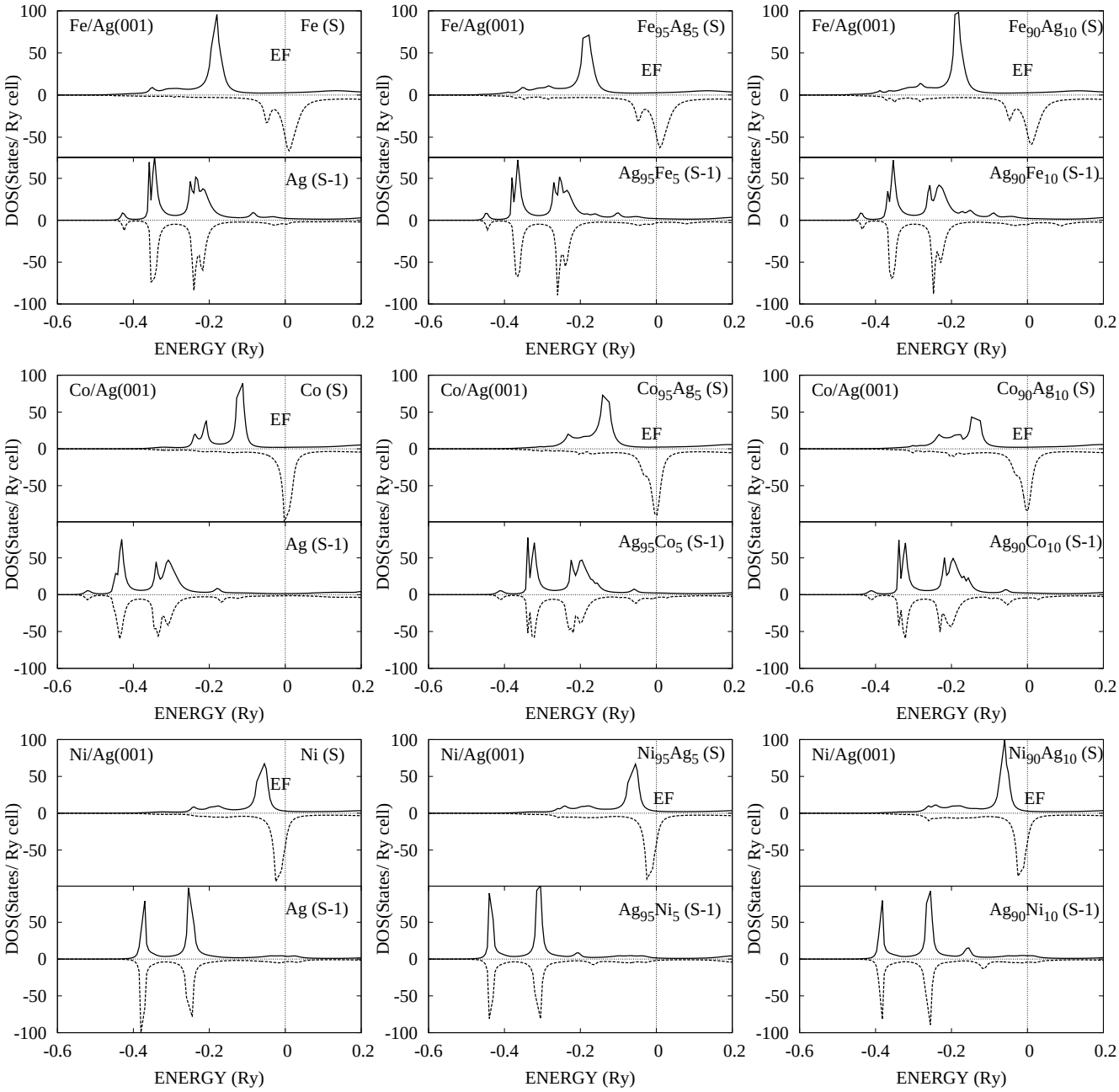

Figure 5.7: Layerwise spin polarized DOS for a single layer of transition metal deposited on Ag substrate. S stands for top most layer of the interface and S-1 is the first substrate layer. Left panel : $x = 0$ (sharp interface), middle panel : $x = 0.05$ and right panel : $x = 0.10$ (rough interface). Solid line: Spin-up DOS. Dotted line: Spin-down DOS. Fermi level is reset at zero.

Table 5.5: Layer-wise magnetic moment (μ_B/atom) for 1 layer (S) of transition metal on Ag metal substrate. S and S-1 are $T_{1-x}M_x$ and $M_{1-x}T_x$ respectively. T and M stand for transition metal and metal atoms respectively. Here $M = Ag$ and $x = 0.05$ (rough interface).

Layers	Fe/Ag(001)			Co/Ag(001)			Ni/Ag(001)		
	μ_T	μ_M	μ_{avg}	μ_T	μ_M	μ_{avg}	μ_T	μ_M	μ_{avg}
S	2.94	0.01	2.80	1.77	-0.04	1.68	0.56	-0.004	0.53
S-1	3.26	0.006	0.17	1.69	0.10	0.18	0.23	0.01	0.02
S-2		0.01			0.06			-0.07	
S-3		0.06			-0.04			0.01	
S-4		0.00			0.00			0.00	

no significant change in the surface spin-down DOS. But a reduction in spin-up electronic states is obtained (figure 5.7). This decreases the magnetic moment of Fe atoms as well as the average magnetic moment of $Fe_{95}Ag_5$ layer (table 5.5). With increase in the amount of Ag to 10% in Fe layer, magnetic moment of Fe as well as average magnetic moment of the layer decreases further (table 5.6). Whereas with increase in the amount of Fe in Ag layers, the average magnetic moment of first substrate layer increases. The magnetic moment of Fe in Ag layers is more than that of Fe overlayers. This agrees with earlier study [63]. The calculated average magnetic moment (tables 5.5 and 5.6) of Fe layer (S) with 5% and 10% Ag atoms agrees well with earlier studies (table 5.2) [19, 50]. In case of Co/Ag, both spin-up and spin-down electronic states show significant change in entire energy region. The spin-up states near Fermi energy decreases while that in lower energy region increases. Hence there is no significant difference in average magnetic moment of top layer for both amount of interdiffusion (tables 5.5 and 5.6). With increase in Co content in first Ag substrate layer, the amount of induced magnetic moment increases. With increase of Ag concentration in Ni overlayer, the peak near Fermi energy in spin-up DOS is significant but there is no significant change in spin-down DOS (figure 5.7). Hence with increase in Ag concentration, the Ni magnetic moment

Table 5.6: Layer-wise magnetic moment (μ_B/atom) for 1 layer (S) of transition metal on Ag metal substrate. S and S-1 are $T_{1-x}M_x$ and $M_{1-x}T_x$ respectively. T and M stand for transition metal and metal atoms respectively. Here $M = Ag$ and $x = 0.10$ (rough interface).

Layers	Fe/Ag(001)			Co/Ag(001)			Ni/Ag(001)		
	μ_T	μ_M	μ_{avg}	μ_T	μ_M	μ_{avg}	μ_T	μ_M	μ_{avg}
S	2.82	0.04	2.54	1.87	0.03	1.69	0.48	-0.02	0.43
S-1	3.29	-0.13	0.21	1.62	0.17	0.32	0.41	0.02	0.06
S-2		0.00			0.01			-0.04	
S-3		-0.07			-0.03			0.02	
S-4		0.00			0.00			0.00	

as well as the average magnetic moment gradually decreases (tables 5.5 and 5.6). The average magnetic moment of first substrate layer increases with increase in amount of Ni.

Tables 5.7 and table 5.8 represent the layerwise variation of magnetic moment with 5% and 10% interdiffusion of atoms in Cu based systems respectively. Figure 5.8 shows there is little change in both spin-up and spin-down states at lower energy value as the concentration of Cu in Fe layer increases. Hence the electrons away from Fermi energy contribute more towards the variation of magnetic moment. But in layer S-1, the peak of the spin-down states decreases slightly with increase amount of Fe impurities. With increase in Fe atoms in the first Cu substrate layer the induced magnetic moment of the layer increases. The calculated average magnetic moment (tables 5.7 and 5.8) for Fe/Cu with 5% and 10% Cu in Fe are comparable to earlier study [50], given in table 5.3. There is slight change in DOS at the lower energy region for top layer in case of Co/Cu. In S-1 layer, with increase in Co impurities the amount of spin-down states decreases but the spin-up states undergo significant change. This contributes towards the induced magnetic moment. Due to presence of Cu impurities on top most Ni layer, the spin DOS show slight variation

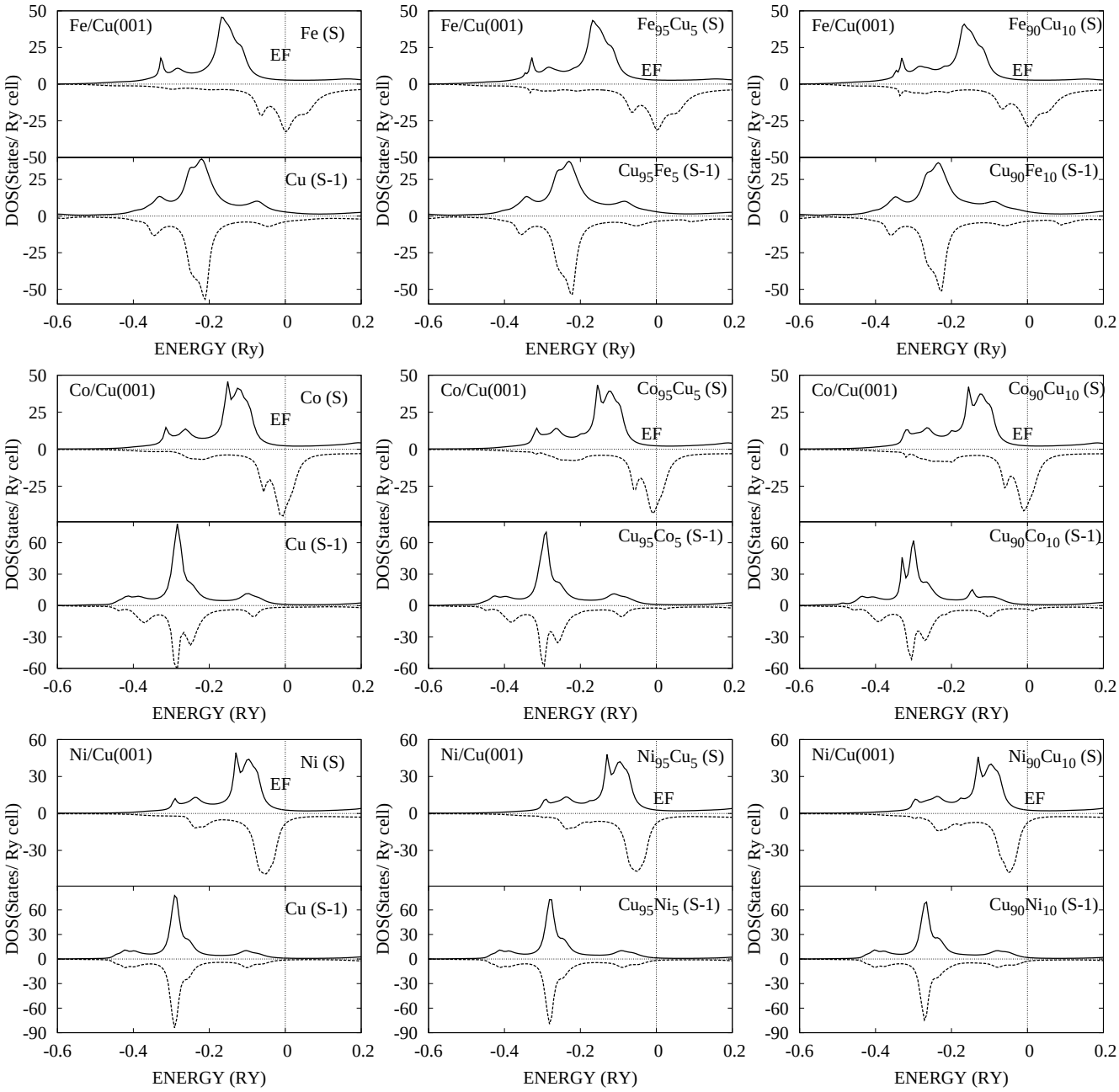

Figure 5.8: Layerwise spin polarized DOS for a single layer of transition metal deposited on Cu substrate. S stands for top most layer of the interface and S-1 is the first substrate layer. Left panel : $x = 0$ (sharp interface), middle panel : $x = 0.05$ and right panel : $x = 0.10$ (rough interface). Solid line: Spin-up DOS. Dotted line: Spin-down DOS. Fermi level is reset at zero.

Table 5.7: Layer-wise magnetic moment (μ_B/atom) for 1 layer (S) of transition metal on Cu metal substrate. S and S-1 are $T_{1-x}M_x$ and $M_{1-x}T_x$ respectively. T and M stand for transition metal and metal atoms respectively. Here $M = Cu$ and $x = 0.05$ (rough interface)

Layers	Fe/Cu(001)			Co/Cu(001)			Ni/Cu(001)		
	μ_T	μ_M	μ_{avg}	μ_T	μ_M	μ_{avg}	μ_T	μ_M	μ_{avg}
S	2.50	-0.005	2.37	1.46	0.26	1.40	0.43	0.03	0.41
S-1	2.98	0.03	0.18	1.96	0.02	0.12	0.61	-0.01	0.02
S-2		0.00			0.14			0.05	
S-3		-0.002			0.00			-0.005	
S-4		0.00			0.00			0.00	

Table 5.8: Layer-wise magnetic moment (μ_B/atom) for 1 layer (S) of transition metal on Cu metal substrate. S and S-1 are $T_{1-x}M_x$ and $M_{1-x}T_x$ respectively. T and M stand for transition metal and metal atoms respectively. Here $M = Cu$ and $x = 0.10$ (rough interface).

Layers	Fe/Cu(001)			Co/Cu(001)			Ni/Cu(001)		
	μ_T	μ_M	μ_{avg}	μ_T	μ_M	μ_{avg}	μ_T	μ_M	μ_{avg}
S	2.52	-0.06	2.26	1.44	0.30	1.32	0.43	0.01	0.39
S-1	3.00	0.02	0.31	1.93	0.02	0.21	0.64	0.03	0.09
S-2		0.01			0.05			0.05	
S-3		-0.002			0.00			-0.005	
S-4		0.00			0.00			0.00	

Table 5.9: Layer-wise magnetic moment (μ_B/atom) for 1 layer (S) of transition metal on Au metal substrate. S and S-1 are $T_{1-x}M_x$ and $M_{1-x}T_x$ respectively. T and M stand for transition metal and metal atoms respectively. Here $M = Au$ and $x = 0.05$ (rough interface).

Layers	Fe/Au(001)			Co/Au(001)			Ni/Au(001)		
	μ_T	μ_M	μ_{avg}	μ_T	μ_M	μ_{avg}	μ_T	μ_M	μ_{avg}
S	2.99	-0.06	2.84	2.04	-0.14	1.93	0.54	-0.007	0.51
S-1	2.94	0.08	0.22	1.59	0.05	0.13	-0.55	-0.03	-0.05
S-2		0.04			0.16			0.05	
S-3		-0.008			-0.006			0.02	
S-4		0.00			0.00			0.00	

in lower energy region in Ni/Cu system. But in first Cu layer with Ni impurities, the amount of electronic states decreases with increase in Ni content. In the case of Ni/Cu system, the DOS for Cu-rich and Ni-rich layers match well with earlier study by KKR-CPA method [163]. In Ni rich layer, the peak near the Fermi level increases as reported earlier [164]. In all the three systems, with increase in Cu atoms in the transition metal layers, the average magnetic moment of the S layer decreases and the induced magnetic moment of the metals in S-1 layer increases. Unlike in Fe/Cu, the presence of different amount of Cu atom in transition metal overlayer in case of Co/Cu and Ni/Cu systems decreases the magnetic moment of the transition metal below its bulk magnetic moments. With interdiffusion of atoms at the interface, the magnetic moment of Co atoms is comparable to earlier report [93].

Tables 5.9 and table 5.10 represent the layerwise variation of magnetic moment with 5% and 10% interdiffusion of atoms at the interface, respectively for Au metal substrate. Figure 5.9 shows that with increase in amount of Au impurities on top most Fe overlayers, the amount of both spin-up and spin-down electronic states decrease gradually. There is slight change in spin-down electronic states at the lower energy region. Though there is negligible change in Fe magnetic moment on

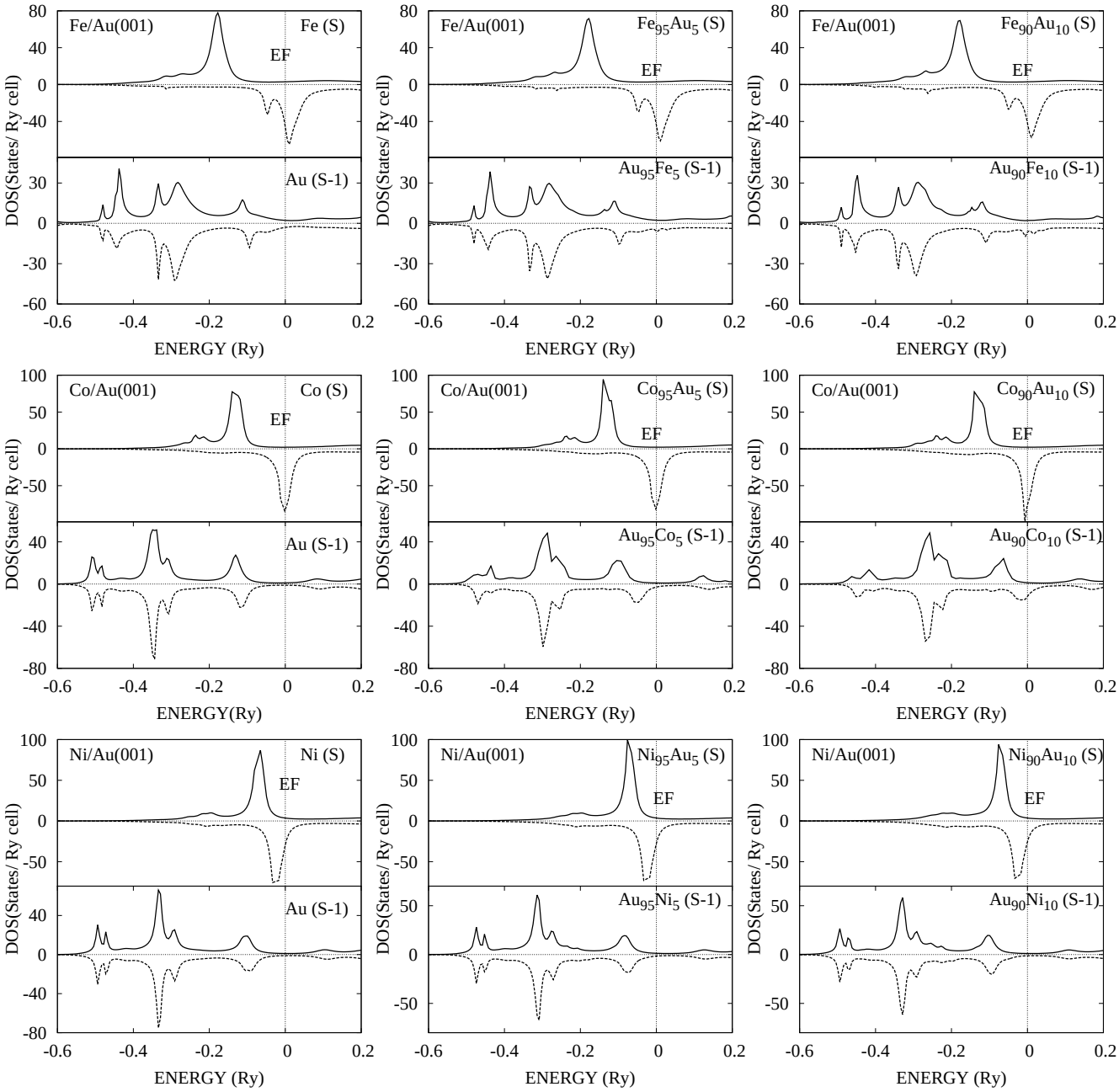

Figure 5.9: Layerwise spin polarized DOS for a single layer of transition metal deposited on Au substrate. S stands for top most layer of the interface and S-1 is the first substrate layer. Left panel : $x = 0$ (sharp interface), middle panel : $x = 0.05$ and right panel : $x = 0.10$ (rough interface). Solid line: Spin-up DOS. Dotted line: Spin-down DOS. Fermi level is reset at zero.

Table 5.10: Layer-wise magnetic moment (μ_B/atom) for 1 layer (S) of transition metal on Au metal substrate. S and S-1 are $T_{1-x}M_x$ and $M_{1-x}T_x$ respectively. T and M stand for transition metal and metal atoms respectively. Here $M = Au$ and $x = 0.10$ (rough interface).

Layers	Fe/Au(001)			Co/Au(001)			Ni/Au(001)		
	μ_T	μ_M	μ_{avg}	μ_T	μ_M	μ_{avg}	μ_T	μ_M	μ_{avg}
S	3.00	-0.05	2.70	1.84	-0.05	1.65	0.52	-0.03	0.47
S-1	2.59	0.12	0.37	1.87	0.07	0.25	-0.40	-0.05	-0.09
S-2		0.04			0.29			-0.006	
S-3		-0.008			0.002			0.01	
S-4		0.00			0.00			0.00	

top most layer but the average magnetic moment of the layer decreases for $Fe_{95}Au_5$ layer. With increase in the amount of Au impurity to 10% in Fe layer, average magnetic moment of the layer decreases further. The calculated average magnetic moment of Fe layer (S) with 5% and 10% Au atoms in Fe are 2.84 μ_B/atom and 2.70 μ_B/atom respectively which agrees with earlier study [50], as given in table 5.4. With increase in the amount of Fe impurity in Au layers, the average magnetic moment of first substrate layer increases (tables 5.9 and 5.10). The amount of both spin-up and spin-down electronic states changes with roughness at the interface in case of Co/Au. The peak of spin-up states decreases with increase in Au impurities from 5% to 10%. Therefore there is a decrement in magnetic moment of Co atom as well as average magnetic moment of the layer (tables 5.9 and 5.10). With increase in Co impurities in first Au substrate layer, the amount of induced magnetic moment increases. The spin-down electronic states of Ni overlayer gradually decreases with increase in Au impurities in case of Ni/Au. Both the spin-up and spin-down states of the first substrate layer decrease gradually with increase in Ni impurities. The magnetic moment of Ni atoms as well as average magnetic moment of the top most layer gradually decreases with increase in Au concentration.

Figures 5.10, 5.11 and 5.12 show the oscillatory behavior in the layerwise magnetic moments. The magnetic moments approaches zero at the fourth substrate layer in all the systems, except for Co/Cu which goes to zero at third substrate layer. The total DOS of the metal substrate approaches bulk DOS at the fourth layer down the top most layer in all the systems with both sharp and rough interfaces (figures 5.1, 5.2 and 5.3). Therefore metal substrates obtain their bulk electronic and magnetic properties at this layer.

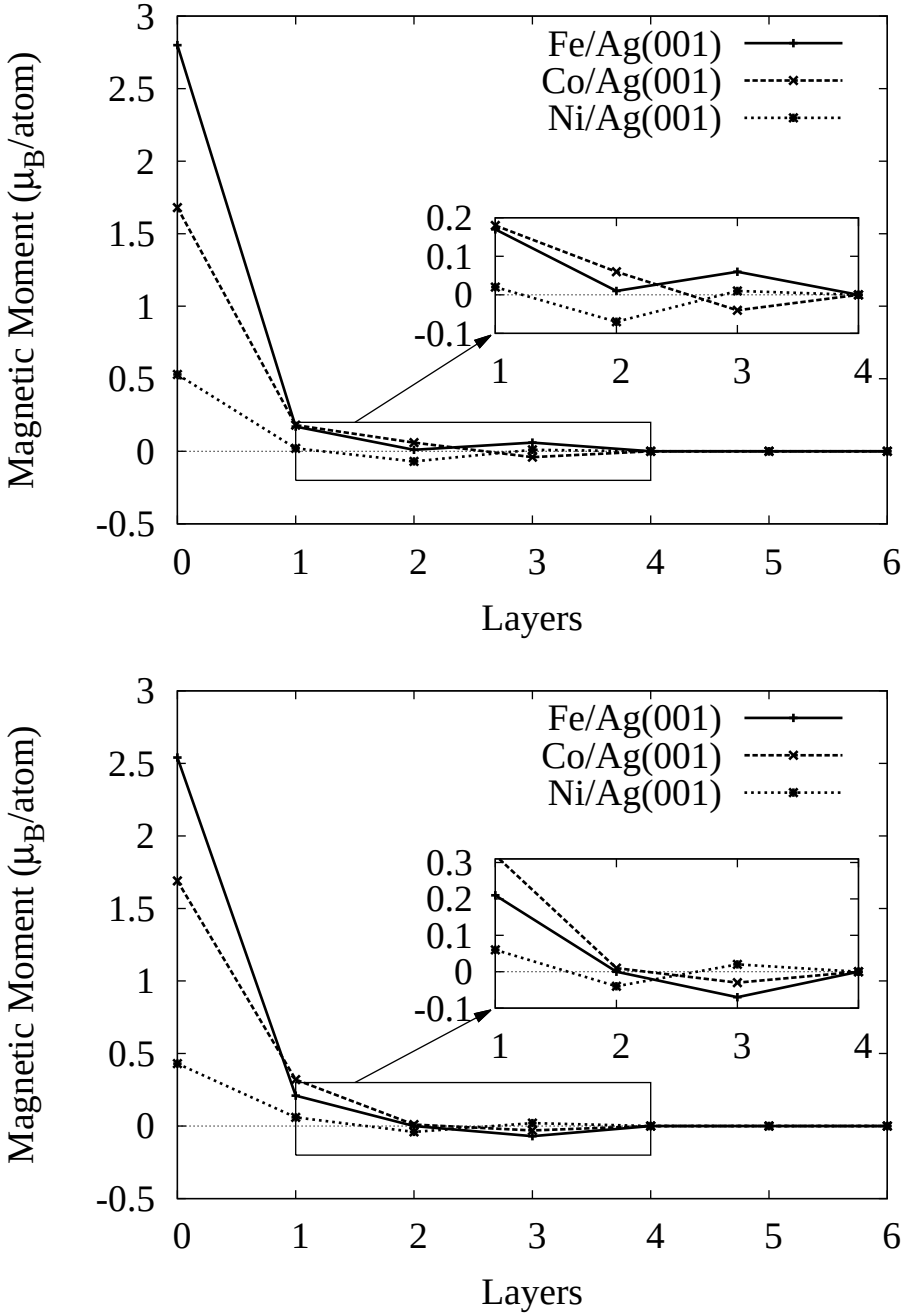

Figure 5.10: Layerwise variation of magnetic moment for a single layer of transition metal deposited on Ag substrate. x = 0.05 (top) and x = 0.10 (bottom). Layers 0 and 1 represent interface.

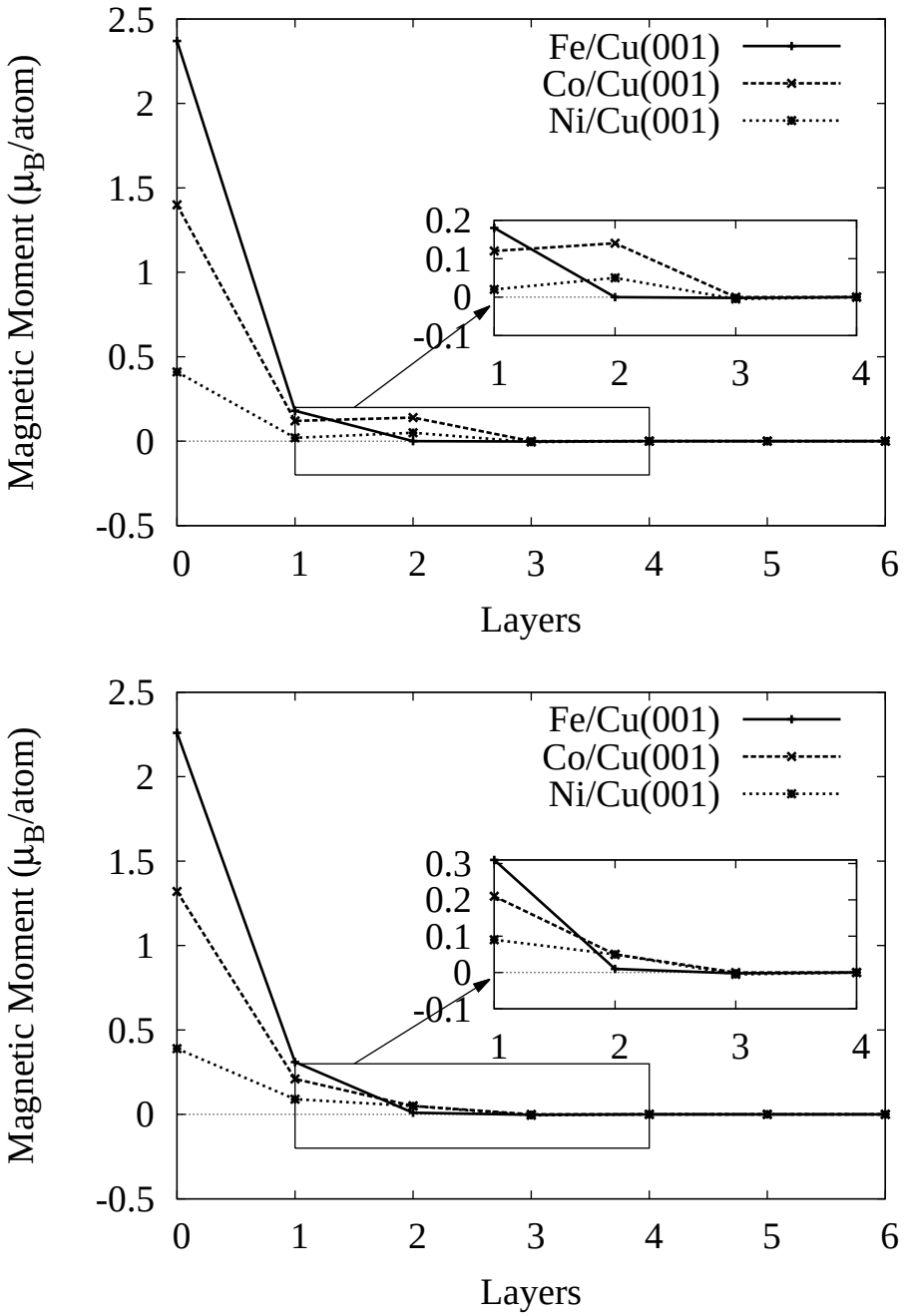

Figure 5.11: Layerwise variation of magnetic moment for a single layer of transition metal deposited on Cu substrate. x = 0.05 (top) and x = 0.10 (bottom). Layers 0 and 1 represent interface.

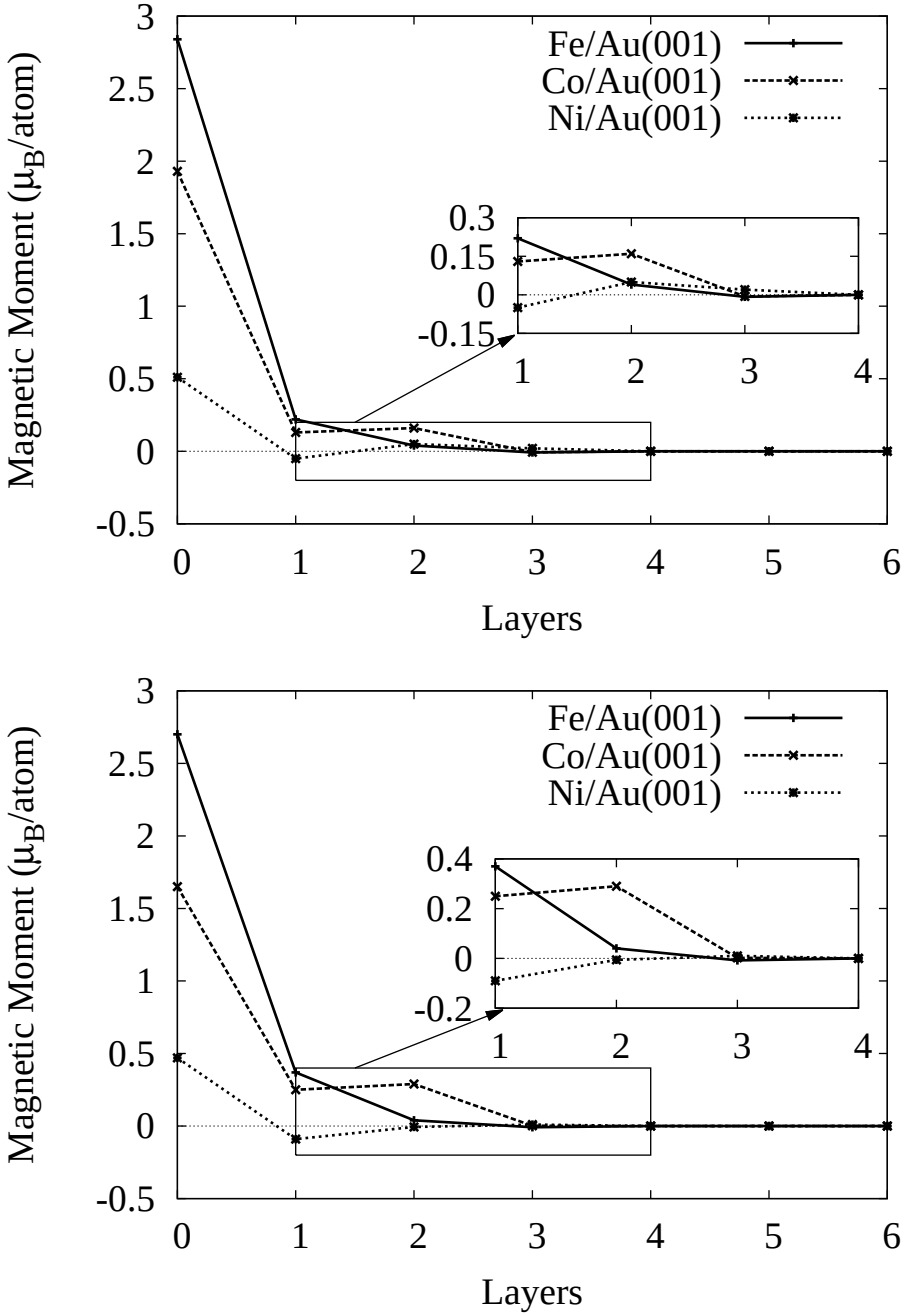

Figure 5.12: Layerwise variation of magnetic moment for a single layer of transition metal deposited on Au substrate. x = 0.05 (top) and x = 0.10 (bottom). Layers 0 and 1 represent interface.

5.2 Two Monolayers of Transition Metal on Metal Substrates

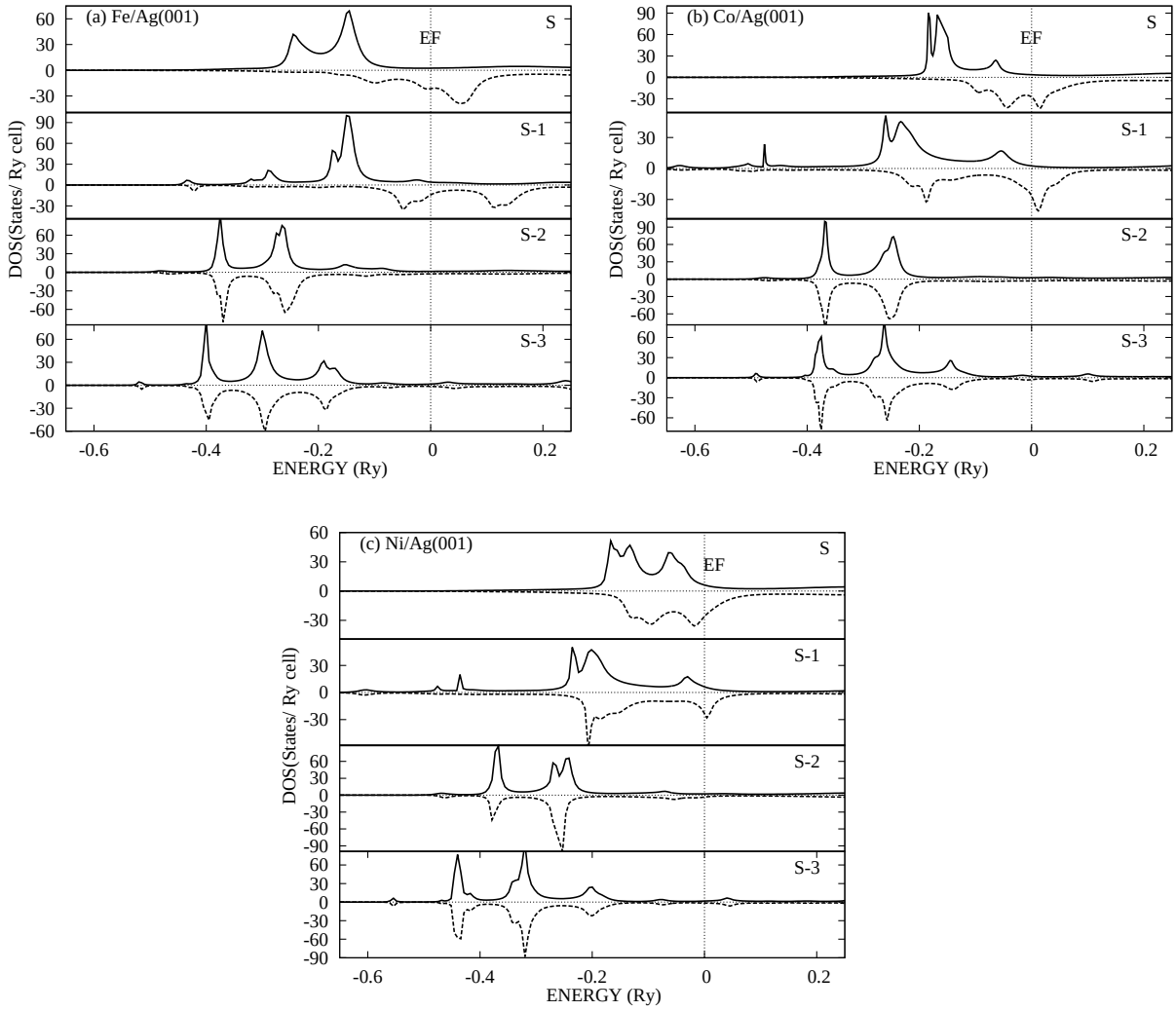

Figure 5.13: Layerwise variation of DOS for two monolayers of transition metal (Fe, Co and Ni) on Ag substrates. Solid curves: spin-up DOS and dashed curves: spin-down DOS. Vertical line at zero represents Fermi level.

We consider the growth of two monolayers of transition metals on semi-infinite metal substrates and carry out their electronic and magnetic properties. Figures 5.13, 5.14 and 5.15 show the layerwise spin polarized DOS for two layers of transition metal overlayers on Ag, Cu and Au substrates respectively. In all these systems, the width of the spin-down electronic states is more than that of the spin-up electronic states for the transition metal layers (S and S-1). The difference in band width for spin-up

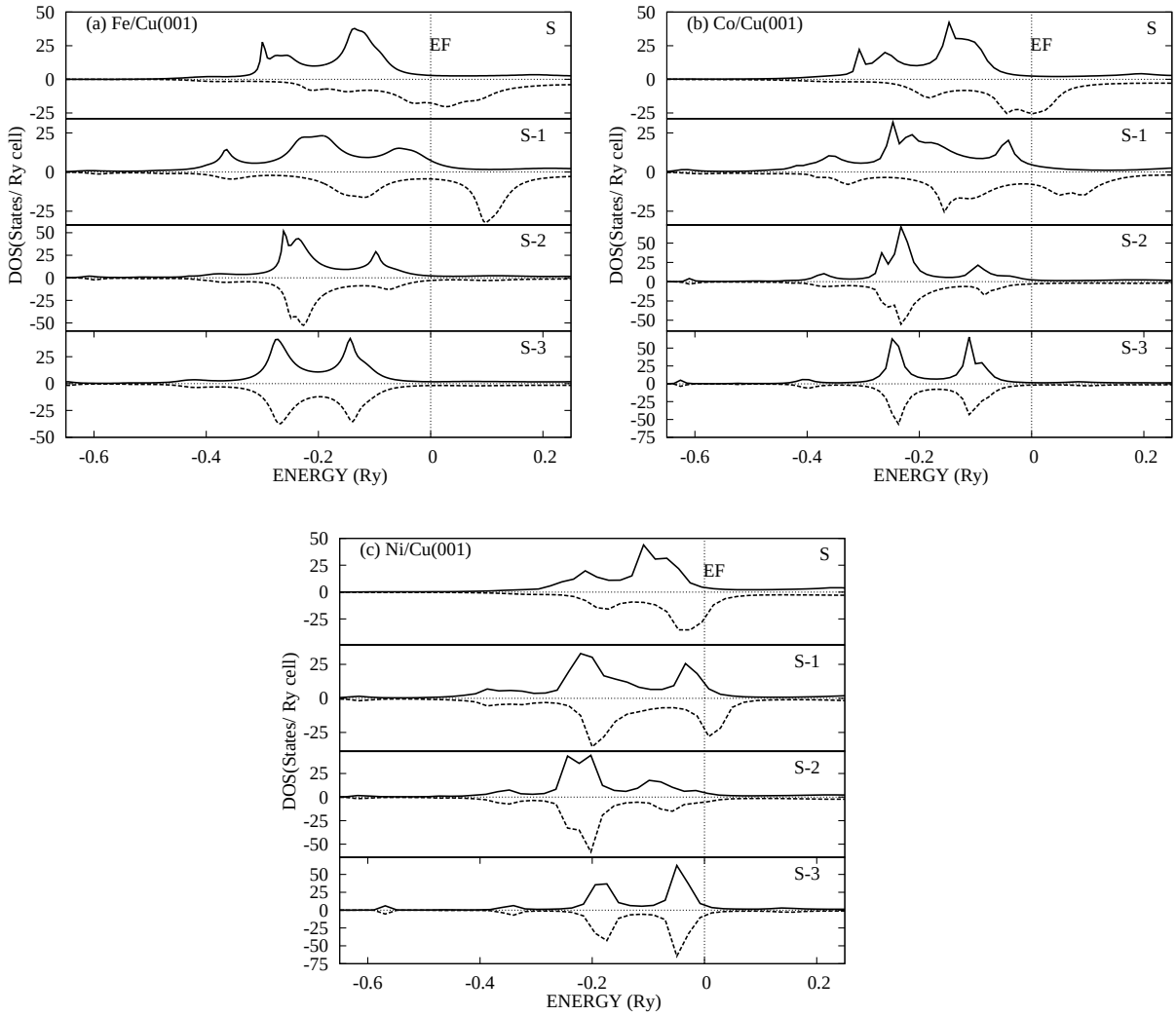

Figure 5.14: Layerwise variation of DOS for two monolayers of transition metal (Fe, Co and Ni) on Cu substrates. Solid curves: spin-up DOS and dashed curves: spin-down DOS. Vertical line at zero represents Fermi level.

and spin-down electronic states decreases from Fe to Ni. The splitting of spin-up and down states are more on surface layer than the subsurface layers. The band narrowing occurs at the surface layer. This is due to reduction of nearest neighbors at the surface. Hence the magnetic moment is maximum at the top most layer (tables 5.11, 5.12 and 5.13). In the subsurface layer (S-1), band width increases due to increase in the nearest neighbors. Therefore there is increase in hybridization which results in reduction of magnetic moment. The spin DOS of surface Fe layer for two layers of Fe on Cu substrate matches well with earlier study using FPLAPW

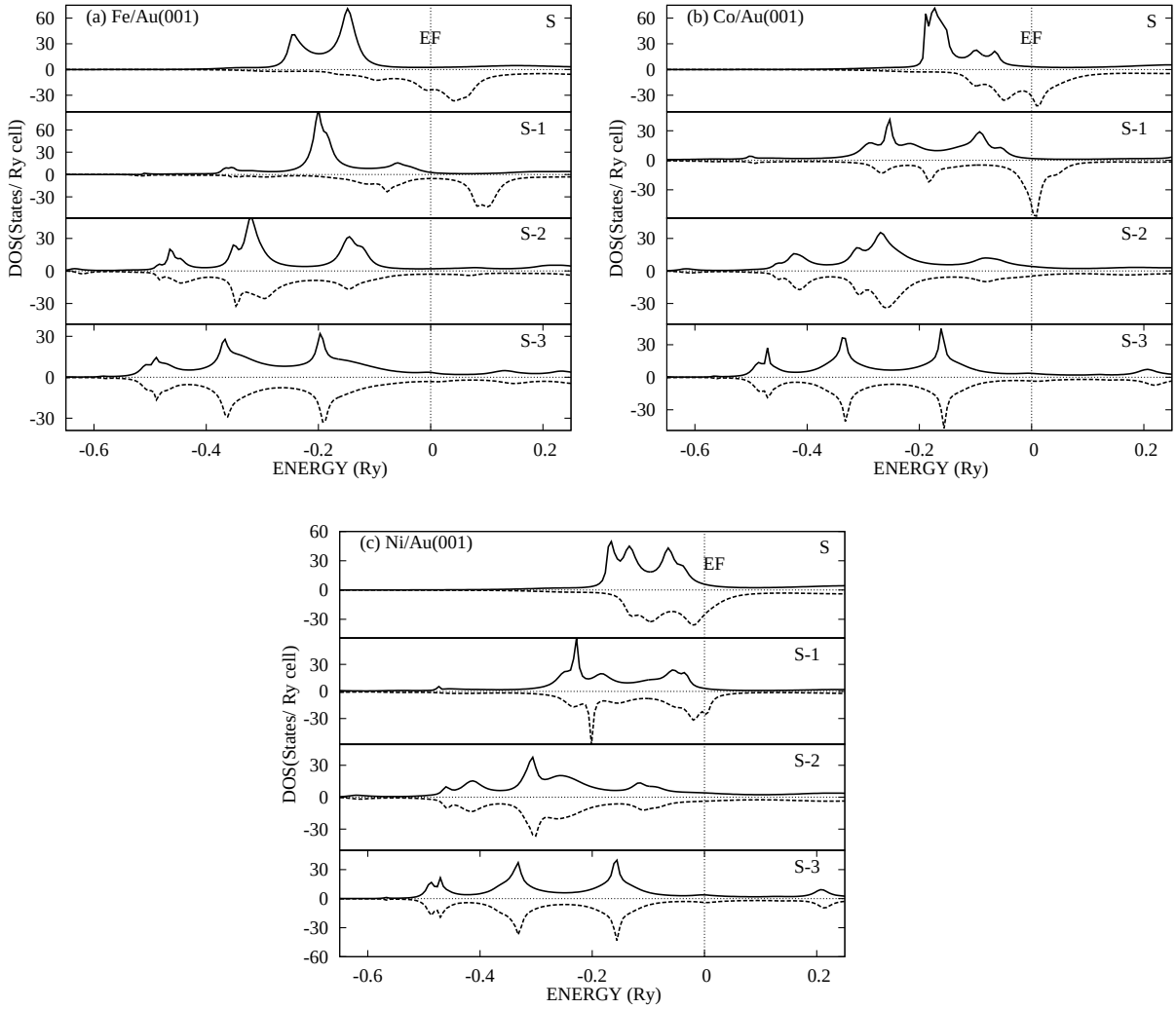

Figure 5.15: Layerwise variation of DOS for two monolayers of transition metal (Fe, Co and Ni) on Au substrates. Solid curves: spin-up DOS and dashed curves: spin-down DOS. Vertical line at zero represents Fermi level.

method [66].

The layered based magnetic moment for these systems are tabulated in tables 5.11, 5.12 and 5.13. The spin-up electronic states contribute more towards the magnetic moment of top two transition metal layers. Magnetic moment at the fourth layer down the top most layer becomes zero for Ag and Cu based systems. Hence metal substrates obtain their bulk magnetic properties at the fourth layer down the top most layer like one ML deposition. But in case of Au based systems, the magnetic moment ceases to zero at the fifth layer down the top most layer (table 5.13

Table 5.11: Layer-wise magnetic moment (μ_B/atom) for two layers of transition metal on Ag metal substrate for sharp interface ($x = 0$). Numbers in square brackets represent reference numbers.

Layers	Fe/Ag	Co/Ag	Ni/Ag
S	2.992 2.94 [13, 40, 60, 61]	2.01	0.70
S-1	2.75 2.63 [13, 40, 60, 61]	1.55	0.53
S-2	0.02	-0.02	-0.03
S-3	-0.16	0.12	0.02
S-4	0.00	0.00	0.00

Refs [13, 40, 60, 61] used FPLAPW method

Table 5.12: Layer-wise magnetic moment (μ_B/atom) for two layers of transition metal on Cu metal substrate for sharp interface ($x = 0$). Numbers in square brackets represent reference numbers.

Layers	Fe/Cu	Co/Cu	Ni/Cu
S	2.48 2.85 [40, 66] 2.84 [60],2.83 [67]	1.65	0.70 0.69 [9, 41] 0.68 [68]
S-1	2.47 2.60 [40, 60, 66] 2.58 [67]	1.61	0.64 0.48 [9, 41] 0.47 [68]
S-2	0.02	0.18	0.01
S-3	-0.004	0.19	-0.08
S-4	0.00	0.00	0.00

Refs. [9, 40, 41, 60, 66–68] used FPLAPW method.

Table 5.13: Layer-wise magnetic moment (μ_B/atom) for two layers of transition metal on Au metal substrate for sharp interface ($x = 0$).

Layers	Fe/Au	Co/Au	Ni/Au
S	3.00	1.87	0.68
S-1	2.96	1.45	0.42
S-2	0.02	0.02	-0.003
S-3	0.005	0.04	0.01
S-4	0.00	0.003	0.001
S-5	0.00	0.00	0.00

and figure 5.16). Table 5.12 shows that the calculated magnetic moment for top two layers in case of Fe/Cu are small compared to earlier reported values by FPLAPW method [40, 60, 66, 67]. The first-layer moment is substantially greater than that of the deeper layers. This result agrees with earlier study using FP-LMTO method [75]. The magnetic moment of the top most layer in the case of Ni/Cu system agrees well with the earlier studies [9, 41, 68], but it is small in the case of second Ni layer. The reasons for this reduction in interface Ni magnetic moment is due to the charge transfer into the d-bands of the interfacial Ni layer from Cu layer, and also the core level shift of surface Ni atom relative to interface Ni atom [41]. The reduction of Ni magnetic moment at the interface is supported by earlier work using tight-binding hamiltonian with the exchange interaction in the single-site approximation [94] and self consistent local orbital method [72]. Unlike one ML of Ni on Ag, the magnetic moment of the top most layer in this case is more compared to smooth fcc Ni(001) surfaces. The magnetic moment of the top most layer in case of Fe/Au is more than that of smooth bcc Fe(001) surface.

It is worth comparing the magnetic moment for the two cases, one ML and two ML transition metal deposition. It is clear that the magnetic moment of the top layer decreases in the case of two layers of transition metals than that of one ML deposition in Fe/Ag and Co/Ag. The splitting of electronic states decreases

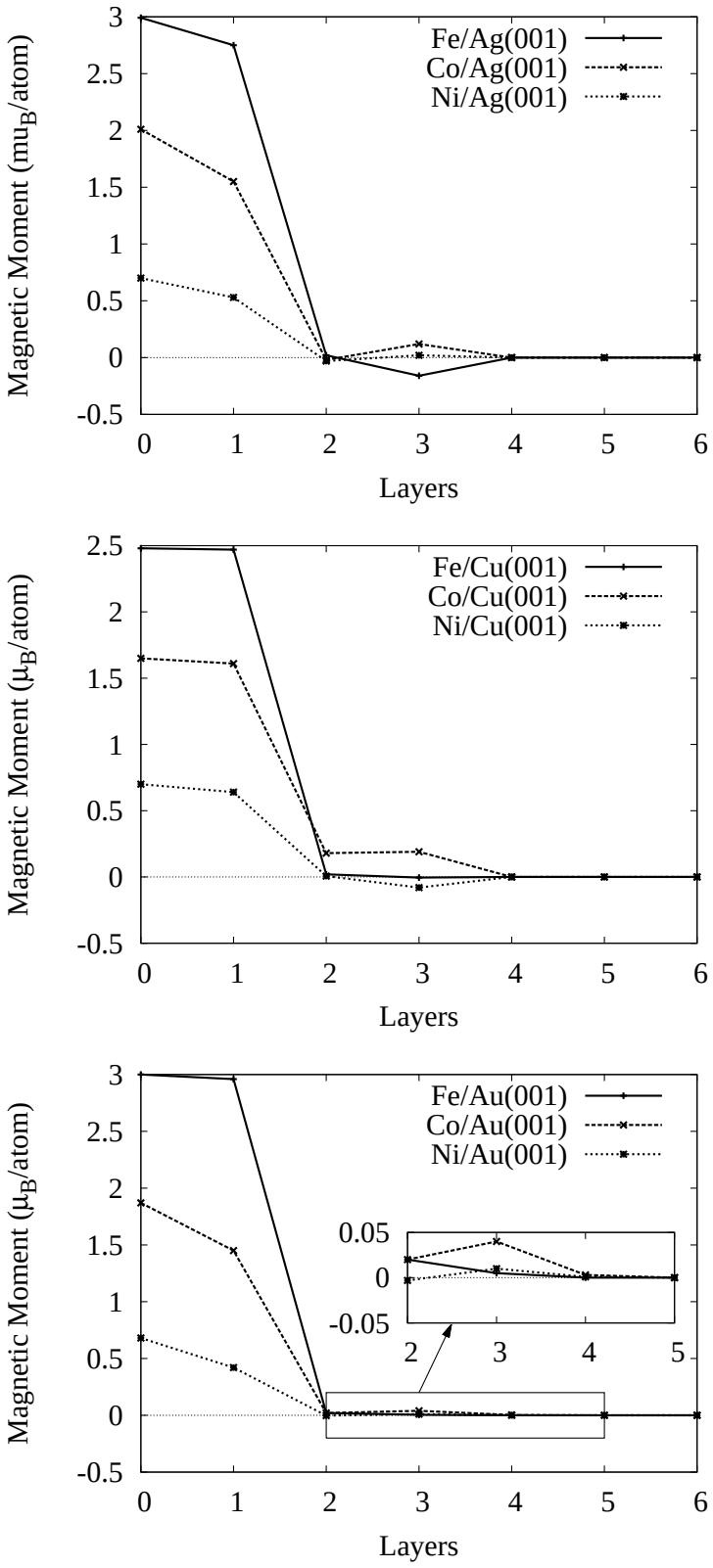

Figure 5.16: Layerwise variation of magnetic moment for 2 ML of transition metal on metal substrates. Layer 0 represents surface layer.

and hybridization increases at the layer S-1. Therefore the magnetic moment at the interface (S-1 layer) for two layer deposition is less than the magnetic moment at the interface (S layer) for one layer deposition. The induced magnetic moment on the first substrate layer is less for two ML case. Magnetic moment of the top layer decreases for two ML case than one ML case of Fe/Cu unlike Co and Ni on Cu substrates. As the splitting of electronic states decreases and the hybridization increases, the magnetic moment of top two transition metal layers are more than the magnetic moment of top layer for one ML case for Co/Cu and Ni/Cu. The induced magnetic moment at the first substrate layer is more for the two ML case except for Fe/Cu. In the case of Fe/Au, magnetic moment of the top layer remains same for both one and two ML of transition metal overlayers. Whereas in case of Co/Au, magnetic moment of top layer for two ML case is less than that of one ML case. In Ni/Au, magnetic moment of top layer with two ML deposition is more than one ML. The layerwise magnetic moments show oscillatory behavior as we go down from the surface (figure 5.16) except for Fe/Cu(001) and Fe/Au(001).

5.3 Interface of Two Layers of Transition Metal and Two Layers of Metal Substrate

To model a more realistic alloyed interface, we define an interface as four atomic layers, two from transition metal side and two from metal substrate side. In these four layers, the transition metal atoms and metal atoms interdiffuse into each other. Therefore the interface is defined by four layers I+2, I+1, I-1 and I-2. The host atom at layers I+2 and I+1 is transition metal atom, whereas the host at layers I-1 and I-2 is substrate metal atom. The composition of the alloyed interface at different layers from top to bottom are $T_{95}M_5$, $T_{90}M_{10}$, $M_{90}T_{10}$ and $M_{95}T_5$ respectively. T stands for transition metal atom and M for metal substrate atom. The compositions shown in the subscripts are in terms of percentage value. There are total four layers of transition metals deposited on semi-infinite metal substrates.

Figure 5.17 shows the effect of interdiffusion of atoms at the interface for Fe deposited on Ag(001) substrate. The spin DOS of the top most (layer I+4) Fe layer is equivalent to that for two layers of Fe on Ag substrate (figure 5.13). As we go down, the change in these electronic states is prominent. Further going down to I+2 layer, the electronic states at the lower energy region is significant. This is because of the presence of Ag impurities. As the Ag impurities in Fe layers increases from 5% to 10%, there is significant change in both spin-up and spin-down DOS. With addition of Ag impurities, the magnetic moment of Fe atoms in I+2 layers increases compared to nearest Fe layer (I+3). With increase in Ag amount in Fe layer, the spin-up states near the Fermi level increases and spin-down states decreases. This reduces the average magnetic moment of I+1 layer compared to I+2 layer. But in Ag layers with Fe impurities, the peaks are shifted towards the lower energy region as that in bulk Ag. Comparing with bulk Ag DOS (figure 5.1), in I-1 layer a peak in spin-down states near Fermi level is missing due to Fe content in that layer, which contribute towards the magnetic moment. The splitting of spin-up and spin-down

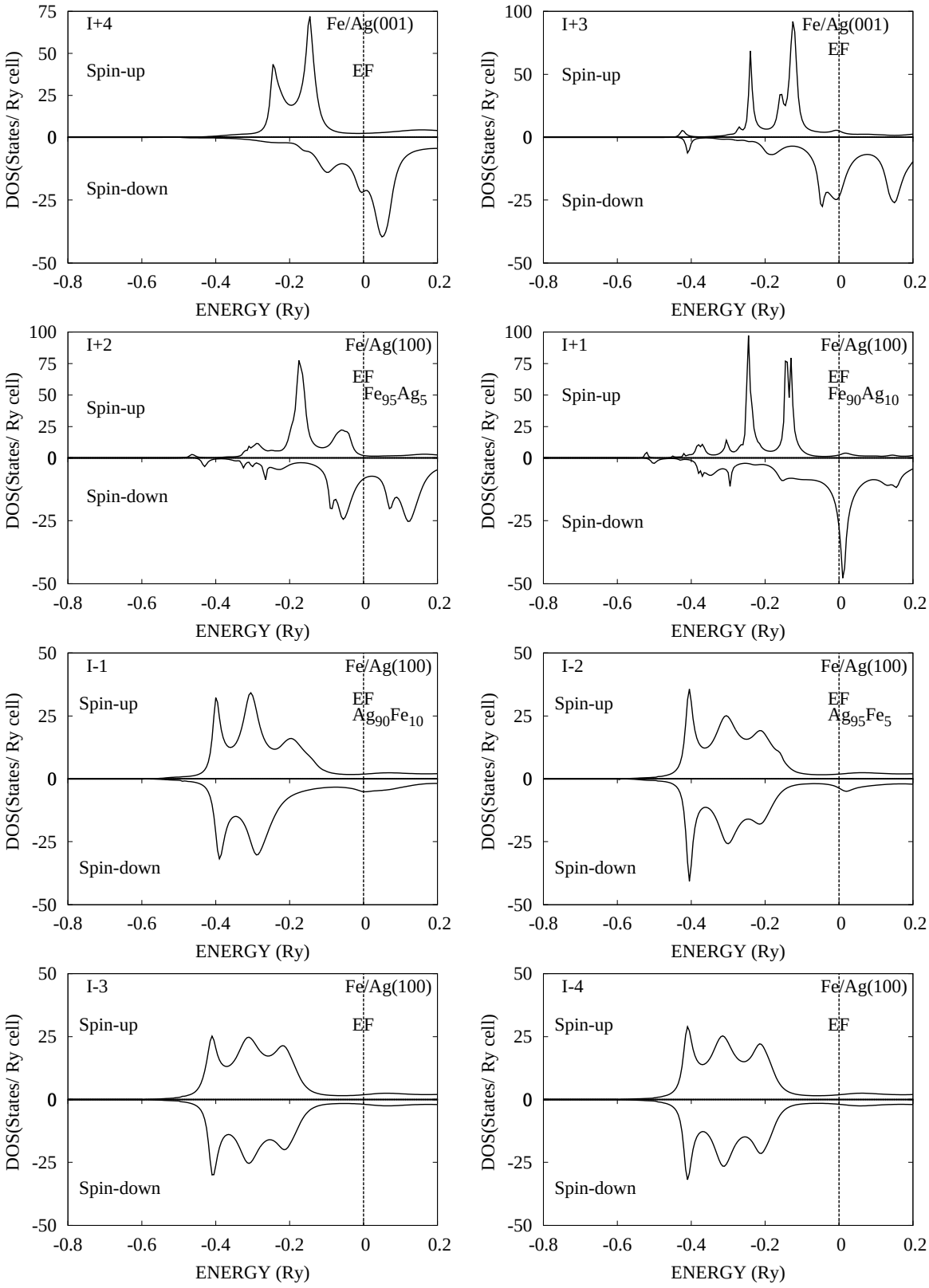

Figure 5.17: Layerwise variation of spin DOS at Fe/Ag(001) with rough alloyed interface. Vertical line represents Fermi level.

states decrease in these regions (I-1 and I-2 layers). As the Fe content is more at I-1 layer therefore average magnetic moment is also more at this layer than I-2 layer (table 5.14). The bulk Ag DOS is obtained at the fourth substrate layer (I-4) from interface.

The spin-up and spin-down electronic states are more on top most Co layer in case of Co/Ag (figure 5.18). It decreases at the next layer. Therefore Co magnetic moment decreases (table 5.14). When Ag impurities increase from 5% to 10%, spin-up states becomes more significant but spin-down states decreases (figure 5.18). The states away from the Fermi energy are more affected with addition of Ag atoms in Co atomic layers. The magnetic moment of Co atom as well as average magnetic moment at the I+1 layer is less than bulk Co magnetic moment (table 5.14). At the Ag atomic layers with different amount of Co impurities, spin DOS approaches towards bulk Ag DOS and attains bulk DOS at the fourth layer (I-4) from the interface. The spin DOS of I-4 layer for Fe/Ag and Co/Ag are equivalent.

When Ni atoms are grown on Ag(001) surface, the spin resolved DOS of the top most layer (figure 5.19) is equivalent to that of two ML deposition case (figure 5.13). There is significant change in electronic states as we go down from the top most layer. An extra peak appears at low energy region. The band narrowing occurs and the states near Fermi level show maximum change at I+2 layer with 5% of Ag impurities. With increase in Ag impurity to 10%, the electronic states near Fermi level increases further and some significant change is also visible at the low energy region due to presence of Ag atoms. The magnetic moment of I+1 layer is less than the Ni bulk magnetic moment (table 5.14). The states near Fermi level changes due to decrease in Ni concentrations as we go away from the interface. DOS approaches bulk value at the fourth Ag layer.

Figure 5.20 shows layerwise spin resolved DOS for Fe deposited on Cu substrate along (001). It clearly shows the effect of interdiffusion of atoms at the interface.

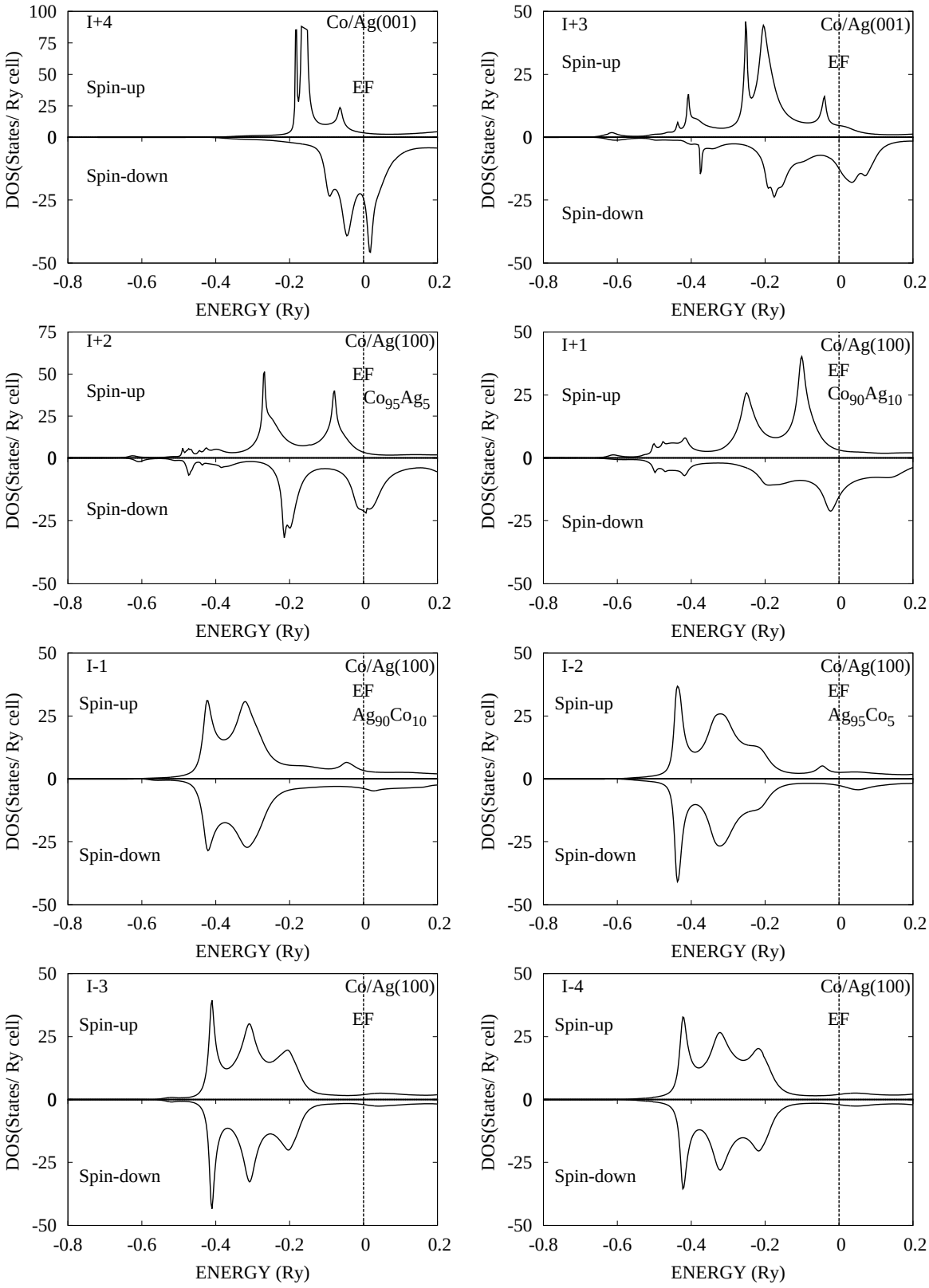

Figure 5.18: Layerwise variation of spin DOS at Co/Ag(001) with rough alloyed interface. Vertical line represents Fermi level.

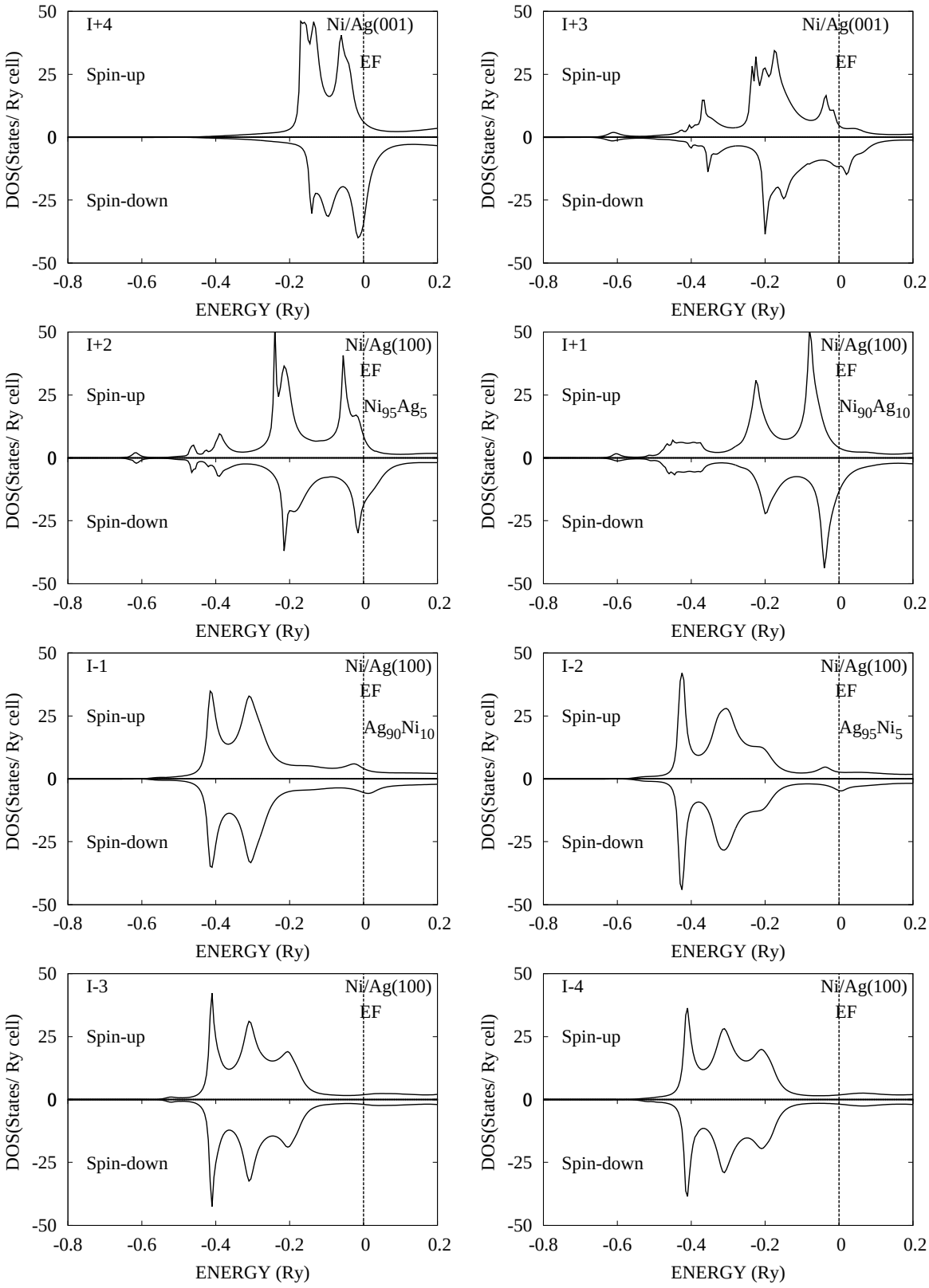

Figure 5.19: Layerwise variation of spin DOS at Ni/Ag(001) with rough alloyed interface. Vertical line represents Fermi level.

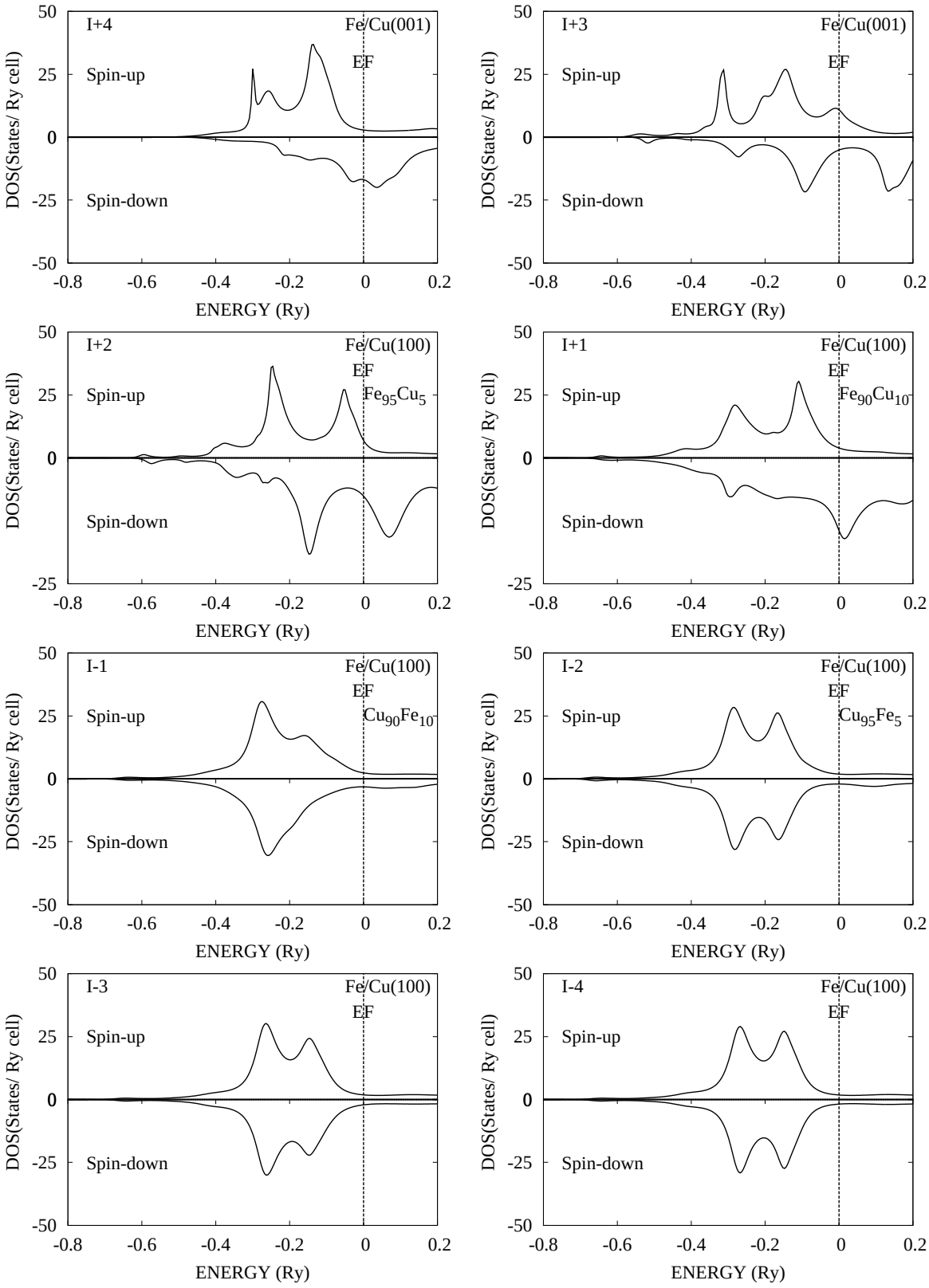

Figure 5.20: Layerwise variation of spin DOS at Fe/Cu(001) with rough alloyed interface. Vertical line represents Fermi level.

The spin DOS of the top most (I+4) Fe layer is equivalent to the top layer spin DOS for two ML case. This means Cu atoms do not have any effect on DOS of Fe at the top layer for two or more layers of Fe on Cu. Both spin-up and down electronic states show significant change due to the presence of Cu impurities at I+2 layer. There is significant change in electronic states when Cu impurities in Fe layers increase from 5% to 10%. The magnetic moment of Fe atoms at I+2 layers increases compared to nearest Fe layer (I+3) (table 5.15). Spin-down states decreases with increase in Cu amount. This reduces the average magnetic moment of I+1 layer compared to I+2 layer. But in Cu layers with Fe impurities, the peaks are shifted towards the lower energy region as for the bulk Cu. Comparing with bulk DOS of Cu (figure 5.2), a peak in spin-down states near Fermi level is missing due to Fe content at I-1 layer. This contributes towards the magnetic moment. The splitting of spin-up and down states decreases in these regions (I-1 and I-2 layers). Since Fe content is more at I-1 layer, therefore average magnetic moment is also more at this layer than I-2 layer (table 5.15). Bulk DOS of Cu is obtained at the fourth substrate layer (I-4) from interface.

Figure 5.21 shows the layerwise variation of spin resolved DOS for Co deposited on Cu(001) substrate. It shows the effect of the interdiffusion of atoms at the interface. The DOS of top layer is equivalent to the surface DOS with two ML case. This shows Cu substrate does not affect the surface DOS of Co when two or more layers of Co deposited on Cu substrates. As we go down to the next layer (I+3), there is significant change in both spin-up and spin-down states at the Fermi level. An extra peak at the Fermi level helps to reduce the magnetic moment of this layer. The spin-up states shifted towards the lower energy region in the next layer with 5% of Cu impurities in Co layer. Therefore the Co magnetic moment as well as average magnetic moment are more than the surface magnetic moment. With further increase in Cu impurities to 10%, the Co magnetic moment and average magnetic moment decreases (table 5.15). In other side of the interface, in Cu layer

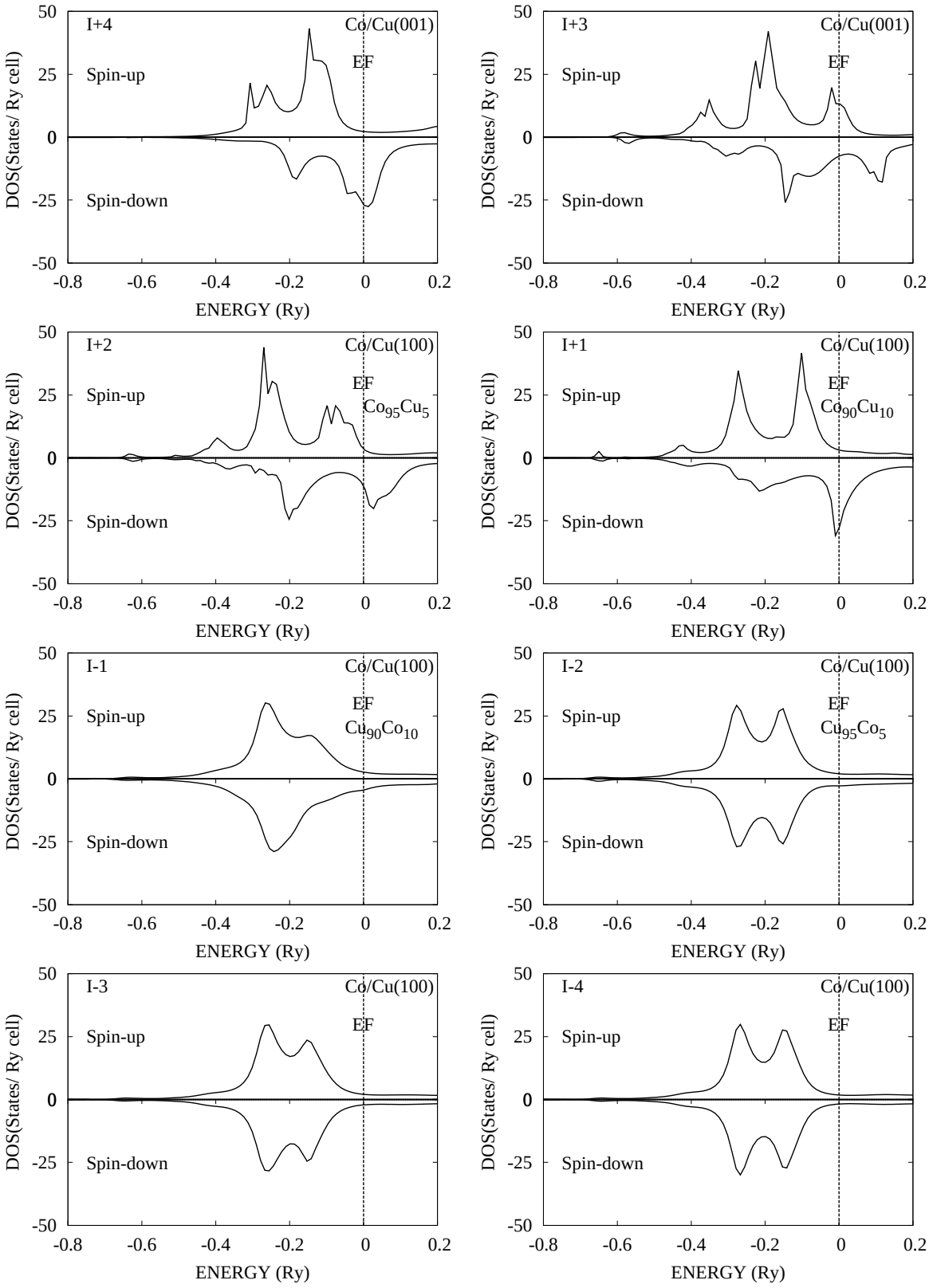

Figure 5.21: Layerwise variation of spin DOS at Co/Cu(001) with rough alloyed interface. Vertical line represents Fermi level.

with Co impurities, the spin-up electronic states has an extra peak comparison to spin-down states. It is due to the presence of 10% Co impurities. As the amount of impurities decreases in the next layer to 5%, the amount of induced magnetic moment decreases. Bulk Cu DOS is obtained at the fourth layer from the interface.

Figure 5.22 shows the layerwise variation of spin DOS for Ni deposited on Cu(001). There is no significant change in top layer spin DOS as compared to the case of two ML deposition (figure 5.14). This shows that Cu substrate do not have any effect on the surface Ni DOS beyond two ML of Ni. At the next layers (I+3 and I+2), the electronic states at the lower energy are more affected due presence of some amount of Cu in I+2 layer. Unlike Co/Cu, the transition metal magnetic moment as well as the average magnetic moment of I+2 layer is less than the surface magnetic moment (table 5.15). The spin DOS of I-1 layer with 10% Ni impurities, resembles with that for Fe/Cu (figure 5.20) and Co/Cu (figure 5.21). The induced magnetic moment in Cu layer decreases with decrease in Ni content in Cu layer. DOS approaches the bulk value and magnetic moment becomes negligible at the fourth layer substrate from the interface. Hence Cu atoms obtains its bulk properties at the fourth substrate layer.

Figure 5.23 shows the layerwise spin resolved DOS for Fe on Au(001) substrate. It shows the effect of interdiffusion of atoms at the interface. The spin DOS of the top most (I+4) Fe layer is equivalent to that of two ML case. The spin-up electronic states at the lower energy region becomes significant in I+2 layer. This is because of the presence of Au impurities. As the Au impurities in Fe layers increases from 5% to 10%, there is significant change in both spin-up and spin-down DOS. With addition of Au impurities, the magnetic moment of Fe atoms at I+2 layers increases compared to nearest Fe layer (I+3). With increase in Au amount in Fe layer, the spin-up states near the Fermi level increases and spin-down states is maximum at the Fermi level. This reduces the average magnetic moment of I+1 layer in comparison to I+2 layer. In Au layers with Fe impurities, the peaks are shifted towards the

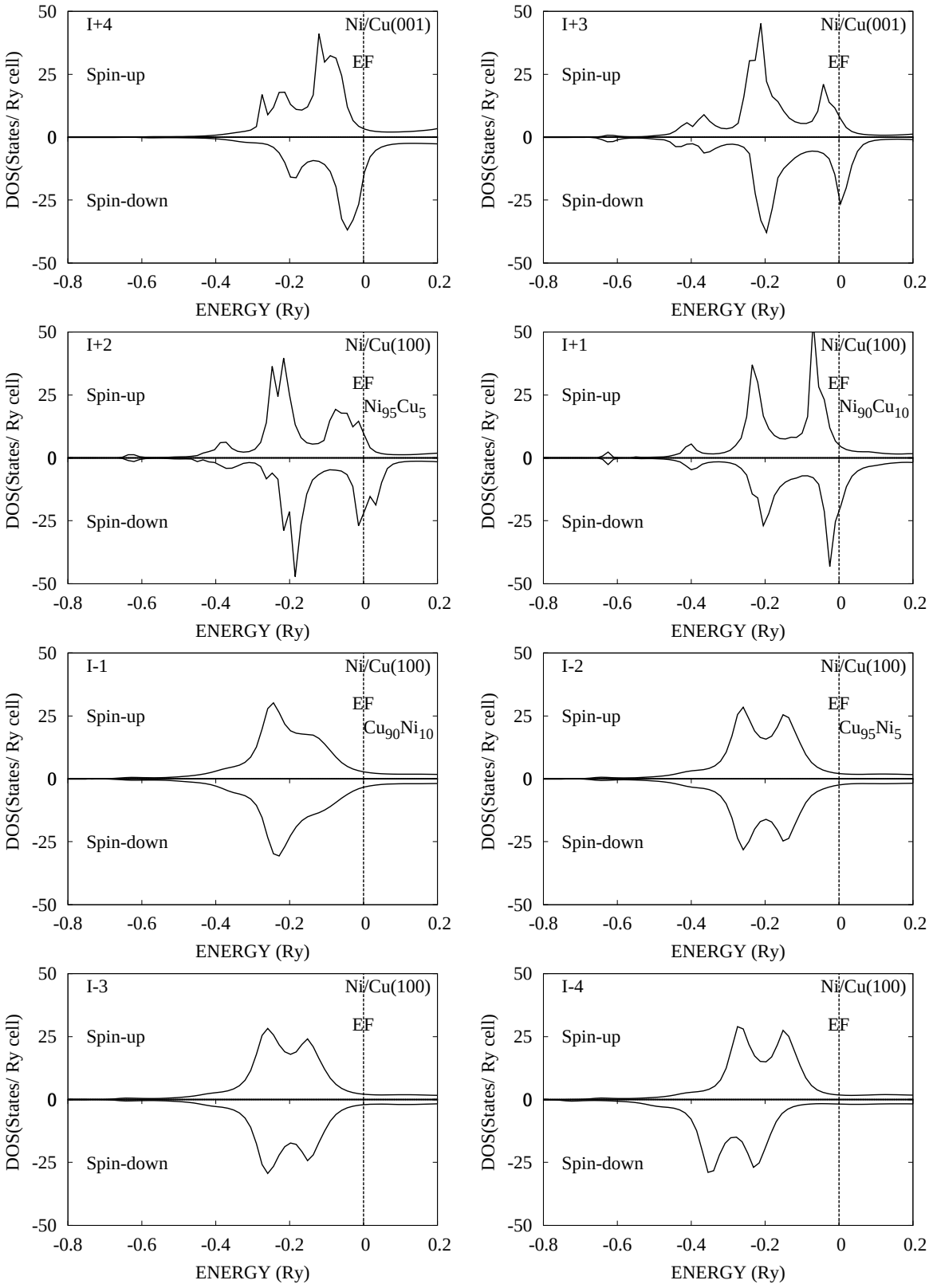

Figure 5.22: Layerwise variation of spin DOS at Ni/Cu(001) with rough alloyed interface. Vertical line represents Fermi level.

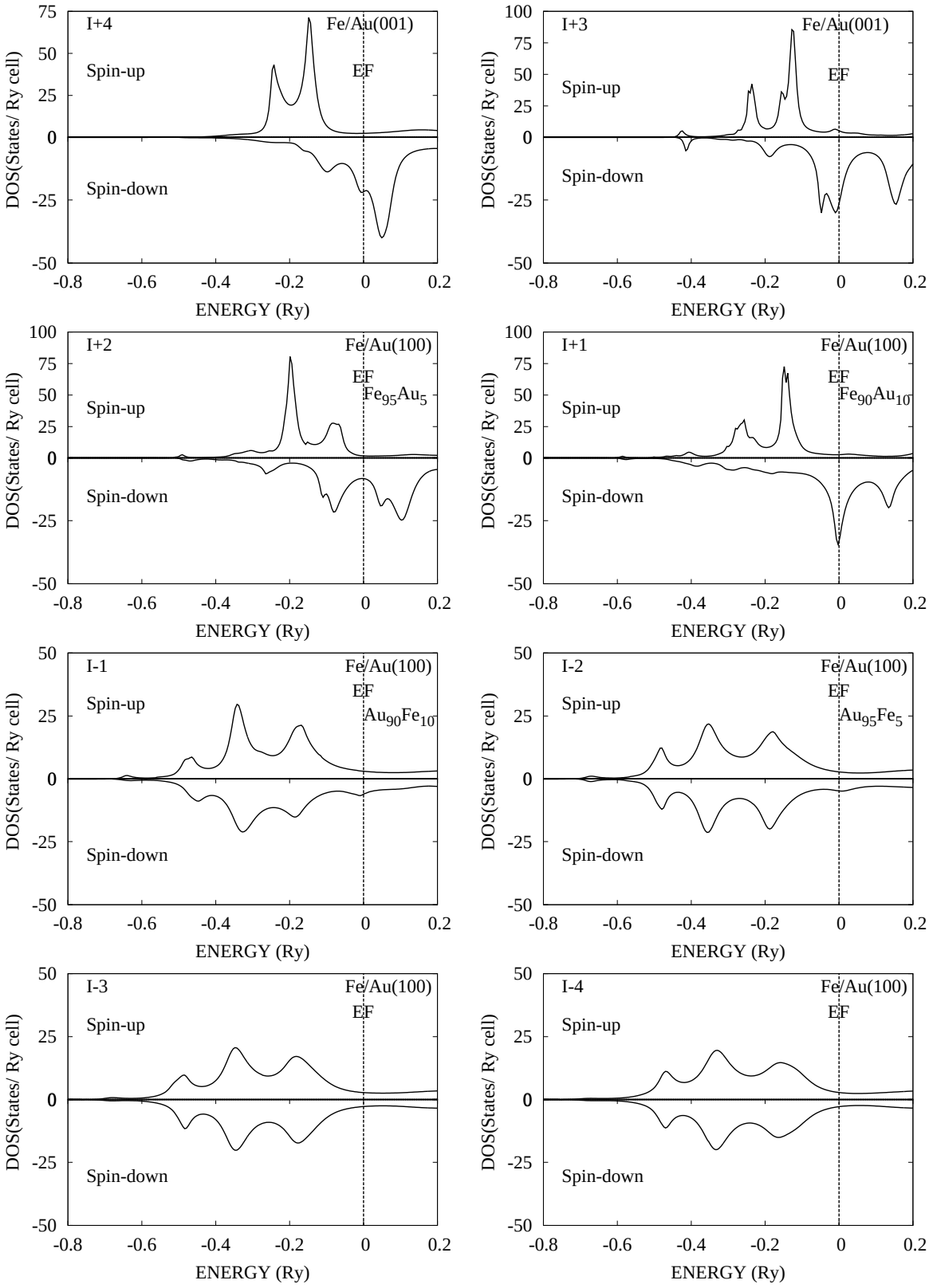

Figure 5.23: Layerwise variation of spin DOS at Fe/Au(001) with rough alloyed interface. Vertical line represents Fermi level.

lower energy region as for the bulk Au. The splitting of spin-up and spin-down states decreases in these regions (I-1 and I-2 layers). Since Fe content is more at I-1 layer therefore average magnetic moment is also more at this layer than I-2 layer (table 5.16). Bulk Au DOS is obtained at the fifth substrate layer (I-5) from interface. The DOS of Fe rich I+1 and Au rich I-1 layers match well with earlier work [56].

The up and down spin electronic states are more at Co top layer in case of Co/Au system. The states decrease at the next layer which reduces the Co magnetic moment. When Au impurities increases from 5% to 10% the spin-up states contribute more to magnetic moment than the spin-down states (figure 5.24). In the region away from Fermi level, electronic states are more affected with increase of Au atoms at Co atomic layers. The magnetic moment of Co atom as well as average magnetic moment at the I+1 layer is less than the bulk Co magnetic moment. DOS attains bulk Au DOS at the fifth substrate layer (I-5) from the interface. With the decrease in Co content in the Au layers the average magnetic moment gradually decreases and becomes zero at the fifth layer (I-5) from the interface (table 5.16).

In the case of Ni/Au (figure 5.25), the top layer spin resolved DOS in this case is equivalent to top layer spin resolved DOS for two ML case. This shows DOS of top most layer does not depend on the number of Ni layers when more than one Ni layers are deposited. This is also true for magnetic moment. There is significant change in electronic states, as we go down from the top most layer. An extra peak appears at low energy region. The band narrowing occurs for the I+2 layer with 5% Au impurities and the states near Fermi level show maximum change. With further increase in Au impurities to 10%, the electronic states near Fermi level increases further and decreases at the low energy region due to presence of Au atoms. The magnetic moment of I+1 layer is less than the Ni bulk magnetic moment. In the substrate layers with Ni impurities, the DOS approaches bulk DOS as we go away from the interface. At the fifth Au layer from the interface (I-5), the DOS becomes

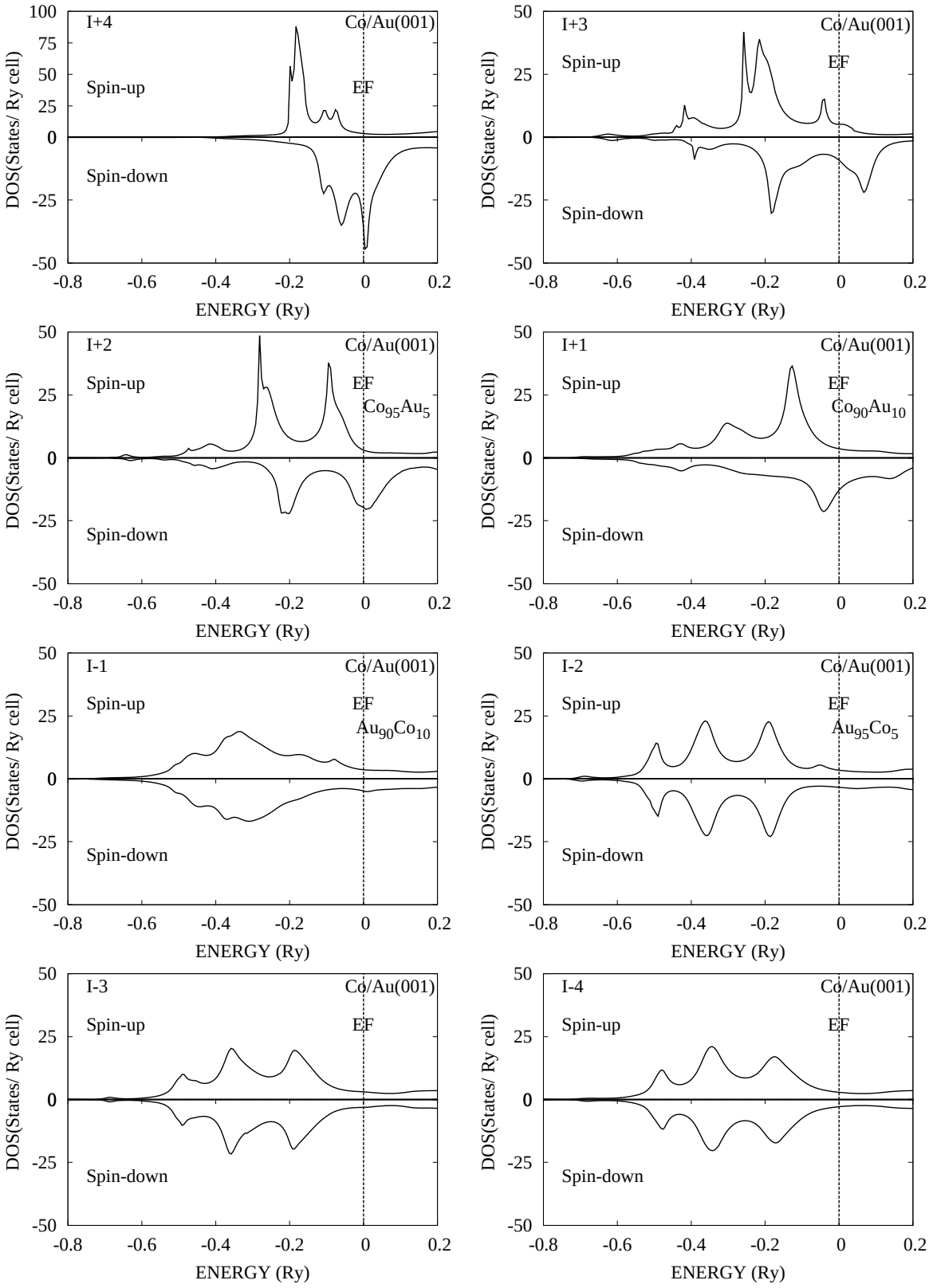

Figure 5.24: Layerwise variation of spin DOS at Co/Au(001) with rough alloyed interface. Vertical line represents Fermi level.

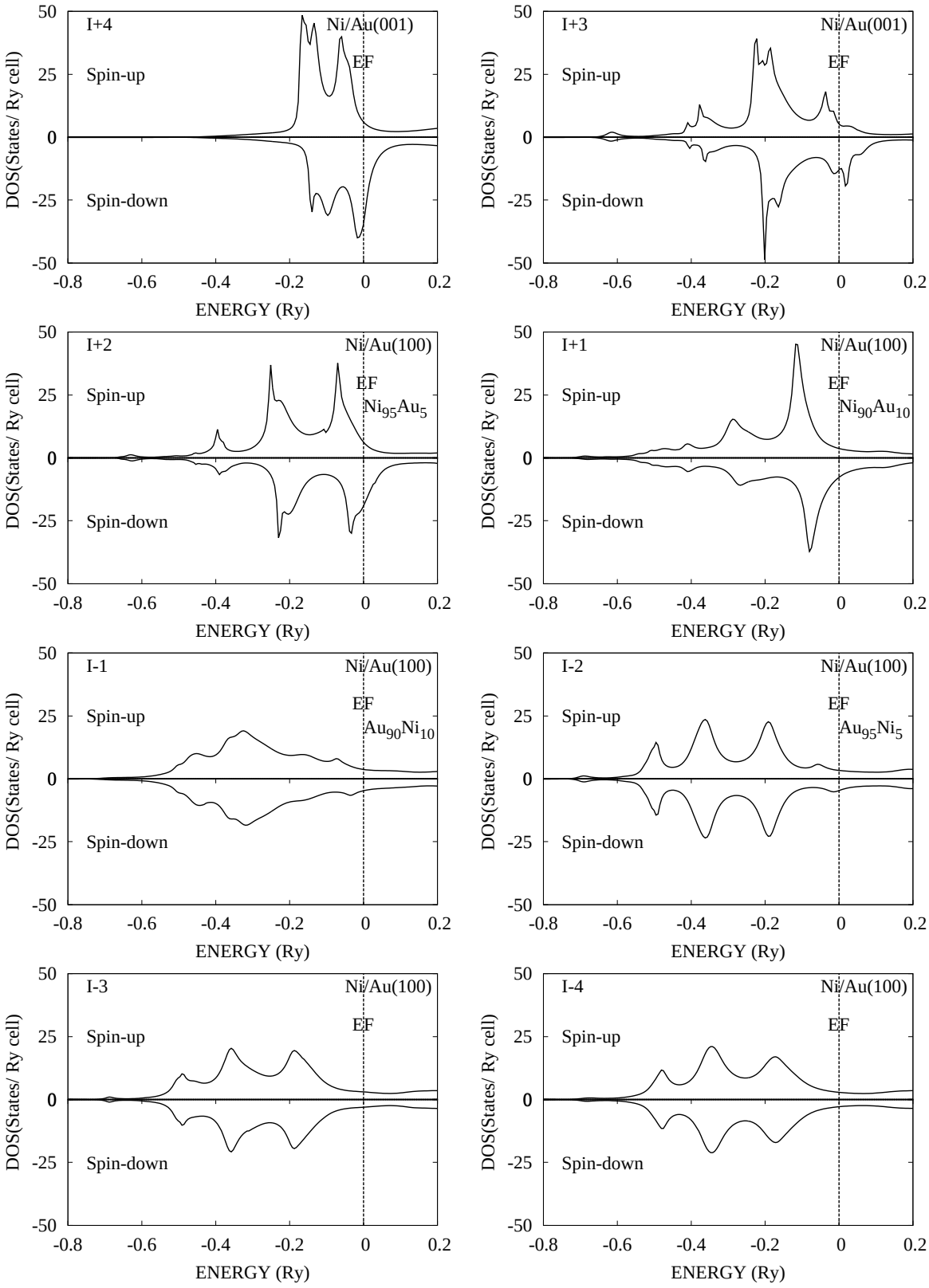

Figure 5.25: Layerwise variation of spin DOS at Ni/Au(001) with rough alloyed interface. Vertical line represents Fermi level.

equivalent to bulk Au DOS (figure 5.3).

Table 5.14: Layerwise magnetic moment (μ_B/atom) at the 4 layers rough interface of 2 layers of transition metal plus 2 layers Ag substrates. I : boundary of transition metal and Ag substrate. Interdiffusion, x = 0.1 at I ± 1 layer and x = 0.05 at I ± 2 layers and x = 0 at other layers.

Layers	Fe/Ag(001)			Co/Ag(001)			Ni/Ag(001)		
	μ_T	μ_M	μ_{avg}	μ_T	μ_M	μ_{avg}	μ_T	μ_M	μ_{avg}
I+4	2.99			2.02			0.69		
I+3	2.74			1.55			0.57		
I+2	2.96	0.16	2.81	1.68	0.65	1.63	0.66	-0.05	0.62
I+1	2.94	0.07	2.66	1.50	-0.13	1.34	0.46	-0.02	0.41
I-1	2.93	-0.04	0.26	2.7	-0.01	0.26	1.40	-0.01	0.13
I-2	3.41	-0.01	0.16	3.27	-0.02	0.16	1.45	-0.001	0.07
I-3		-0.01			-0.02			0.00	
I-4		0.00			-0.004			-0.001	
I-5		0.00			0.00			0.00	
I-6		0.00			0.00			0.00	

Table 5.14 shows the layerwise variation of magnetic moment with four layered rough interface of transition metals on Ag substrate. This variation in magnetic moment is shown in figure 5.26. Figure 5.26 shows there is small induced magnetic moment at the third metal layer from the interface for Ag based systems. The magnetic moment becomes zero at the fifth layer from the interface. First four Ag layers from the interface are therefore magnetic. In the transition metal overlayers (I+4 to I+1), the magnetic moment for all the four systems show oscillatory behavior. The magnetic moment gradually decreases to zero from I-1 layer to I-6 layer in the case of Ag substrate. The magnetism is due to induced magnetic moment from the transition metal impurities in this region.

The magnetic moment of Fe sharp interface layer calculated by FPLAPW method [83] is found to be more compared to other layers. In this FPLAPW

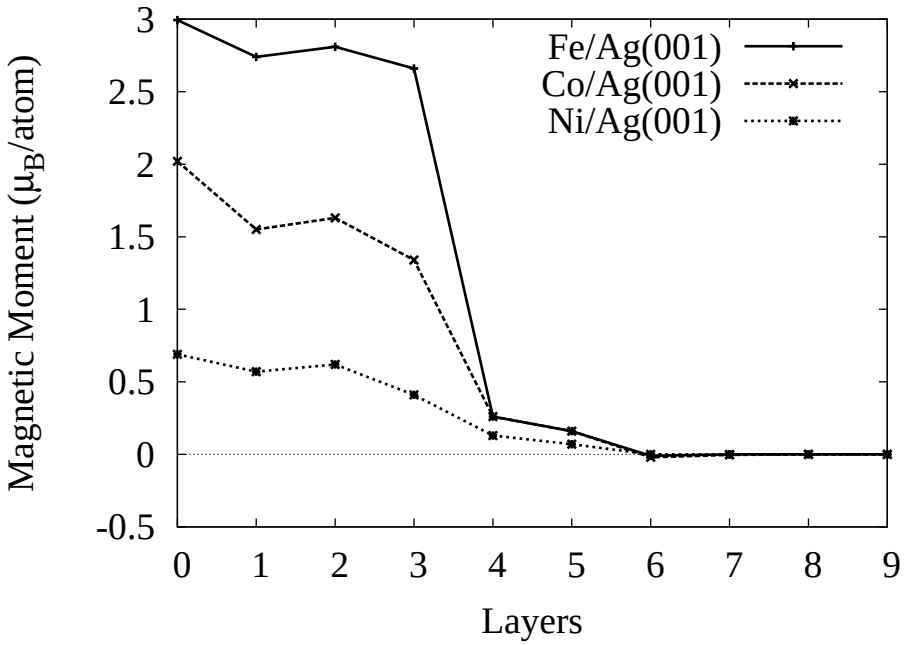

Figure 5.26: Layerwise variation of magnetic moment (μ_B/atom) at the 4 layers rough interface of 2 layers of transition metal plus 2 layers Ag substrates (4 layers of transition metal deposited). Layer 0 represents surface layer. Layers 2 to 5 define interface. Interdiffusion, $x = 0.1$ at layers 3 & 4 and $x = 0.05$ at layers 2 & 5 and $x = 0$ at other layers.

method [83] a supercell calculation was carried out with 5 layers of Fe on 5 layers of Ag. Since we consider interdiffusion of atoms at the interface, therefore average magnetic moment decreases as Ag content increases at the interface. The interface magnetic moments of Fe atoms in Fe/Ag systems with and without roughness are reported to be $2.55\mu_B$/atom and $2.4\mu_B$/atom respectively using TBLMTO-ASA method [55]. A DFT based embedded atom method [81] found surface and interface magnetic moment of Fe atom to be 2.99 μ_B and 2.82 μ_B respectively. In an experimental study [89] of Fe deposited on Ag, it is observed that Fe intermixed with three Ag layers with 50%, 25% and 12.5% concentration respectively. The average magnetic moment is measured to be 2.6 μ_B/atom. Our calculated values for 10% and 5% of Ag at the interface, the average magnetic moment of Fe atom is found to 2.95 μ_B. The average Co and Ni magnetic moment are 1.59 μ_B and 0.56 μ_B respectively for Co/Ag and Ni/Ag. For rough interface, the magnetic moment of

the transition metal gradually decreases from surface to interface. The magnetic moment gradually becomes zero after fourth Ag layer as we approach inner layers.

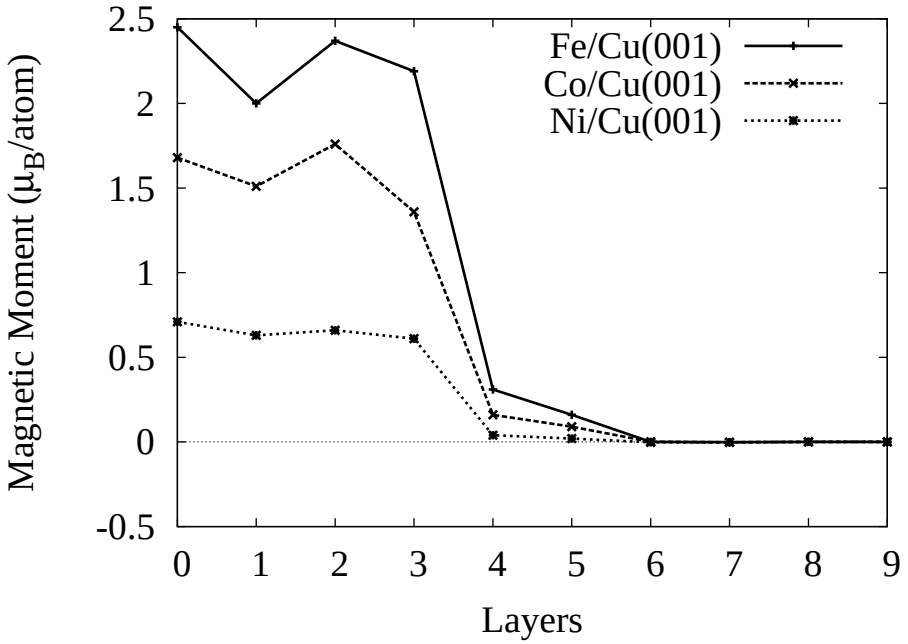

Figure 5.27: Layerwise variation of magnetic moment (μ_B/atom) at the 4 layers rough interface of 2 layers of transition metal plus 2 layers Cu substrates (4 layers of transition metal deposited). Layer 0 represents surface layer. Layers 2 to 5 define interface. Interdiffusion, $x = 0.1$ at layers 3 & 4 and $x = 0.05$ at layers 2 & 5 and $x = 0$ at other layers.

Table 5.15 shows the layerwise variation of magnetic moment for Cu based systems with four layered rough alloyed interface. Figure 5.27 clearly shows that in all Cu based systems, there is a little amount of induced magnetic moment upto third metal layer from the interface. At the fifth layer from the interface the magnetic moment ceases to zero in this case also. Therefore Cu atoms are magnetic upto fourth substrate layer from the interface. The magnetic moment for all the four systems show oscillatory behavior at the transition metal overlayers (I+4 to I+1) for these systems also. The magnetic moment gradually decreases to zero from I-1 to I-6 layers for Cu based systems. The magnetism in this region is due to induced magnetic moment from the transition metal impurities. The magnetic moment gradually ceases to zero as we go away from the interface.

Table 5.15: Layerwise magnetic moment (μ_B/atom) at the 4 layers rough interface of 2 layers of transition metal plus 2 layers Cu substrates. I : boundary of transition metal and Cu substrate. Interdiffusion, x = 0.1 at I $\pm$ 1 layer and x = 0.05 at I $\pm$ 2 layers and x = 0 at other layers.

Layers	Fe/Cu(001)			Co/Cu(001)			Ni/Cu(001)		
	μ_T	μ_M	μ_{avg}	μ_T	μ_M	μ_{avg}	μ_T	μ_M	μ_{avg}
I+4	2.45			1.68			0.71		
I+3	2.00			1.51			0.63		
I+2	2.49	-0.04	2.37	1.86	-0.04	1.76	0.71	-0.44	0.66
I+1	2.44	-0.02	2.19	1.50	0.09	1.36	0.69	-0.14	0.61
I-1	3.09	-0.001	0.31	1.60	-0.003	0.16	0.37	0.001	0.04
I-2	3.23	-0.04	0.16	1.88	-0.006	0.09	0.41	0.00	0.02
I-3		0.00			0.001			-0.002	
I-4		-0.001			-0.002			-0.002	
I-5		0.00			0.00			0.00	
I-6		0.00			0.00			0.00	

Earlier reported result by FP-LMTO method [75] show that the first-layer moment is substantially greater than that of the deeper layers. This matches with our results. Using neutron scattering technique it is reported that average magnetic moment for Ni-Cu alloy decreases with increase in Cu concentration [120]. Our calculation also shows the same trend for average magnetic moment (table 5.15). The average magnetic moment at I-1 layer and I-2 layer is very less in the case of Ni/Cu system. This is because of least magnetic interaction between Ni and Cu atoms. And since both are adjacent in periodic table, there is a small charge transfer between these two atoms [165].

Table 5.16 shows the layerwise variation of magnetic moment for the case of four layered rough alloyed interface having Au substrate. This variation in magnetic moment is shown in figure 5.28. The roughness of Fe-Au interface is reported earlier using scanning tunnelling microscopy [134]. Using molecular dynamics simulation

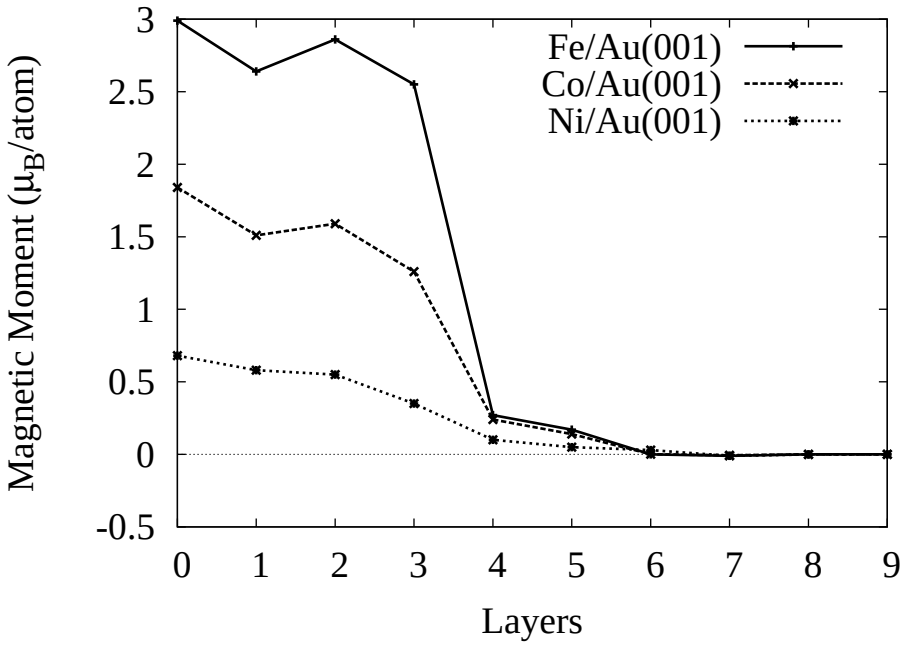

Figure 5.28: Layerwise variation of magnetic moment (μ_B/atom) at the 4 layers rough interface of 2 layers of transition metal plus 2 layers Au substrates (4 layers of transition metal deposited). Layer 0 represents surface layer. Layers 2 to 5 define interface. Interdiffusion, $x = 0.1$ at layers 3 & 4 and $x = 0.05$ at layers 2 & 5 and $x = 0$ at other layers.

with embedded atom method [132], it is reported that the deposition of Ni on Au(001) involves interspecies mixing leading to strained films and the growth of the overlayer is 3D from the initial stages of growth process. Figure 5.28 shows that magnetic moment becomes zero at the fifth layer from the interface in all Au based systems. Therefore Au remains magnetic upto fourth substrate layer from the interface. The magnetic moment at the transition metal overlayers (I+4 to I+1) for these systems show oscillatory behavior except for Ni/Au(001). The magnetic moment gradually decreases to zero from I-1 layer to I-6 layers. The magnetism is due to induced magnetic moment from the transition metal impurities in this region. The magnetic moment of the transition metal gradually decreases from surface to interface in this case.

Table 5.16: Layerwise magnetic moment (μ_B/atom) at the 4 layers rough interface of 2 layers of transition metal plus 2 layers Au substrates. I : boundary of transition metal and Au substrate. Interdiffusion, x = 0.1 at I $\pm$ 1 layer and x = 0.05 at I $\pm$ 2 layers and x = 0 at other layers.

Layers	Fe/Au(001)			Co/Au(001)			Ni/Au(001)		
	μ_T	μ_M	μ_{avg}	μ_T	μ_M	μ_{avg}	μ_T	μ_M	μ_{avg}
I+4	2.99			1.84			0.68		
I+3	2.64			1.51			0.58		
I+2	3.01	0.06	2.86	1.68	-0.07	1.59	0.58	0.11	0.55
I+1	2.83	-0.001	2.55	1.40	0.01	1.26	0.39	0.005	0.35
I-1	2.52	0.02	0.27	2.30	0.004	0.24	0.85	0.01	0.10
I-2	2.90	0.02	0.17	2.95	-0.009	0.14	1.12	-0.002	0.05
I-3		0.00			0.001			0.03	
I-4		-0.01			-0.006			-0.01	
I-5		0.00			0.00			0.00	
I-6		0.00			0.00			0.00	

5.4 Three Monolayers of Transition Metal on Metal Substrates

We have carried out the properties for three ML of transition metal overlayers with both sharp and rough interface to compare our results with the experimental studies. Some experimental works [85, 89] are reported considering three ML of Fe on Ag substrates. Hence for comparison of our results with the experimental data, we consider 5% interdiffusion of atoms at the interface.

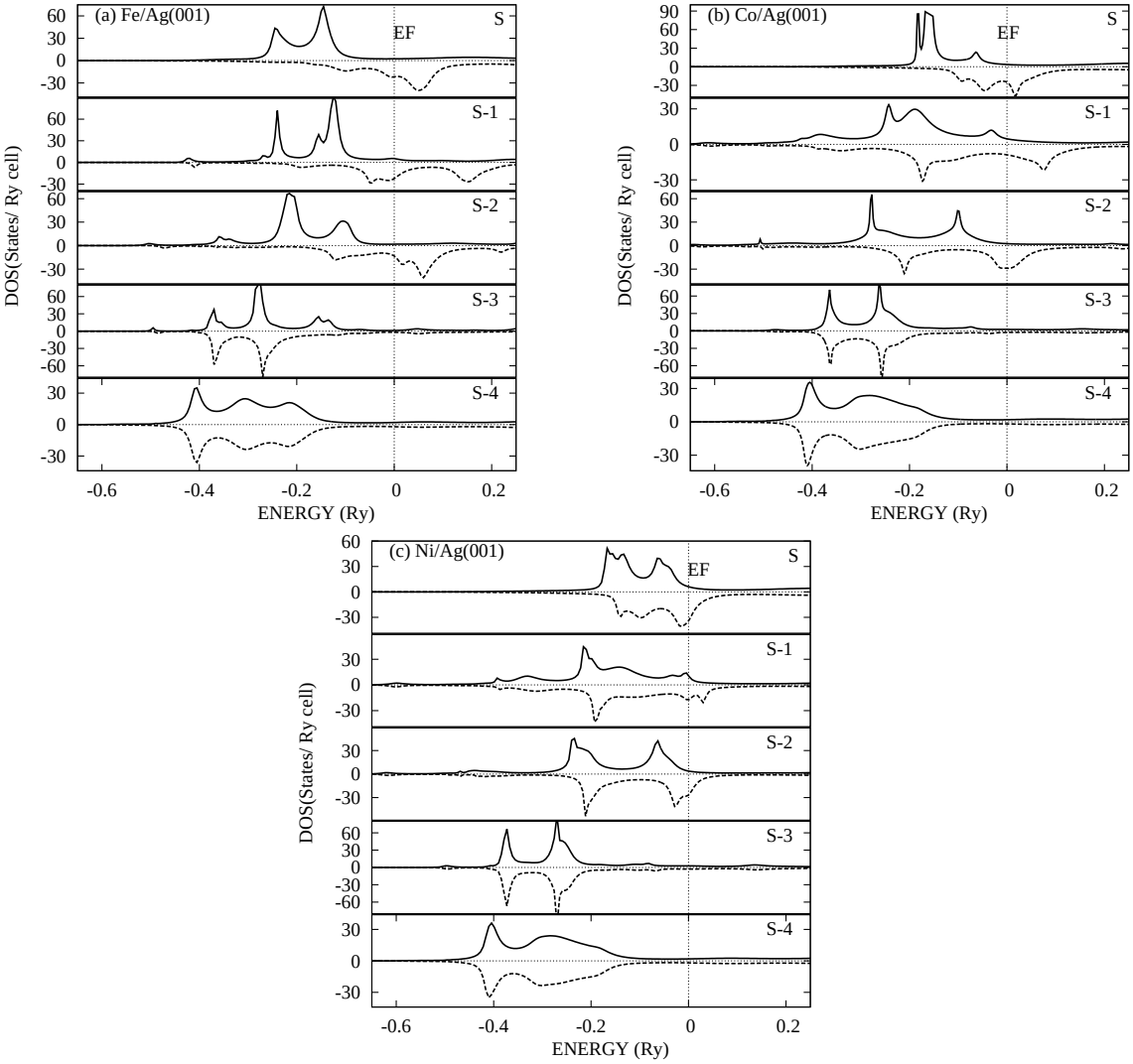

Figure 5.29: Layerwise spin DOS for three monolayers of transition metal on Ag substrates. Solid curve: spin-up DOS and dashed curve: spin-down DOS. Fermi energy is reset at zero.

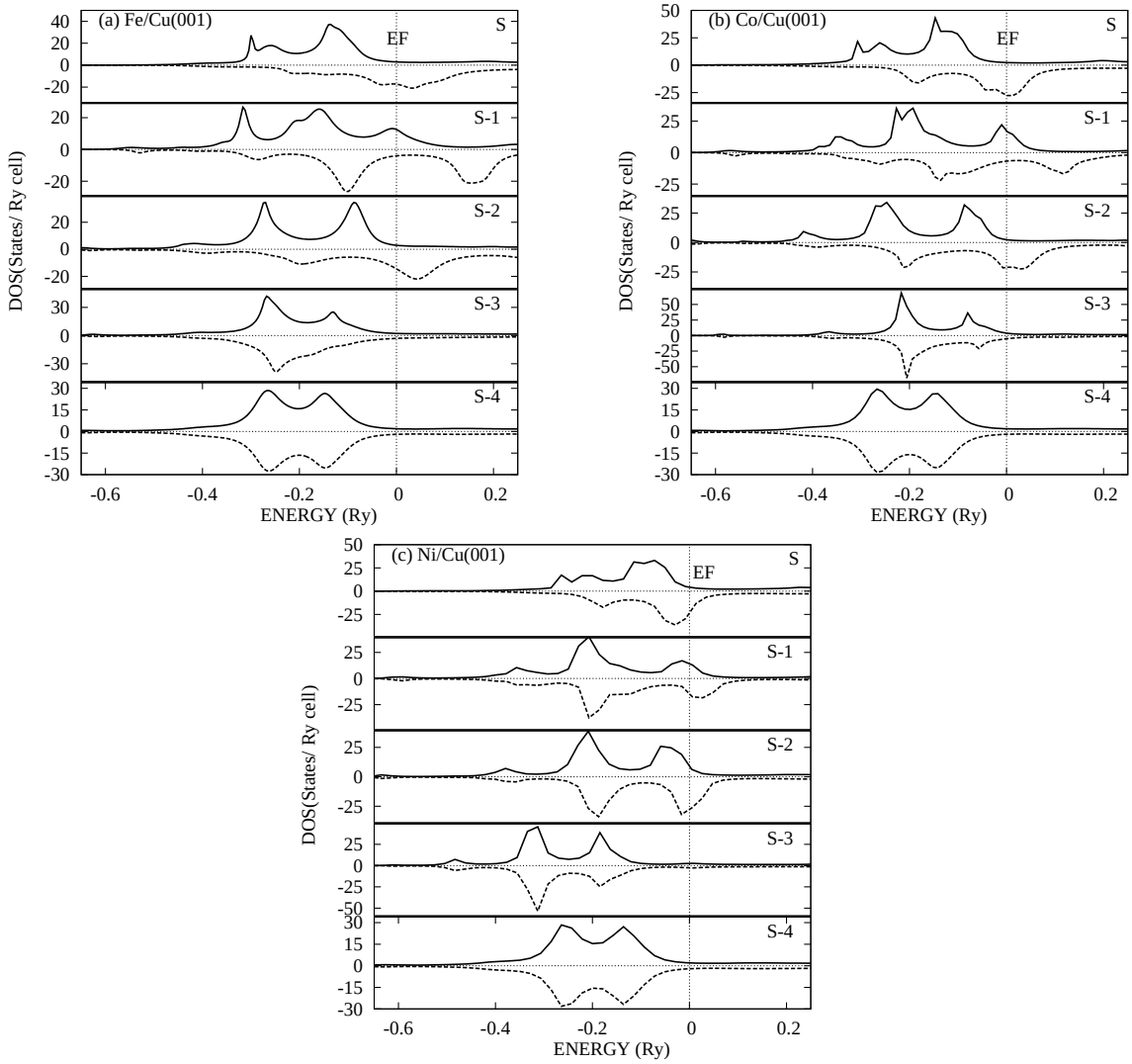

Figure 5.30: Layerwise spin DOS for three monolayers of transition metal on Cu substrates. Solid curve: spin-up DOS and dashed curve: spin-down DOS. Fermi energy is reset at zero.

Figures 5.29, 5.30 and 5.31 show the layerwise spin resolved DOS for three ML of transition metals on Ag, Cu and Au substrates respectively. The width of the spin-down electronic states of transition metal is more than spin-up states in all the systems. The splitting of spin-up and down states are more for Fe overlayers compared to Co and Ni on metal substrate. Therefore the magnetic moment is more in this case. The splitting decreases as the d-electrons of the transition metal are filled. As we go down from the top most layer, the width of the DOS increases. Therefore the magnetic moment decreases due to band widening. At the fifth layer

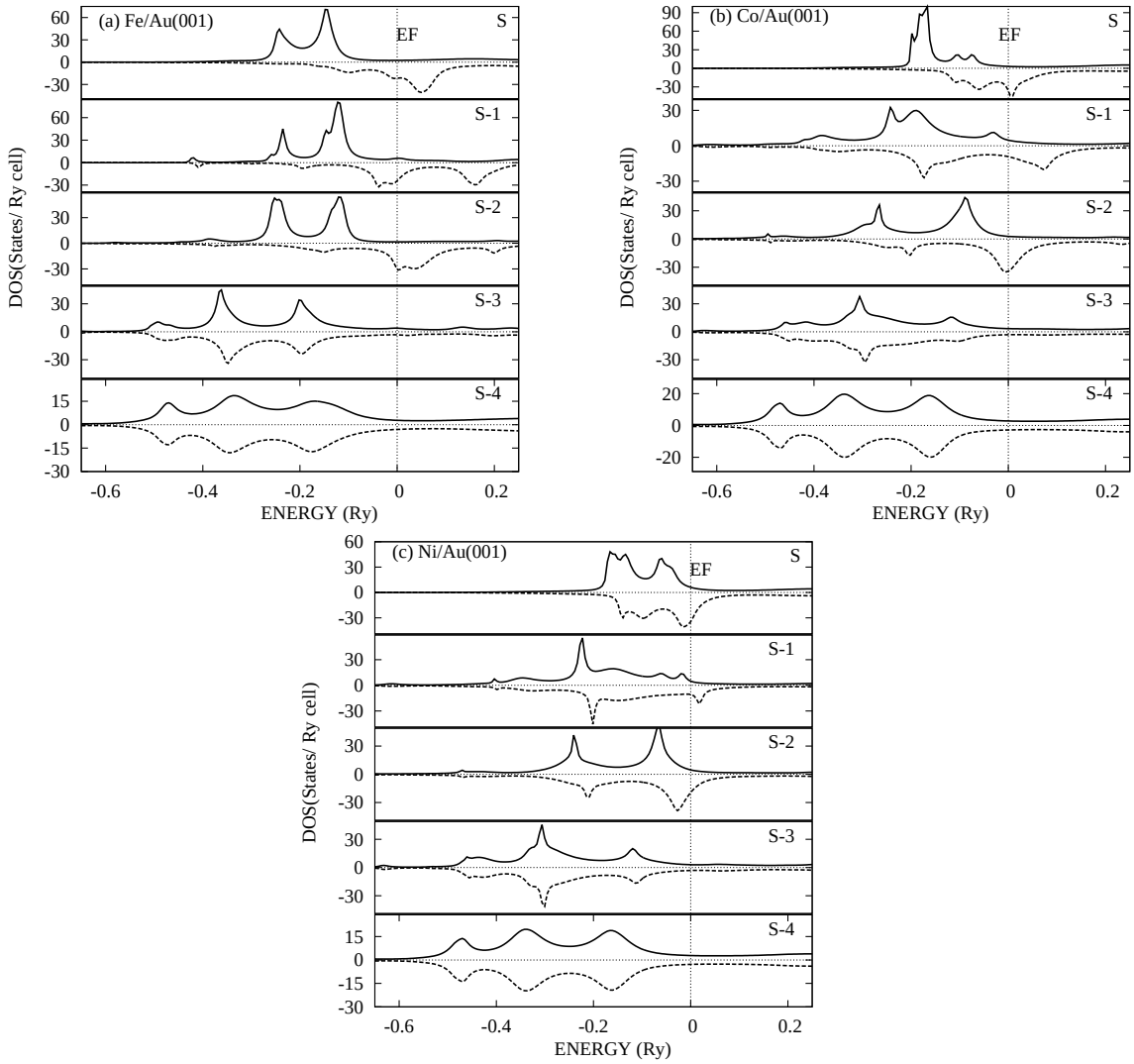

Figure 5.31: Layerwise spin DOS for three monolayers of transition metal on Au substrates. Solid curve: spin-up DOS and dashed curve: spin-down DOS. Fermi energy is reset at zero.

down the top most layer (S-5), Ag and Au DOS approaches bulk values. In case of Cu based systems, bulk DOS is attained at the sixth layer down the top most layer (S-6). Hence for three layers of transition metals overlayers, Ag and Au obtain their bulk electronic properties at the third substrate layer and Cu obtains at the fourth substrate layer from the interface.

Table 5.17 represents the layerwise variations of magnetic moments. These variations in magnetic moments also shown in figure 5.32. As we go down from the surface, the magnetic moment show oscillatory behavior. Table 5.18 shows the

Table 5.17: Layer-wise magnetic moment(μ_B/atom) for three ML of transition metal deposited on metal substrate. S stands for top most layer. S-2 and S-3 are sharp interface layers ($x = 0.0$).

Layers	Ag(001)			Cu(001)			Au(001)		
	Fe	Co	Ni	Fe	Co	Ni	Fe	Co	Ni
S	3.00	2.03	0.69	2.46	1.68	0.70	3.00	1.84	0.68
S-1	2.72	1.53	0.58	1.89	1.47	0.55	2.63	1.55	0.60
S-2	3.08	1.63	0.61	2.62	1.75	0.70	3.06	1.56	0.48
S-3	0.04	-0.005	-0.07	0.01	0.03	0.15	0.00	0.01	0.01
S-4	-0.005	0.00	0.00	-0.005	-0.004	-0.001	0.005	-0.003	0.00
S-5	0.00	0.00	0.00	0.00	0.00	0.00	0.00	0.003	0.001
S-6	0.00	0.00	0.00	0.00	0.00	0.00	0.00	0.00	0.00

Table 5.18: Average and interface magnetic moments (in μ_B/atom) for three layers of transition metals on metal substrates. Numbers in square bracket show reference numbers.

Magnetic Moments	Ag(001)			Cu(001)			Au(001)		
	Fe	Co	Ni	Fe	Co	Ni	Fe	Co	Ni
Average	2.93^a	1.73^a	0.63^a	2.32^a	1.63^a	0.65^a	2.90^a	1.65^a	0.59^a
	2.87^b	1.72^b	0.64^b	2.34^b	1.62^b	0.67^b	2.82^b	1.67^b	0.58^b
	2.67 [85]								
	2.80 [89]								
	3.05 [86]								
Interface	3.08^a	1.63^a	0.69^a	2.62^a	1.73^a	0.70^a	3.06^a	1.56^a	0.48^a
	2.93^b	1.53^b	0.65^b	2.49^b	1.67^b	0.62^b	2.89^b	1.49^b	0.42^b
	2.87 [85]								

^{a}sharp interface ($x = 0.0$) and ^{b}rough interface ($x = 0.05$) are calculated values. Refs [85] used SQUID magnetometry; [89] used X-ray Magnetic Circular Dichroism; [86] used KKR method. Ref [85] deals with 2.9 ML of Fe.

average and interface magnetic moment of the transition metals for three layers of transition metal on metal substrates. The average magnetic moment of Fe atoms decreases with the increase in Fe thickness, as found in an experimental study by alternate vapor deposition [91]. We have also calculated the magnetic moment for these systems with 5% interdiffusion of atoms at the interface layers (S-2 and S-3). Our results with rough interface ($x = 0.05$) for Fe/Ag(001) agrees well with the experimental results [85, 89]. Table 5.18 shows that our result with sharp interface overestimate experimental results. Hence theoretical modelling of rough interface is more realistic than sharp interface.

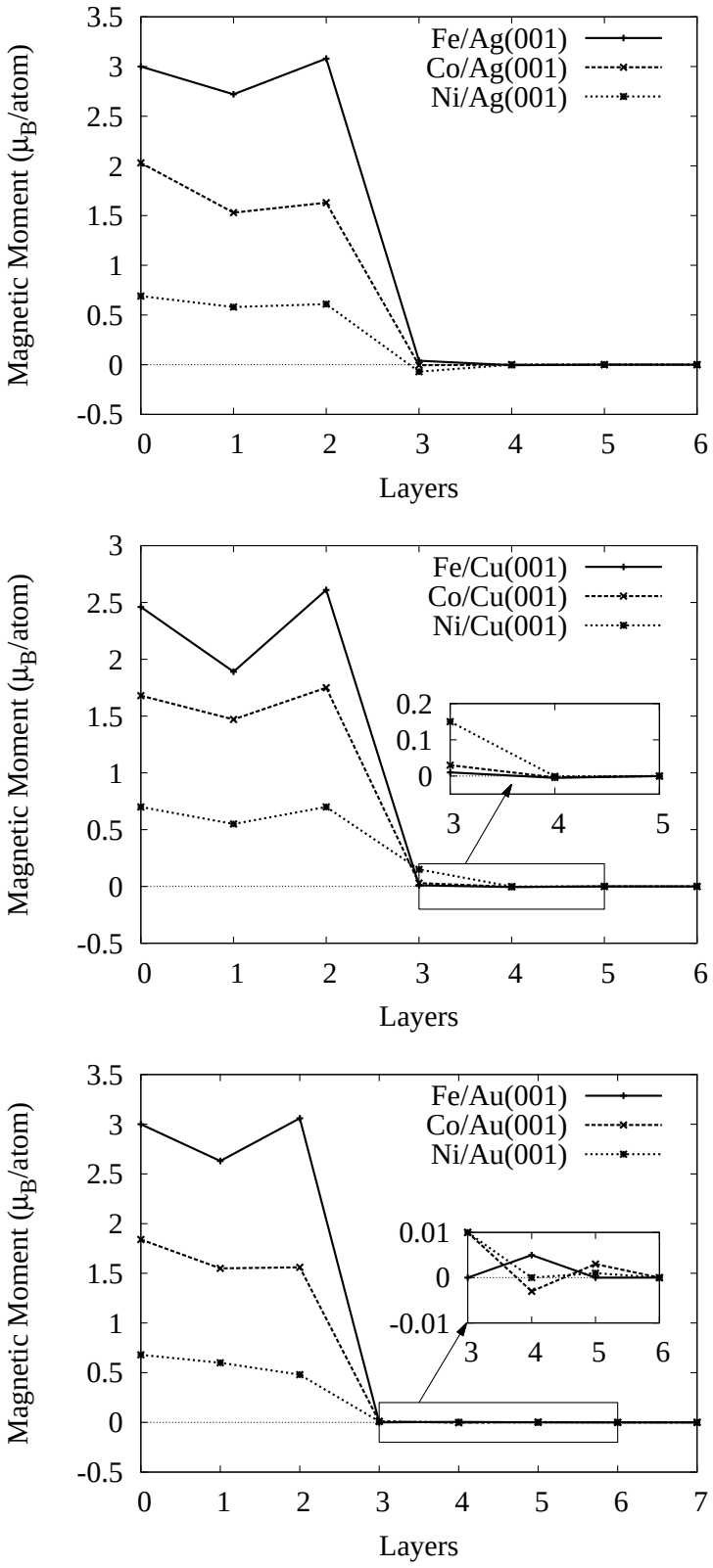

Figure 5.32: Layerwise variation of magnetic moment for 3 ML of transition metal on metal substrates. Layer 0 represents surface layer.

Chapter 6

Conclusions and Future Works

6.1 Conclusions

It is clear from the present study that Augmented Space Formalism (ASF), which is a real space technique, is not only suitable for the study of disordered binary alloys, it also can be applied to cases where surface is rough and interface layers between substrate and film deposited are disordered. The disordered interface is due to interdiffusion of atoms. It is also successfully applied to study almost smooth surfaces in the limit of zero disorderedness. ASF is applied for the calculation of layer dependent surface properties of bcc Fe(001), fcc Co(001) and fcc Ni(001) and interface properties of Fe, Co and Ni on (001) surface of Ag, Cu and Au substrates. Two types of rough surfaces are considered. In the first case only the top most layer is rough. In the second case first four layers with different degrees of randomness are considered. The comparison is made between these two rough surfaces. In the case of four layered rough interface, different amount (10% and 5%) of interdiffusion of atoms are considered in different atomic layers. The layer based density of states (DOS), magnetic moments are calculated. We have also calculated the work function. The following results are obtained from the present work.

Surface Properties:

1. The 5%, 16% and 9% lattice relaxations of the top layer are obtained for bcc Fe(001), fcc Co(001) and Ni(001) respectively.

2. The bulk properties of the systems are attained at the 9^{th} layer from the top in the case of Fe(001) whereas they are attained at 8^{th} layer in the cases of Co(001) & Ni(001) for four layered rough surfaces.

3. The trend in the variation of the width and the structure of DOS among the layers changes when a realistic surface is considered in comparison to a smooth surface.

4. Comparison between two types of rough surfaces shows there is slight difference in surface magnetic moment of Fe(001), significant difference for Co(001) and no change in the case of Ni(001).

5. In both type of roughening, the magnetic moment of the top layer is maximum for Fe(001) and Co(001). Maximum value is obtained at the 3^{rd} layer down the top most layer in case of Ni(001). Layered based magnetic moment is also found to be different in both type of rough surfaces.

6. Work functions of all the systems are found to be almost same for both types of rough surfaces.

7. d-band has significant contribution towards the magnetic moment in all the cases.

8. The appearance of new peaks in DOS for all these systems, with change in roughness correspond to disorderedness.

9. The surface magnetic moment is found to be 2.78 μ_B/atom, an enhancement of 28% compared to its bulk value in case of Fe(001) when surface is modeled by introducing 50% empty spheres in bcc Fe unit cell instead of relaxing it. When

the roughness of the top most layer is more than 50%, the surface magnetic moment increases and it approaches to atomic magnetic moment.

10. ASF is also successfully applied to almost smooth surfaces.

11. When nine layers of (001) smooth surfaces of Fe, Co and Ni are taken, the top most layers are relaxed by 5%, 16% and 9% respectively.

12. The magnetic moment get enhanced at the smooth surface compared to the bulk value by 30%, 19% and 32% for Fe(001), Co(001) and Ni(001) respectively.

13. Layer wise magnetic moments show Friedel oscillations.

14. The enhancement of surface magnetic moment is due to narrowing down of d-band, which support earlier studies.

15. The orbital resolved density of states show the significant contribution of d-orbital towards the surface as well as bulk magnetic moments.

16. It is observed that bulk magnetic moment is attained at the 5^{th} layer down the top most layer in the case of Fe(001) and at the 4^{th} layer in the cases of Co(001) and Ni(001).

17. The calculated work functions are 4.15 eV, 5.33 eV and 4.79 eV for Fe(001), Co(001) and Ni(001) respectively. These results are same for rough surfaces also except for Co(001) surface.

Interface Properties:

1. The lattice mismatch of Fe layer with Ag or Au substrate is minimized when Fe is deposited with a rotation of 45° w.r.t. (001) Ag or Au plane.

2. The lattice mismatch between Co/Ag and Ni/Ag is minimized when lattice parameter of Co and Ni are relaxed by 17% and 10% respectively.

3. The lattice mismatch between Co/Au and Ni/Au is minimized when lattice parameter of Co and Ni are relaxed by 15.5% and 10% respectively.

4. The magnetic moment of the overlayer get enhanced compared to its bulk value, for one smooth monolayer of transition metal deposited on Ag and Au substrate. Whereas it get enhanced for Fe overlayer but not for Co and Ni, in case of one smooth monolayer of transition metal on Cu substrate.

5. The induced magnetic moment on the Cu substrate layer is more than that of Ag and Au for 1 ML of Fe and Co deposition.

6. The magnetic moment of transition metal deposited on Ag and Au get enhanced more than Cu based systems. This is due to the effect of weak hybridization in Ag and Au based systems.

7. The surface magnetic moment in the case of two ML transition metal decreases compared to one ML transition metal. And the next layer magnetic moment is less than the top most layer. Therefore the induced moment on the top substrate layer is less in this cases except for Co/Cu(001), Ni/Cu(001) and Ni/Au(001).

8. The surface magnetic moment of Ni for two ML Ni/Cu is more compared to one ML Ni/Cu which agrees with earlier theoretical studies.

9. Average magnetic moment for overlayers is 2.93 μ_B/atom and the interface magnetic moment is 3.08 μ_B/atom for three ML of Fe on Ag (001). These are within 10% difference from the experimental values.

10. The substrate obtains its bulk electronic and magnetic properties at the fourth substrate layer from the interface in the case of one ML of transition metals.

11. The bulk electronic and magnetic properties of the substrate are obtained at the third substrate layer from the interface for two and three ML of transition metals on Ag and Cu, and at the fourth layer from the interface in case of Au.

12. The average magnetic moment of the top layer decreases and the average induced magnetic moment of the top substrate layer increases when 5% interdiffusion of atoms is considered than that of without interdiffusion case for one ML of transition metal, except for Ni/Ag(001). In the case of Ni/Ag, average induced magnetic moment decreases. But with increase in the amount of interdiffusion from 5% to 10%, the average magnetic moment of the overlayer decreases further but it increases for the substrate, except for Ni/Au(001).

13. The magnetic moment of the transition metal as well as the average magnetic moment of these interface layers gradually decreases to zero for four layered rough interface.

14. The substrate obtains its bulk electronic and magnetic properties at the fourth substrate layer for four layered rough interface with Ag and Cu substrate, whereas they are obtained at the fifth substrate layer in case of Au.

15. The magnetic moment of transition metal as well as the average magnetic moment of the overlayers show oscillatory behavior for the top four layers in case of four layer roughening except for Ni/Au(001).

6.2 Future Works

The present work can be extend to carry out the following studies.

1. In the present study, homogeneous randomness is considered. It can be extended to include inhomogeneous and correlated randomness in future.

2. The study of the effect of short range ordering on the properties of rough interfaces.

3. The study the effect of oxygen adsorption on transition metals deposited on metal substrate.

4. The study of the magnetic properties of metal-ceramic interface.

5. The study of dilute magnetic semiconductors (DMS) based on various semiconductors doped with magnetic transition metals.

Bibliography

[1] R.Haydock, "Locality in electronic structure an introduction to recursion method," in *Electronic structure of alloys, surfaces and clusters* (A. Mookerjee and D. Sarma, eds.), London and New York: Taylor & Francis, 2003.

[2] P.Mohn, *Magnetism in the Solid state An introduction.* Germany: Springer, 2006.

[3] S.Blundell, *Magnetism in Condensed Matter.* New York: Oxford University Press Inc., 2001.

[4] A.Mehta, B.Sanyal, and A.Mookerjee, "Growth, electonic and magnetic structure of rough surfaces," in *Electronic structure of alloys, surfaces and clusters* (A. Mookerjee and D. Sarma, eds.), London and New York: Taylor & Francis, 2003.

[5] J.E.Inglesfield and G.A.Benesh, "Surface electronic structure: Embedded self-consistent calculations," *Phys. Rev. B*, vol. 37, p. 6682–6700, 1988.

[6] R.Wu, D.Wang, and A.J.Freeman, "First Principles investigation of MCD spectra and sum rules for 3d transition metal surfaces," *J.Mag. Magn. Mater.*, vol. 132, pp. 103–123, 1994.

[7] O.Eriksson, G.W.Fernando, R.C.Albers, and A.M.Boring, "Enhanced orbital contribution to surface magnetism," *Solid State Comm.*, vol. 78, pp. 801–806, 1991.

[8] A.M.N.Niklasson, B.Johansson, and H.L.Skriver, "Interface magnetism of 3d transition metals," *Phys. Rev. B*, vol. 59, pp. 6373–6382, 1999.

[9] A.J.Freeman, D.S.Wang, and H.Krakauer, "Magnetism of surfaces and interfaces," *J. Appl. Phys.*, vol. 53, pp. 1997–2001, 1982.

[10] A.Huda and A.Mookerjee, "Magnetism on a rough surface," *J. Mag. Magn. Mater.*, vol. 267, pp. 97–104, 2003.

[11] M.Chakraborty, A.Mookerjee, and A.K.Bhattacharya, "Magnetism in surfaces: an orbital-resolved study," *J. Magn. Mag. Mater.*, vol. 285, pp. 210–223, 2005.

[12] S.Ohnishi, A.J.Freeman, and M.Weinert, "Surface magnetism of Fe(001)," *Phys. Rev. B*, vol. 28, pp. 6741–6748, 1983.

[13] A.J.Freeman, C.L.Fu, and T.Oguchi, "Structural, electronic and magnetic properties of surfaces, interfaces and superlattices," *Mat. Res. Soc. Symp. Proc.*, vol. 63, pp. 1–6, 1985.

[14] A.J.Freeman and R.Wu, "Electronic structure theory of surface, interface and thin-film magnetism," *J. Magn. Mag. Mater.*, vol. 100, pp. 497–514, 1991.

[15] C.Li, A.J.Freeman, and C.L.Fu, "Electronic structure and surface magnetism of fcc Co (001)," *J. Magn. Magn. Mater.*, vol. 75, pp. 53–60, 1988.

[16] E.Wimmer, A.J.Freeman, and H.Krakauer, "Magnetism at the Ni (001) surface: A high-precision, all-electron local-spin-density-functional study," *Phys. Rev. B*, vol. 30, pp. 3113–3123, 1984.

[17] O.Eriksson, A.M.Boring, R.C.Albers, G.W.Fernando, and B.R.Cooper, "Spin and orbital contributions to surface magnetism in 3d elements," *Phys. Rev. B*, vol. 45, pp. 2868–2875, 1992.

[18] M.Alden, S.Mirbt, H.L.Skriver, N.M.Rosengaard, and B.Johansson, "Surface magnetism in iron, cobalt, and nickel," *Phys. Rev. B*, vol. 46, pp. 6303–6312, 1992.

[19] B.Sanyal, P.Biswas, A.Mookerjee, H.G.Salunke, G.P.Das, and A.K.Bhattacharyya, "An augmented space recursion study of the electronic structure of rough epitaxial overlayers," *J.Phys.: Condens. Matter*, vol. 10, pp. 5767–5779, 1998.

[20] C.S.Wang and A.J.Freeman, "Surface states, surface magnetization, and electron spin polarization: Fe(001)," *Phys. Rev. B*, vol. 24, pp. 4364–4371, 1981.

[21] P.Bruno and J.-P.Renard, "Magnetic surface anisotropy of transition metal ultrathin films," *Appl. Phys. A*, vol. 49, pp. 499–506, 1989.

[22] N.P.Dahal and S.K.Lamichhane, "Nanotopographical Analysis of iron by AFM," *The Himalayan Physics*, vol. 2, pp. 73–75, 2011.

[23] J.N.Eckstein, "Growth of magnetic materials using molecular beam epitaxy," in *Handbook of Magnetism and Advanced Magnetic Materials* (H. Kronmuller and S. Parkin, eds.), John wiley & Sons, Ltd., 2007.

[24] M.D.Johnson, C.Orme, A.W.Hunt, D.Graff, J.Sudijono, L.M.Sander, and B.G.Orr, "Stable and unstable growth in molecular beam epitaxy," *Phys. Rev. Lett.*, vol. 72, pp. 116–119, 1994.

[25] M. Canepa, S. Terreni, P. Cantini, A. Campora, and L. Mattera, "Initial growth morphology in a heteroepitaxial system at low temperature: Fe on Ag(100)," *Phys. Rev. B*, vol. 56, pp. 4233–4242, 1997.

[26] B.T.Jonker, K.H.Walker, E.Kisker, G.A.Prinz, and C.Carbone, "Spin-polarized photoemission study of epitaxial Fe(001) films on Ag(001)," *Phys. Rev.Lett.*, vol. 57, pp. 142–145, 1986.

[27] J.Izquierdo, A.Vega, L.C.Balbas, D.S.Portal, J.Junquera, E.Artacho, J.M.Soler, and P.Ordejon, "Systematic ab initio study of the electronic and magnetic properties of different pure and mixed iron system," *Phys. Rev. B*, vol. 61, pp. 13639–13646, 2000.

[28] D.J.Sellmyer, M.Zheng, and R.Skomski, "Magnetism of Fe, Co and Ni nanowires in self-assembled arrays," *J. Phys.: Condens. Metter*, vol. 13, p. R433–R460, 2001.

[29] H.C.Siegmann and P.S.Bagus, "Magnetic properties of the (100) surface of Fe," *Phys. Rev. B*, vol. 38, pp. 10434–10439, 1988.

[30] S.A.Ziganshina, A.A.Bukharaev, L.I.Shamsetdinova, A.P.Chuklanov, and D.A.Bizyaev, "Atomic force microscopy of cobalt nanoparticles with electrocatalytic properties," *J. Surf. Investigation. X-ray, synchrotron and neutron techniques*, vol. 3, pp. 725–729, 2009.

[31] L.N.Liebermann, D.R.Fredkin, and H.B.Shore, "Two dimensional ferromagnetism in iron," *Phys. Rev. Lett.*, vol. 22, pp. 539–541, 1969.

[32] L.Liebermann, J.Clinton, D.M.Edwards, and J.Mathon, "Dead layers in ferromagnetic transition metals," *Phys. Rev. Lett.* , vol. 25, pp. 232–235, 1970.

[33] S.F.Alvarado, H.Hopster, and M.Campagna, "Surface Magnetism on Ni(001) by spin polarized electron scattering," *Surf. Sci.*, vol. 117, pp. 294–299, 1982.

[34] N.B.Brookes, A.Clarke, P.D.Johnson, and M.Weinert, "Magnetic surface states on Fe(001)," *Phys. Rev. B*, vol. 41, pp. 2643–2645, 1990.

[35] H.Danan, A.Herr, and A.J.P.Meyer, "New determinations of the saturation magnetization of nickel and iron," *J.Appl.Phys.*, vol. 39, pp. 669–670, 1968.

[36] C.Rau and S.Eichner, "Electron-spin polarization at single crystalline cr and ni surfaces determined with electron-capture spectroscopy," *Phys. Rev. Lett.*, vol. 47, pp. 939–942, 1981.

[37] H.A.Mook, "Magnetic moment distribution of nickel metal," *The Phys. Rev.*, vol. 148, pp. 495–501, 1966.

[38] M.Landolt and M.Campagna, "Spin polarization of field-emitted and magnetism at the (100) surface of Ni," *Phys.. Rev. Lett.*, vol. 38, pp. 663–666, 1977.

[39] A.M.Turner, Y.J.Chang, and J.L.Erskine, "Surface states and the Photoelectron Spin Polarized of Fe(100)," *Phys. Rev. Lett.*, vol. 48, pp. 348–351, 1982.

[40] A.J.Freeman and C.L.Fu, "Strongly enhanced 2d magnetism at surfaces and interfaces (invited)," *J. Appl. Phys.*, vol. 61, pp. 3356–3361, 1987.

[41] A.J.Freeman, "Electronic structure and magnetism of surfaces and interfaces," *J. Mag. Magn. Mater.*, vol. 35, pp. 31–36, 1983.

[42] A.J.Freeman, H.Krakauer, S.Ohnishi, D.S.Wang, M.Weinert, and E.Wimmer, "Magnetism at surfaces and interfaces," *j. Mag. Magn. Mater.*, vol. 38, pp. 269–272, 1983.

[43] O.Hjortstam, J.Trygg, J.M.Wills, B.Johansson, and O.Eriksson, "Calculated spin and orbital moments in the surfaces of the 3d metals Fe, Co, and Ni and their overlayers on Cu(001)," *Phys. Rev. B*, vol. 53, pp. 9204–9213, 1996.

[44] H.Krakauer, A.J.Freeman, and E.Wimmer, "Magnetism of the Ni(110) and Ni(100) surfaces: Local spin density functional calculations using the thin-slab linearized augmented plane wave method," *Phys. Rev. B*, vol. 28, pp. 610–623, 1983.

[45] C.S.Wang and A.J.Freeman, "Surface states, surface magnetization, and electron spin polarization: Ni (001)," *Phys. Rev. B*, vol. 21, pp. 4585–4591, 1980.

[46] M.Chakraborty and A.Mookerjee, "Electronic structure and magnetism of nickel thin films," *Int. J. Mod. Phys. B*, vol. 17, pp. 5839–5848, 2003.

[47] J.Kubler, "Magnetic moment of ferromagnetic and antiferromagnetic bcc and fcc iron," *Phys. Lett.*, vol. 81A, pp. 81–83, 1981.

[48] P.H.Citrin and G.K.Wertheim, "Photoemission from surface-atom core levels, surface densitites of states, and metal-atom clusters: a unified picture," *Phys. Rev. B*, vol. 27, pp. 3176–3200, 1983.

[49] T.Ohwaki, D.Wortmann, H.Ishida, S.Blugel, and K.Terakura, "Spin-polarized field emission from Ni(001) and Ni(111) surfaces," *Phys. Rev. B*, vol. 73, pp. 2354241–2354249, 2006.

[50] B.Sanyal, "Magnetism of rough overlayers - an augmented space recursive study," *Computational Mater. Sci.*, vol. 20, pp. 429–435, 2001.

[51] H.B.Michaelson, "The work function of the elements and its periodicity," *J.Appl.Phys.*, vol. 48, pp. 4729–4733, 1977.

[52] A.P.Kurpin, L.Cheng, Z.Altounian, and D.H.Ryan, "Influence of the Interfaces on Magnetic Properties of Fe/Ag and Fe/Cu Multilayers Prepared by Sputtering," *Hyperfine Interactions*, vol. 144/145, pp. 141–149, 2002.

[53] B.T.Jonker and G.A.Prinz, "Comment on "The growth of Fe overlayers on Ag (100)" by G.C. Smith, H.A. Padmore and C. Norris," *Surf. Sci. Lett.*, vol. 172, pp. L568–L570, 1986.

[54] F.J.Himpsel, "Exchange splitting of epitaxial fcc Fe/Cu (100) versus bcc Fe/Ag(100)," *Phys. Rev. Lett.*, vol. 67, pp. 2363–2366, 1991.

[55] S.Krompiewski, U.Krauss, and U.Krey, "Magnetic properties of Fe/Ag multilayers with interface roughness by a first-principle tight-binding LMTO method," *J. Magn. Mag. Mater.*, vol. 92, pp. L295–L300, 1991.

[56] M.Benoit, C.Langlois, N.Combe, H.Tang, and M.J.Casanove, "Structural and electronic properties of the Au(001)/Fe(001) interface from density functional theory calculations," *Phys. Rev. B*, vol. 86, pp. 075460(1–12), 2012.

[57] G.C.Smith, H.A.Padmore, and C.Norris, "The growth of Fe overlayers on Ag (100)," *Surf. Sci.*, vol. 119, pp. L287–L291, 1982.

[58] G.Gladyszewski, K.Temst, K.Mae, R.Schad, F.Belien, E.Kunnen, G.Verbanck, Y.Bruynseraede, R.Moons, A.Vantomme, S.Blasser, and G.Langouche, "Structure of Ag/Fe superlattices probed at different length scales," *Thin solid films*, vol. 366, pp. 51–62, 2000.

[59] F.Ciccacci and S.D.Rossi, "Empty electronic states in magnetic thin films: Fe on Au(100), Ag(100) and Cu(100)," *Phys.Rev.B*, vol. 51, pp. 11538–11545, 1995.

[60] C.L.Fu and A.J.Freeman, "Giant two-dimensional ferromagnetic moments on metallic overlayers and interfaces," *J. Magn. Mag. Mater.*, vol. 54-57, pp. 777–778, 1986.

[61] C.L.Fu, A.J.Freeman, and T.Oguchi, "Prediction of strongly enhanced two-dimensional ferromagnetic moments on metallic overlayers, interfaces, and superlattices," *Phys. Rev. Lett.*, vol. 54, pp. 2700–2703, 1985.

[62] C.Li, A.J.Freeman, H.J.F.Jansen, and C.L.Fu, "Magnetic anisotropy in low-dimensional ferromagnetic systems: Fe monolayers on Ag(001), Au(001) and Pd(001) substrates," *Phys. Rev. B*, vol. 42, pp. 5433–5442, 1990.

[63] S.Blugel, B.Drittler, R.Zellet, and P.H.Dederichs, "Magnetic properties of 3d transition metal monolayers on metal substrates," *App. Phys. A*, vol. 49, pp. 547–562, 1989.

[64] S.C.Hong, A.J.Freeman, and C.L.Fu, "Structural, electronic and magnetic properties of a Ni monolayer on Ag(001): Ni adsorption versus Ag surface segregation," *Phys. Rev. B*, vol. 39, pp. 5719–5725, 1989.

[65] C.Li, A.J.Freeman, and C.L.Fu, "Electronic structure and magnetism of surfaces and interfaces: selected examples," *J. Magn. Mag. Mater.*, vol. 83, pp. 51–56, 1990.

[66] C.L.Fu and A.J.Freeman, "Electronic and magnetic properties of the fcc Fe(001) thin films: Fe/Cu(001) and Cu/Fe/Cu(001)," *Phys. Rev. B*, vol. 35, pp. 925–932, 1987.

[67] M.F.Onellion, C.L.Fu, M.A.Thompson, J.L.Erskine, and A.J.Freeman, "Electronic structure and properties of epitaxial Fe on Cu(100): Theory and experiment," *Phys. Rev. B*, vol. 33, pp. 7322–7325, 1986.

[68] D.S.Wang, A.J.Freeman, and H.Krakauer, "Electronic Structure and Magnetism of Ni overlayers on Cu(001) substrate," *Phys. Rev. B*, vol. 26, pp. 1340–1351, 1982.

[69] D.S.Wang, A.J.Freeman, and H.Krakauer, "Surface magnetism of a Ni overlayer on a Cu(001) substrate," *Phys. Rev. B*, vol. 24, pp. 1126–1129, 1981.

[70] C.Li, A.J.Freeman, and C.L.Fu, "Monolayer Magnetism: Electronic and Magnetic Properties of Fe/Au (001)," *J. Mag. Magn. Mater.*, vol. 75, pp. 201–208, 1988.

[71] R.Richter, J.G.Gay, and J.R.Smith, "Spin separation in a metal overlayer," *Phys. Rev. Lett.*, vol. 54, pp. 2704–2707, 1985.

[72] X.Y.Zhu, H.Huang, and J.Hermanson, "Electronic structure and magnetism of the Cu/Ni100 interface: Self-consistent local-orbital calculations," *Phys. Rev. B*, vol. 29, pp. 3009–3014, 1984.

[73] H.Huang, X.Y.Zhu, and J.Hermanson, "Ni overlayer on a Cu100 substrate: Magnetism and surface states," *Phys. Rev. B*, vol. 29, pp. 2270–2273, 1984.

[74] V.S.Stepanyuk, W.Hergert, P.Rennert, K.Wildberger, R.Zeller, and P.H.Dederichs, "Magnetic dimers of transition-metal atoms on the Ag(001) surface," *Phys. Rev. B*, vol. 54, pp. 14121–14126, 1996.

[75] T.Kraft, P.M.Marcus, and M.Scheffler, "Atomic and Magnetic Structure of fcc Fe/Cu(100)," *Phys. Rev. B*, vol. 49, pp. 11511–11514, 1994.

[76] I.Turek, J.Kudrnovsky, V.Drchal, and P.Weinberger, "Itinerant magnetism of disordered Fe-Co and Ni-Cu alloys in two and three dimensions," *Phys. Rev. B*, vol. 49, pp. 3352–3362, 1994.

[77] D.Schmitz, C.Charton, A.Scholl, C.Carbone, and W.Eberhardt, "Magnetic moment of fcc Fe overlayers on Cu(100) and Co(100)," *Phys.Rev.B*, vol. 59, pp. 4327–4333, 1999.

[78] P.Srivastava, F.Wilhelm, A.Ney, M.Farle, H.Wende, N.Haack, G.Ceballos, and K.Baberschke, "Magnetic moments and Curie temperatures of Ni and Co thin films and coupled trilayers," *Phys.Rev.B*, vol. 58, pp. 5701–5706, 1998.

[79] A.Ney, P.Poulopoulos, M.Farle, and K.Baberschke, "Absolute determination of co magnetic moments: Ultrahigh-vacuum high t_c magnetometry," *Phys.Rev.B*, vol. 62, pp. 11336–11339, 2000.

[80] A.Ney, P.Poulopoulos, F.Wilhelm, A.Scherz, M. Farle, and K. Baberschke, "Absolute determination of the magnetic moments of Co monolayers: a combination of UHV magetometries," *J. Mag. Magn. Mater.*, vol. 226-230, pp. 1570–1572, 2001.

[81] S.Lu, Q.-M.Hu, M.P.J.Punkkinen, B. Jahansson, and L. Vitos, "First-principles study of fcc-Ag/bcc-Fe interfaces," *Phys. Rev. B*, vol. 87, pp. 224104–(1–11), 2013.

[82] T.Phalet, M.J.Prandolini, W.D.Brewer, P. Moor, P.Schuurmans, N.Severijns, B.G.Turrell, A. Geert, B.Vereecke, and S.Versyck, "Noncollinear Magnetic Hy-

perfine Fields in the Ag Spacers of Fe/ Ag Multilayers," *Phys. Rev. Lett.*, vol. 86, pp. 902–905, 2001.

[83] C.O.Rodriguez, M.V.Ganduglia-Pirovano, E. y Blanca, M.Petersen, and P.Novak, "Orbital and dipolar contributions to the hyperfine fields in bulk bcc Fe, hcp Co, and at the Fe/Ag(100) interface: the inclusion of orbital polarization," *Phys. Rev. B*, vol. 63, pp. 1844131–1844137, 2001.

[84] S.Ohnishi, M.Weinert, and A.J.Freeman, "Interface magnetism in metals: Ag/Fe(001)," *Phys.Rev.B*, vol. 30, pp. 36–43, 1984.

[85] C.L.Wooten, J.Chen, G.A.Mulhollan, J.L.Erskine, and J.T.Markert, "Direct observation of enhanced magnetic moment in Fe/Ag(100)," *Phys. Rev. B*, vol. 49, pp. 10023–10026, 1994.

[86] C.Sommers, J.Zabloudil, C.Uiberacker, P.Weinberger, and L.Szunyogh, "Multiple reorientation transition of the magnetization of free surfaces of Fe on Ag(100)," *Phys. Rev. B*, vol. 58, pp. 5539–5543, 1998.

[87] Z.C.Li, D.P.Yu, and B.X.Liu, "Manipulation of ordered layered structure by interface-assisted ion-beam mixing in immiscible Ag-Co and Ag-Ni systems," *Phys.Rev.B*, vol. 65, pp. 245403(1–6), 2002.

[88] R.Krishnan and M.Tessier, "Magnetization and FMR studies in multilayer Ni-Ag Films," *Solid State Comm.*, vol. 60, pp. 637–639, 1986.

[89] A.Hahlin, C.Andersson, J. Dunn, B.Sanyal, O.Karis, and D.Arvanitis, "Structure and magnetic of ultrathin epitaxial Fe on Ag (100)," *Phys. Rev. B*, vol. 73, pp. 1344231–1344238, 2006.

[90] N.C.Koon, B.T.Jonker, F.A.Volkening, J.J.Krebs, and G.A.Prinz, "Direct evidence for perpendicular spin orientations and enhanced hyperfine fields in ultrathin Fe(100) films on Ag(100)," *Phys. Rev. Lett.*, vol. 59, pp. 2463–2466, 1987.

[91] F.Pan, T.Yang, K.Tao, and B.X.Liu, "Magnetic properties of Fe/Ag nano-multilayers," *J. Phys: Condens. Matter*, vol. 4, pp. L519–L524, 1992.

[92] L.Szunyogh, B.Ujfalussy, C.Blaas, U.Pustogowa, C.Sommers, and P.Weinberger, "Oscillatory behavior of the magnetic anisotropy energy in Cu(100)/Co_n multilayer systems," *Phys.Rev.B*, vol. 56, pp. 14036–14044, 1997.

[93] A.Ney, P.Poulopoulos, and K.Baberschke, "Surface and interface magnetic moments of Co/Cu(001)," *Europhys. Lett.*, vol. 54, pp. 820–825, 2001.

[94] J.Tersoff and L.M.Falicov, "Magnetic and electronic properties of Ni films, surfaces, and interfaces," *Phys. Rev. B*, vol. 26, pp. 6186–6200, 1982.

[95] J.Tersoff and L.M.Falicov, "Interface magnetization: Cu films on Ni(100)," *Phys.Rev.B*, vol. 25, pp. 2959–2961, 1982.

[96] M.E.McHenry, J.M.MacLaren, and D.P.Clougherty, "Monolayer magnetism of 3d transitson metals in Ag, Au, Pd, and Pt hosts: Systematics of local moment variation," *J. Appl. Phys.*, vol. 70, pp. 5932–5934, 1991.

[97] M.E.McHenry, J.M.MacLaren, M.E.Eberhart, and S.Crampin, "Electronic and magnetic properties of Fe/Au multilayers and interfaces," *J.Mag.Magn.Mater.*, vol. 88, pp. 134–150, 1990.

[98] S.D.Rossi, F.Ciccacci, and S.Crampin, "Magnetism of Fe on Au(100) in the monolayer limit," *Phys.Rev.B*, vol. 52, pp. 3063–3066, 1995.

[99] B.C.Bolding and E.A.Carter, "Effect of strain on thin film growth: deposition of Ni on Ag(100)," *Surface Sci.*, vol. 268, pp. 142–154, 1992.

[100] J.Thomassen, F.May, B.Feldmann, M.Wuttig, and H.Ibach, "Magnetic live surface layers in Fe/Cu(100)," *Phys.Rev.Lett.*, vol. 69, pp. 3831–3834, 1992.

[101] S.H.Lu, J.Quinn, D.Tian, F.Jona, and P.M.Marcus, "Structural properties of epitaxial films of Fe on Cu and Cu-based surface and bulk alloys," *Surf. Sci.*, vol. 209, pp. 364–378, 1989.

[102] S.Muller, P.Bayer, C.Reischl, K.Heinz, B.Feldmann, H.Zillgen, and M.Wuttig, "Structural instability of ferromagnetic fcc Fe films on Cu(100)," *Phys. Rev. Lett.*, vol. 74, pp. 765–768, 1995.

[103] Y.Gotoh, K.Yamashita, and T.Ichikawa, "Synthesis and structural studies of Fe/Ag metallic superlattices," *J. Mag. Magn. Mater.*, vol. 126, pp. 38–40, 1993.

[104] R.Gupta, M.Weisheit, H.Krebs, and P.Schaaf, "Interface structure of Fe/Ag multilayers prepared by pulsed laser deposition," *Phys. Rev. B*, vol. 67, pp. 0754021–0754027, 2003.

[105] T.Kingetsu, Y.Kamada, and M.Yamamoto, "Epitaxial growth of binary and ternary metallic strained superlattices and their magnetic properties," *Science and Technology of Advanced Materials*, vol. 2, pp. 331–347, 2001.

[106] J.Q.Xiao, A.Gavrin, G.Xiao, J.R.Childress, W.A.Bryden, C.L.Chien, and A.S.Edelstein, "Structural studies and magnetic properties of Fe/Ag superlattices," *J. Appl.Phys.*, vol. 67, pp. 5388–5390, 1990.

[107] P.Etienne, S.Lequien, F.Nguyen-Van-Dau, R.Cabanel, G.Creuzet, A.Friederich, J.Massies, A.Fert, A.Barthelemy, and F. Petroff, "A comparative study of the molecular-beam epitaxial growth of Ag/Fe, Ag/Cr, and Fe/Cr superlattices on GaAs(001)," *J.Appl.Phys.*, vol. 67, pp. 5400–5402, 1990.

[108] A.Tunyogi, F.Paszti, Z.Osvath, F.Tancziko, M.Major, and E.Szilagyi, "Asymmetric interfaces in Fe/Ag and Ag/Fe bilayers prepared by molecular beam

evaporation," *Nuclear Instruments and Methods in Physics Research B*, vol. 249, pp. 384–386, 2006.

[109] G.Sharma, R.Gupta, D.Kumar, and A.Gupta, "Anomalous evolution of interfaces in Fe/Ag magnetic multilayer," *J.Phys.D: Appl. Phys.*, vol. 46, pp. 505302(1–7), 2013.

[110] G.E.Thayer, N.C.Bartelt, V.Ozolins, A.K.Schmid, S.Chiang, and R.Q.Hwang, "Linking surface stress to surface structure: Measurement of atomic strain in a surface alloy using scanning tunneling microscopy," *Phys. Rev. Lett.*, vol. 89, pp. 0361011–0361014, 2002.

[111] M.Canepa, E.Magnano, A. Campora, P.Cantini, M.Salvietti, and L.Mattera, "Diffusion by atomic place exchange in ultrathin iron films on Ag(100): an ion scattering spectroscopy study," *Surf. Sci.*, vol. 352-354, pp. 36–40, 1996.

[112] M.Csontos, J.Balogh, D.Kaptas, L.F.Kiss, A.Kovacs, and G.Mihaly, "Magnetic and transport properties of Fe-Ag granular multilayers," *Phys. Rev. B*, vol. 73, pp. 1844121–1844129, 2006.

[113] E.Agostinelli, D.Fiorani, S.Foglia, S.Kaciulis, A.M.Testa, and M.V.Antisari, "Microstructure and magnetotransport properties of nanocrystalline laser processed Co-Ag films," *J. Metastable and Nanocrystalline*, vol. 12, pp. 111–125, 2002.

[114] W.C.Chiang, W.P.Pratt, M.Herrold, and D.V.Baxter, "Effect of sputtering pressure on the structure and current-perpendicular-to-the-plane magnetotransport of Co/Ag multilayered films," *Phys. Rev. B*, vol. 58, pp. 5602–5610, 1998.

[115] Y.G.Pogorelov, G.N.Kakezei, J. ad A.F.Kravets, N.A.Lesnik, M.M.P.Azevedo, M.Malinowska, and P.Panissod, "Structural and magnetic study of heteroge-

neous $co_x ag_{1-x}$ films by resonance and magnetometric techniques," *Phys. Rev. B*, vol. 60, pp. 12200–12206, 1999.

[116] A.Azizi, S.M.Thompson, K. Ounadjela, J.Gregg, P.Vennegues, A. Dinia, J. Arabski, and C.Fermon, "Correlation between the structural and transport properties of granular CoAg systems prepared by MBE," *J. Mag. Magn. Mater.*, vol. 148, pp. 313–314, 1995.

[117] T.J.Colla, H.M.Urbassek, K.Nordlund, and R.S.Averback, "Ion-induced mixing and demixing in the immiscible Ni-Ag system," *Phys. Rev. B*, vol. 63, pp. 1042061–1042067, 2001.

[118] G.Weiming, P.Yong, Z.Kunhua, and G.Junmei, "First Principle Study on the Interface of Ag-Ni Composites," *Rare Metal Materials and Engineering*, vol. 39, pp. 1339–1343, 2010.

[119] K.Y.Yu, Y.Liu, S.Rios, H.Wang, and X.Zhang, "Strengthening mechanism of ag/ni immiscible multilayers with fcc/fcc interface," *Surface & Coatings Technology*, vol. 237, pp. 269–275, 2013.

[120] A.T.Aldred, B.D.Rainford, T.J.Hicks, and J.S.Kouvel, "Magnetic Moment distribution in Ferromagnetic Ni-Cu Alloys," *Phys. Rev. B*, vol. 7, pp. 218–229, 1973.

[121] J.Fassbender, R.Allenspach, and U.Dtirig, "Intermixing and growth kinetics of the first Co monolayers on Cu(001)," *Surf. Sci. Lett.*, vol. 383, pp. L742–L748, 1997.

[122] I.Kramer and G.Bergmann, "The magnetic behavior of Co atoms on the surface and in the interior of the noble metals Au, Ag and Cu," *Z. Phys. B - Condensed Matter*, vol. 47, pp. 321–325, 1982.

[123] S.Ghosh and A.Mookerjee, "Magnetic properties of disordered CoCu alloys: a first-principles approach," *J. Mag. Magn. Mater*, vol. 214, pp. 291–300, 2000.

[124] H.H.Brongersma, P.A.J.Ackermans, and A.D.vanLangeveld, "Composition of Cu-Ni alloy surfaces," *Phys.Rev.B*, vol. 34, pp. 5974–5976, 1986.

[125] S.Granroth, R.Knut, M.Marcellini, G.Andersson, S.Svensson, O.Karis, M.Gorgoi, F.Schafers, W.Braun, W.Eberhardt, W.Olovsson, E.Holmstrom, and N.Martensson, "Investigation of interface properties of Ni/Cu multilayers by high kinetic energy photoelectron spectroscopy," *Phys. Rev. B*, vol. 80, pp. 0941041–0941049, 2009.

[126] S.H.Kim, K.S.Lee, H.G.Min, J.Seo, S.C.Hong, T.H.Rho, and J.S.Kim, "Subsurface growth of Ni atoms deposited on Cu(001) surface," *Phys. Rev. B*, vol. 55, pp. 7904–7909, 1997.

[127] L.V.Pourovskii, N.V.Skorodumova, Yu.Kh.Vekilov, B.Johansson, and I.A.Abrikosov, "Calculated properties of surface and subsurface nickel monolayers on copper," *Surf. Sci.*, vol. 439, pp. 111–119, 1999.

[128] H.L.Meyerheim, D.Sander, N.N.Negulyaev, V.S.Stepanyuk, R.Popescu, I.Popa, and J.Kirschner, "Buried Ni/Cu (001) Interface at the Atomic Scale," *Phys. Rev. Lett.*, vol. 100, pp. 1461011–1461014, 2008.

[129] J.C.J.Saez, J.D.Vazquez, A.M.C.P.Martin, and J.J.J.Rodriguez, "Molecular dynamics study of a Ni/Cu(001) interface," *Nanotechnology*, vol. 14, pp. 701–708, 2003.

[130] V.Blum, Ch.Rath, S.Muller, L.Hammer, K.Heinz, J.M.Garcia, J.E.Ortega, J.E.Prieto, O.S.Hernan, J.M.Gallego, A. Parga, and R.Miranda, "Fe thin-film growth on Au(100): A self-surfactant effect and its limitations," *Phys. Rev. B*, vol. 59, pp. 15966–15974, 1999.

[131] T.R.McGuire, J.A.Aboaf, and E.Klokholm, "Magnetic and transport properties of Fe-Au and Co-Au films," *J.Appl.Phys.*, vol. 52, pp. 2205–2207, 1981.

[132] W.D.Luedtke and U.Landman, "Metal-on-metal thin-film growth: Au/Ni(001) and Ni/Au(001)," *Phys. Rev. B*, vol. 44, pp. 5970–5972, 1991.

[133] A.M.Begley, S.K.Kim, J.Quinn, F.Jona, H.Over, and P.M.Marcus, "Growth of ultrathin films of Fe on Au001," *Phys.Rev.B*, vol. 48, pp. 1779–1785, 1993.

[134] M.M.J.Bischoff, T.Yamada, A.J.Quinn, R. der Krann, and H. Kempen, "Direct Observation of Surface Alloying and Interface Roughening: Growth of Au on Fe(001)," *Phys. Rev. Lett.*, vol. 87, pp. 2461021–2461024, 2001.

[135] P.Weinberger, J.Banhart, G.H.Schadler, A.M.Boring, and P.S.Riseborough, "Calculation of magnetic impurities in a nonmagnetic host: Fe in Au," *Phys.Rev.B*, vol. 41, pp. 9444–9451, 1990.

[136] F.Wilhelm, P.Poulopoulos, V.Kapaklis, J.-P.Kappler, N.Jaouen, A.Rogalev, A.N.Yaresko, and C.Politis, "Au and Fe magnetic moments in disrdered Au-Fe alloys," *Phys.Rev.B*, vol. 77, pp. 224414(1–6), 2008.

[137] I.Turek, V.Drchal, J.Kudrnovsky, M.Sob, and P.Weinberger, *Electronic structure of disordered alloys, surfaces and interfaces.* USA: Kluwer Academic Publishers, 1997.

[138] R.M.Martin, *Electronic structure: Basic theory and practical methods.* New York: Cambridge University Press, 2008.

[139] P.Hohenberg and W.Kohn, "Inhomogeneous electron gas," *Phys. Rev.*, vol. 136, pp. B864–B871, 1964.

[140] W.Kohn and L.J.Sham, "Self-consistent equations including exchange and correlation effects," *Phys. Rev.*, vol. 140, pp. A1133–A1138, 1965.

[141] N.W.Ashcroft and N.D.Mermin, *Solid state Physics.* Brooks/Cole: Thomson Learning, Inc., 2007.

[142] E.Wigner and F.Seitz, "On the constitution of metallic sodium," *Phys.Rev.*, vol. 43, pp. 804–810, 1933.

[143] E.Wigner and F.Seitz, "On the constitution of metallic sodium. ii," *Phys.Rev.*, vol. 46, pp. 509–524, 1934.

[144] J.C.Slater, "Wave functions in a periodic potential," *Phys. Rev.*, vol. 51, pp. 846–851, 1937.

[145] J.Korringa, "On the calculation of the energy of a bloch wave in a metal," *Physica*, vol. 13, pp. 392–400, 1947.

[146] W.Kohn and N.Rostoker, "Solution of the schroedinger equation in periodic lattices with an application to metallic lithium," *Phys. Rev.*, vol. 94, pp. 1111–1120, 1954.

[147] C.Herring, "A new method for calculating wave functions in crystals," *Phys.Rev.*, vol. 57, pp. 1169–1177, 1940.

[148] P.Soven, "Coherent-potential model of substitutional disordered alloys," *Phys.Rev.*, vol. 156, pp. 809–813, 1967.

[149] A.Mookerjee, "Introduction to augmented space method," in *Electronic structure of alloys, surfaces and clusters* (A. Mookerjee and D. Sarma, eds.), London and New York: Taylor & Francis, 2003.

[150] A.Mookerjee, "A new formalism for the study of configuration-averaged properties of disordered systems," *J.Phys. C: Solid state Phys.*, vol. 6, pp. L205–L208, 1973.

[151] A.Mookerjee, "Averaged density of states in disordered systems," *J.Phys. C: Solid state Phys.*, vol. 6, pp. 1340–1349, 1973.

[152] R.Haydock, V.Heine, and M.J.Kelly, "Electronic structure based on the local atomic environment for tight-binding bands," *J.Phys. C: Solid state Phys.*, vol. 5, pp. 2845–2858, 1972.

[153] R.Haydock and R.L.Te, "Accuracy of the recursion method," *Phys.Rev.B*, vol. 49, pp. 10845–10850, 1994.

[154] T.Saha, I.Dasgupta, and A.Mookerjee, "Electronic structure of random binary alloys," *J. Phys.: Condens. Matter*, vol. 8, pp. 1979–1996, 1996.

[155] M.U.Luchini and C.M.M.Nex, "A new procedure for appending terminators in the recursion method," *J.Phys. C: Solid state Phys.*, vol. 20, pp. 3125–3130, 1987.

[156] V.S.Viswanath and G.Muller, "Recursion method in quantum spin dynamics: The art of terminating a continued fraction," *J.Appl.Phys.*, vol. 67, pp. 5486–5488, 1990.

[157] V.S.Viswanath and G.Muller, *The Recursion Method: Application to Many-body Dynamics*. Berlin Heidelberg: Springer-Verlag, 1994.

[158] A.Magnus, "Asymptotic behavior of continued fraction coefficients related to singularities of the weight function," in *The Recursion Method and Its Applications* (D.G.Pettifor and D.L.Weaire, eds.), Berlin Heidelberg: Springer Verlag, 1985.

[159] U. von Barth and L. Hedin, "A local exchange-correlation potential for the spin polarized case: I," *J.Phys.C: Solid State Phys.*, vol. 5, pp. 1629–1642, 1972.

[160] O.K.Andersen, "Linear methods in band theory," *Phys. Rev. B*, vol. 12, pp. 3060–3083, 1975.

[161] L.Pauling and F.J.Ewing, "The ratio of valence electrons to atoms in metals and intermatallic compounds," *Rev. Mod. Phys.*, vol. 20, pp. 112–122, 1948.

[162] B.Lazarovits, L.Szunyogh, and P.Weinberger, "Fully relativistic calculation of magnetic properties of Fe, Co, and Ni adclusters on Ag(100)," *Phys. Rev. B*, vol. 65, pp. 1044411–1044418, 2002.

[163] G.M.Stocks, W.M.Temmerman, and B.L.Gyorffy, "Complete Solution of the Korringa-Kohn-Rostoker Coherent-Potential-Approximation Equations: Cu-Ni Alloys," *Phys.Rev.Lett.*, vol. 41, pp. 339–343, 1978.

[164] G.M.Stocks, R.W.Willams, and J.S.Faulkner, "Densities of States of Paramagnetic Cu-Ni Alloys," *Phys.Rev.B*, vol. 4, pp. 4390–4405, 1971.

[165] I.Dasgupta and A.Mookerjee, "An augmented-space recursive method for the study of concentration profiles at CuNi alloy surfaces," *J.Phys.:Condens.Matter*, vol. 8, pp. 4125–4138, 1996.